12-2018

# Optimization of Laser Shock Peening Process Using Finite Element Modeling

Sai Hamsini Kosaraju
*Clemson University*, skosara@clemson.edu

# OPTIMIZATION OF LASER SHOCK PEENING PROCESS USING FINITE ELEMENT MODELING

---

A Thesis
Presented to
the Graduate School of
Clemson University

---

In Partial Fulfillment
of the Requirements for the Degree
Master of Science
Mechanical Engineering

---

by
Sai Hamsini Kosaraju
December 2018

---

Accepted by:
Dr. Xin Zhao, Committee Chair
Dr. Oliver J. Myers
Dr. Hongseok Choi

## ABSTRACT

Laser shock peening is a cold working process which is used to improve material properties like surface hardness, fatigue life, wear and corrosion resistance, etc. It is widely used to treat turbines, fans, compressor blades, aircraft and automotive parts. When the material is irradiated by high power density laser beams, shock waves are generated, which plastically deforms the material surface and induces high compressive stresses within subsurface area. The amount of residual compressive stress and plastically affected depth depend on laser parameters (laser power density, pulse duration, wavelength, repetition rate, spot size and shape), materials, ambient environment, etc. To improve the application of laser shock peening, it is of critical importance to optimize the process by fully understanding the effects of different parameters. Extensive studies have been devoted to this area. Recently, thanks to the advance of laser technology, high repetition rate lasers could significantly improve this technique by increasing compressive residual stress and plastically affected depth. This research studies the effect of laser repetition rate at different spot sizes and different scanning patterns of shot application on the final shock peening results by finite element modeling.

A two-dimensional finite element model is developed to simulate the interaction between metal samples and laser-induced shock waves. Multiple laser impacts are applied at each location to increase plastically affected depth and compressive stress. The in-depth and surface residual stress profiles are analyzed at various repetition rates and spot sizes. It is found that the residual stress is not sensitive to repetition rate until it reaches a very high level. At extremely high repetition rate (100 MHz), the delay between two shock waves is even shorter than their duration, and there will be shock wave superposition. It is revealed that the interaction of metal with shock wave is significantly different, leading to a different residual stress profiles. Stronger residual

stress with deeper distribution will be obtained comparing with lower repetition rate cases. The effect of repetition rate at different spot sizes is also studied. It is found that with larger laser spot, the peak compressive residual stress decreases but the distribution is deeper at extremely high repetition rates.

A three-dimensional finite element model is developed to study the effect of scanning pattern and repetition rate. The final residual stress distributions are studied at repetition rates of 0.1 MHz, 1 MHz, 10 MHz and 20 MHz for 5 different patterns. It is found that there are no major differences in residual stress profiles due to variation of scanning patterns except for circular pattern. It is also revealed that the minimum residual stress decreases and non-uniformity increases with increase in repetition rate due to interaction of relaxation waves with incoming pressure pulses. To minimize the effect of relaxation waves, two zig-zag patterns are studied. The overlap between successive spots is less in zig-zag pattern-1, and it is completely absent in zig-zag pattern-2. It is found that by applying the newly proposed zig-zag pattern-2, the residual stress uniformity can be significantly improved at repetition rates higher than 0.1 MHz.

## DEDICATION

I would like to dedicate this thesis to my grandparents, parents and friends, who are my strength and always encouraged me throughout my graduate studies.

## ACKNOWLEDGEMENTS

My sincere gratitude to my Advisor Dr. Xin Zhao for his constant guidance, motivation and valuable inputs throughout my graduate study at Clemson University. I would like to thank my committee members Dr. Oliver J. Myers and Dr. Hongseok Choi for being part of my research committee and extending their support throughout this research work. I would like to acknowledge Clemson University for the allotment of computational time on Palmetto cluster. I would also like to thank all the staff members of Mechanical Department for their constant assistance. I would like to extend my gratitude to my fellow research group members Ankit, Kewei, Yuxin and Xiao for their valuable inputs. I would also like to thank my family and friends for their constant support and encouragement.

## TABLE OF CONTENTS

## LIST OF TABLES

## LIST OF FIGURES

# CHAPTER 1: INTRODUCTION TO LASER SHOCK PEENING

## 1.1 Introduction

Fatigue failure due to stress corrosion cracking, foreign object damage, corrosion and wear is a common phenomenon which occur in mechanical structures. This degeneration of material mostly starts on the surface. It is desired to increase the life of a mechanical component and decrease its operation and maintenance costs. Hence surface enhancement techniques are employed to prevent the degeneration of material. These techniques impart residual stresses on the surface which retards crack initiation and propagation, increasing the life of a component. There are many thermal, chemical and mechanical ways for inducing residual stresses. Among these, laser shock peening (LSP) is a promising technique to improve material properties like surface hardness, fatigue life, wear and corrosion resistance, etc. LSP is widely used to treat turbines, fans, compressor blades, aircraft and automotive parts, due to its great advantages in high residual stress, deep stress distribution, high flexibility, and low cost. In this chapter, different mechanical processes for inducing residual stresses on the surface are briefly explained followed by discussion of physical process, advantages and applications of laser shock peening. The mechanism of residual stress generation and relaxation in LSP are explained.

## 1.2 Mechanical surface enhancement techniques

### 1.2.1. Shot peening

In this process, the surface of the workpiece is bombarded with spherical shots at high pressure (Figure 1.1). This creates a dimple on the surface. The material under the dimple is plastically deformed resulting in compressive residual stresses. Multiple spherical shots create overlapping dimples and residual stresses throughout the surface. It is not controllable and hence

cannot produce uniform residual stress distribution. Surface finish is compromised and hence it is not suitable for all applications [1].

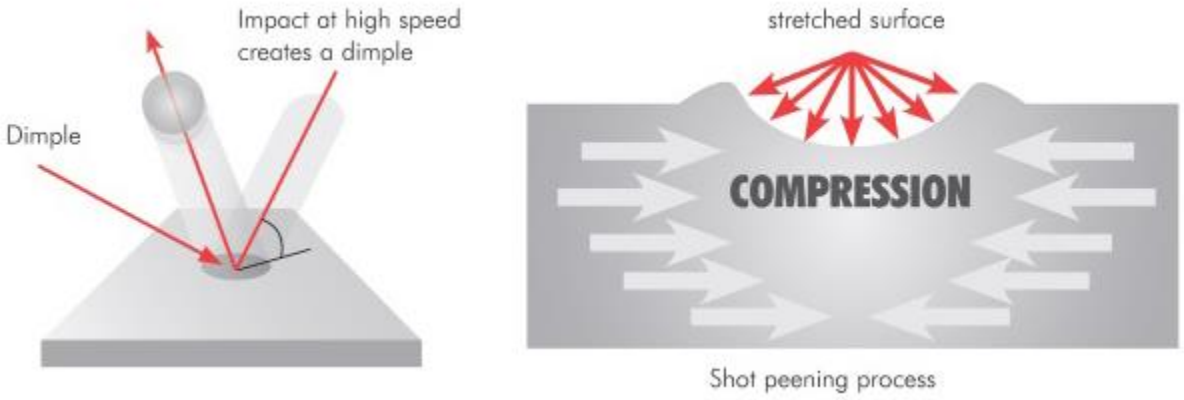


**Figure 1.1: Illustration of shot peening and generation of residual stresses [2]**

1.2.2. Ultrasonic impact peening

As shown in Figure 1.2, a frequency controller is calibrated, and steel pins are attached to it. The vibrations of the controller cause pins to vibrate with high frequency. Plastic deformation of workpiece occurs when high energy pins strike the workpiece surface. The apparatus is handheld and portable. The residual stresses are deeper than shot peening, but the surface is roughened. Repeatability and flexibility are challenging because of handheld tools [3].

**Figure 1.2: Ultrasonic peening process representation [3]**

1.2.3. Water jet peening

In this process, the surface of the workpiece is collided with high pressure water jet (Figure 1.3). A pressure load that exceeds yield strength of the material is created by the water droplet. This causes permanent plastic deformation and compressive residual stresses in the subsurface region of the workpiece. This process is environmentally friendly and surface finish is high. The major disadvantages of this process are cavitation and erosion of workpiece.

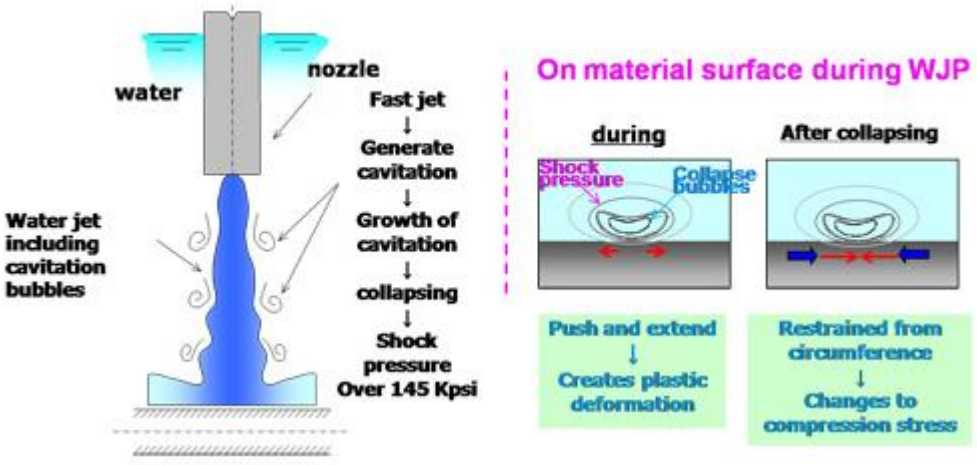


**Figure 1.3: Water jet peening process representation [4]**

1.2.4. Low plasticity burnishing

In this process, a spherical ball supported in a hydrostatic bearing is used as the tool (Figure 1.4). A hydraulic cylinder is used to apply normal force between the tool and the workpiece. When the ball is made to roll on the workpiece surface in required path, the pressure applied by ball creates residual stresses within the subsurface region of workpiece. Deeper residual stress and fine surface finish are achieved in this process. But the requirement of fluid between the ball and socket makes it difficult to treat workpieces with complex and curved geometries.

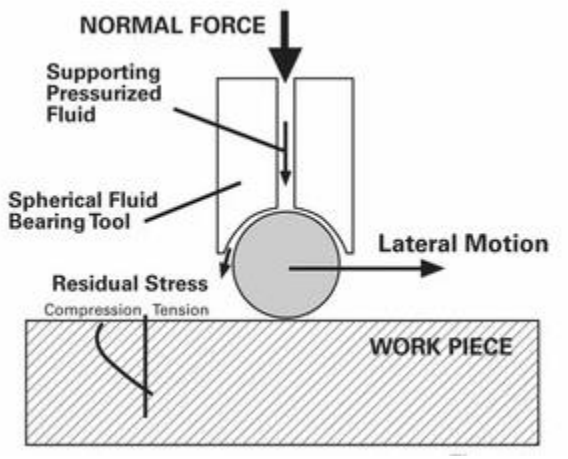


**Figure 1.4: Low plasticity burnishing process representation [5]**

## 1.3 Laser shock peening

### 1.3.1 Mechanism

The work piece is first coated with aluminum or black paint and placed in transparent overlay such as water or glass. When the material is irradiated by high power laser, the coating vaporizes generating high energy plasma which expands in all directions. The expansion of plasma is confined by the transparent overlay, which generates shock waves of high pressure and short duration into the sample. The shock waves plastically deform the material surface and induce high compressive stresses within subsurface area. The aluminum or black paint coating is used to

protect the material surface from thermal damage. LSP can be performed without coating but low power lasers must be used to prevent damage to the surface. Figure 1.5 illustrates laser shock peening process.

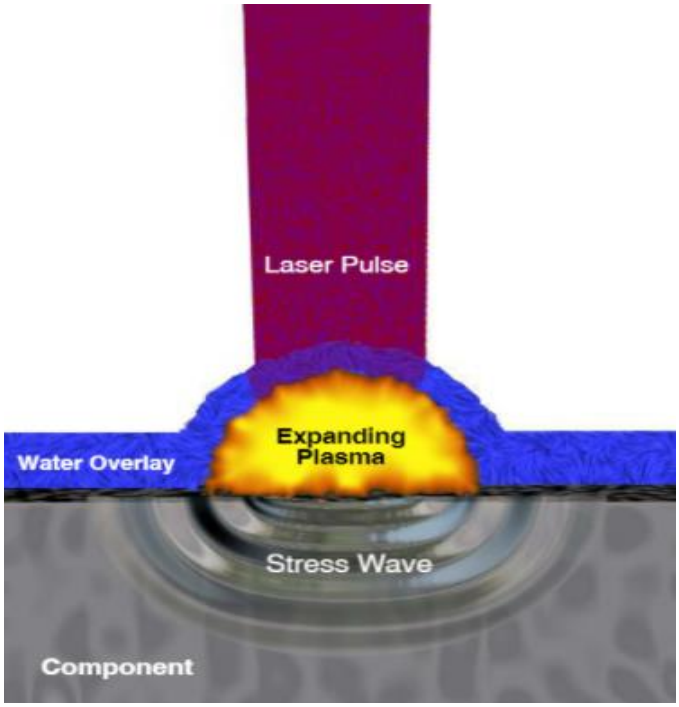


**Figure 1.5: Laser shock peening process representation [6]**

### 1.3.2 Advantages of laser shock peening

Laser shock peening improves the fatigue life of the component by increasing its resistance to stress corrosion cracking, crack propagation, fretting fatigue, cavitation, foreign object damage, stress concentration, pitting etc. Compared to shot peening and ultrasonic impact peening, the compressive residual stress and plastically affected depth are much higher. Unlike shot peening, this process is highly controllable and the effect on surface finish of the component is less. It can be used to treat workpieces with complex geometries [6, 30, 42].

### 1.3.4 Applications of laser shock peening

LSP is used in Aviation industry to treat blades of turbines, fans and compressors, engine parts, fastener holes and fasteners, brakes, welded aircraft parts, wheels etc. In medical field, it is used to improve fatigue performance of orthopedic implants. It is used in automotive industry to treat engine parts, gears, transmission axles etc. In power generation industry, it is used to treat components in steam and gas turbine engines. In tooling industry, it is used to treat drill bits and components of other machine tools [6, 28, 40, 42].

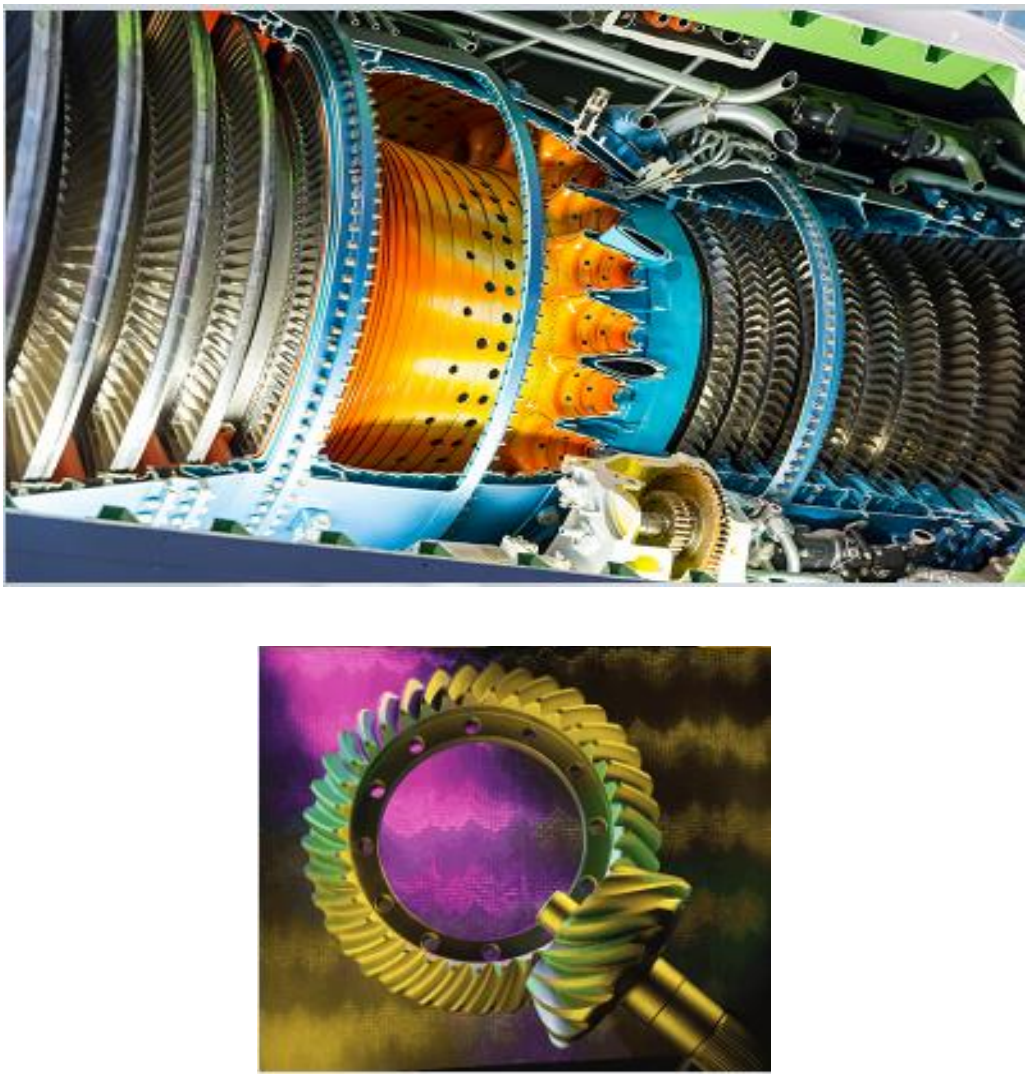

**Figure 1.6: Application of LSP in treating turbines and gears [6]**

### 1.4 Mechanism of residual stress generation

The propagation of shock waves through the metal causes it to deform plastically when the pressure of shock wave is greater than Hugoniot limit of the material [7, 8, 9]. Hugoniot elastic limit is the maximum stress a material can withstand in uniaxial direction without undergoing plastic deformation. It is given by

$$\sigma_{yd} = \sigma_{HEL}\left(\frac{1-2\nu}{1-\nu}\right) \quad \textbf{(1.1)}$$

where $\sigma_{yd}$ is the dynamic yield stress, $\sigma_{HEL}$ is the Hugoniot elastic limit and $\nu$ is the poisson's ratio. Figure 1-7 shows the effect of shock waves on the material. The top layers of the material under the influence of shock wave expand plastically. The expansion of material decreases with increase in depth and finally becomes zero. The tensile plastic deformation of the surface layers induces compressive residual stress which decreases with increase in depth. The expanded layers try to push away the material surrounding it inducing compressive plastic deformation. The residual stress becomes tensile around the affected area because of the compressive plastic deformation [15].

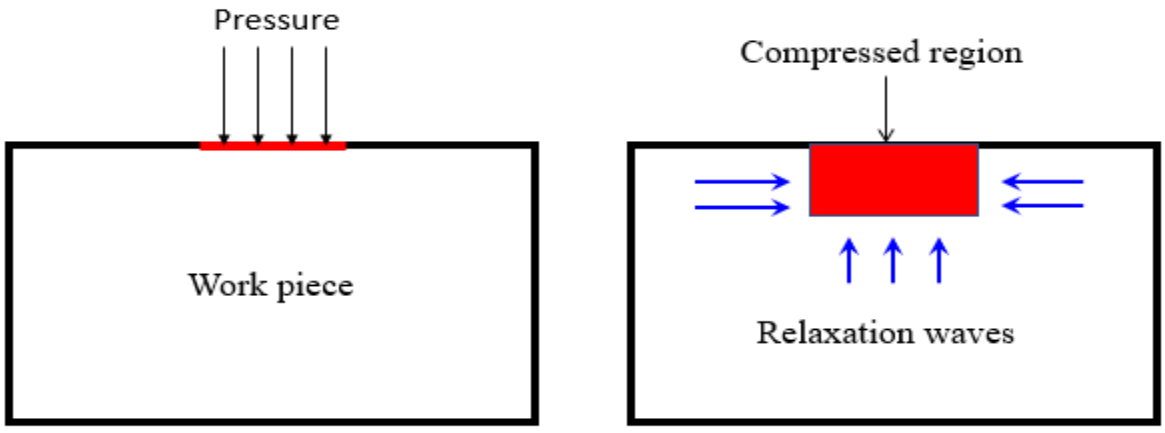


**Figure 1-7. Generation of residual stress**

Figure 1-8 shows the variation of residual stress in depth direction for 1mm spot diameter. It varies from -426.08MPa to 82.85MPa. The peak value of tensile stress is less than peak value of compressive stress. But the volume of material in tensile state is greater than the volume in compressive state to attain equilibrium in the workpiece.

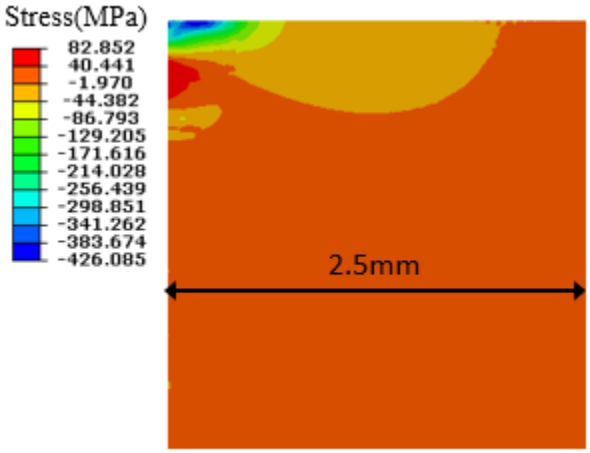


**Figure 1-8: Residual stress distribution along depth for 1mm spot size predicted using axe-symmetric model.**

### 1.5 Relaxation of residual stress

After the pressure is removed, the relaxation waves generated at the boundary of affected area causes reverse straining, resulting in a decrease in residual stress [9, 21, 40, 42]. The reverse straining is more in the top layers of the material because of the free degree of freedom in z-direction. It causes stress hole at the center of circular spot because of the concentration of relaxation waves. This effect is less for square or rectangular spot shapes because of the absence of concentration of relaxation waves [21]. High magnitude and long duration of pressure pulses also increases the strength of relaxation waves. This is because of the increase in deformation of the material which generates stronger opposition from the boundary of the spot.

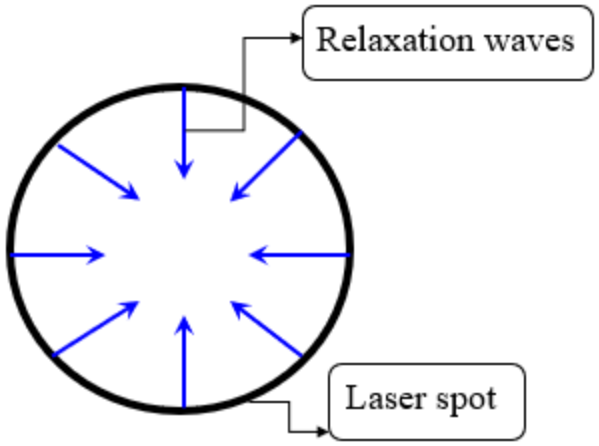


**Figure 1-9: Origin and path of relaxation waves for circular spot shapes**

The magnitude and depth of compressive stress in LSP depend on different parameters such as laser spot size and shape, laser intensity, wavelength, pulse duration, material properties, ambient environment etc. To improve the application of laser shock peening, it is of critical importance to optimize the process by fully understanding the effects of different parameters. Extensive studies have been devoted to this area. Previous studies have demonstrated the benefit of using multiple shocks at the same location to increase the magnitude and depth of residual stresses. But the effect of time interval between successive spots which is determined by repetition rate has not been studied yet. Recently, thanks to the advance of laser technology, high repetition rate lasers could significantly improve this technique. This research studies the effect of laser repetition rate at different spot sizes on the final shock peening results such as peak residual stress and plastically affected depth by finite element modeling. In addition, a sequence of laser shocks is required to scan a large workpiece, which will determine the final residual stress distribution. Hence, an optimum scanning pattern which is not affected by repetition rate needs to be designed to induce uniform residual stresses.

# CHAPTER 2: LITERATURE REVIEW

A two-dimensional (2D) model was initially developed to study laser shock peening numerically. The results from the numerical model were compared with experimental results to find the feasibility of the model. Later the model was used to study the effect of various LSP input parameters. Braisted and Brockman [7] developed a 2D model to study LSP using ABAQUS/Explicit and Standard codes. Elastic perfectly plastic (EPP) material model and a uniform triangular pressure pulse were used. After comparing the finite element analysis (FEA) results for Ti-64 and 35CD4 with experimental results, FEA was found to be a feasible tool for predicting residual stress profiles in LSP. Peyre *et al* [8] adopted a 2D axisymmetric model to study the peening of 12% Cr steel, pure aluminum and 7075-T7351 Al alloys. Ding and Ye [9] adopted a 2D model to study the effect of multiple impacts at the same location in 35CD4 30 HRC steel. It was found that deeper residual stresses were produced with multiple impacts. Plastically affected depth and affected area increases with increase radius of spot. Also, the radius of the spot affects the tensile region formed inside the spot area due to radial stress waves. Peyre *et al* [10] studied the effect of peak pressure, impact size, pulse duration and sacrificial overlay using a 2D axisymmetric model.

Since a 2D model limits the study of LSP parameters like spot shape, sequence of shock application, workpiece geometry etc., a three-dimensional (3D) model was developed. Ding [11] developed a 3D model to calculate surface and in-depth residual stress profiles in 35CD4 50 HRC using ABAQUS Explicit and standard codes. The simulation results were in good agreement with experimental results. EPP material model is used to determine material behavior. The effect of multiple spots, impact pressure, pressure pulse duration, spot size and shape on residual stress profiles are studied using numerical model.

The yield stress and elastic modulus of the material change because of high strain rates ($10^6$/s) in LSP. The EPP material model is not sufficient to accurately determine the material behavior. Amarchinta *et al* [12] studied non-linear material models to represent material behavior and compared them with experimental results. Inconsistent results are produced by EPP material model, whereas Zerilli-Armstrong (ZA) model exaggerate residual stresses. Johnson-Cook (JC) model produces results compatible with experimental results.

In the previous models, the spatial and temporal profiles of the pressure were not precisely considered. A user subroutine is required to model space and time variation of pressure simultaneously. After determining proper material model and pressure profiles, the effect of various LSP process parameters on different materials were studied by various authors. Different code combinations were used by researchers to solve the final equation of motion. Rohit *et al* [13] developed 3D model using ABAQUS Explicit. JC model is used to determine the material behavior of annealed AISI 1053 steel. A VDLOAD user subroutine is used to control the position of the pressure. After validating a 2D model with experimental results, a 3D model is used to study the effect of overlapping spots on final residual stress distribution. 50% overlap produced maximum compressive residual stresses in the workpiece. Zhang *et al* [14] studied the effect of peening intensity, multiple spots and overlapped spots on Ti-6Al-4V alloy. Gulshan Singh *et al* [15] developed a 3D model using ABAQUS Explicit and Implicit algorithms to study the impact of laser parameters on Ti-6Al-4V. It is found that the peak compressive stress, tensile stress, effect depth and volume increase with increase in pressure magnitude and spot radius. Spot shape and thickness of the sample affect the compressive and tensile residual stresses significantly. The maximum tensile stress is higher for circular spot shape than other shapes. Residual stress profiles are sensitive to overlap ratio and the shot sequence. Warren *et al* [16] studied the effect of intensity,

peening spacing and spot size in a massive parallel shock peening. The magnitude of stress and affected depth increases with increase in laser intensity and spot size. Peen spacing plays a critical role in obtaining uniform mechanical properties. K.Y. Luo *et al* [17] adopted ABAQUS/Explicit and standard codes to determine the residual stress distribution in Ti-6Al-4V alloy at different LSP parameters. It is found that with increase in overlapping rate and spot diameter, high compressive stresses with low fluctuation rate can be induced at constant laser power density. Magnitude of plastically affected depth and residual stress increases with increase in laser power density. A 50% overlap ratio is an optimum choice to treat massive samples. Wei *et al* [18] also studied the effect of power density, spot size, full width at half maximum (FWHM) of pressure pulse, multiple impacts at same region and the effect of overlap using a 3D model in 35CD4 steel. The effect of FWHM on stress profile is complex. With increase in FWHM, the surface stress decreases whereas plastically affected depth increases.

Yongxiang *et al* [19] developed a 3D model using ANSYS and LS-DYNA to perform static and dynamic analysis respectively. The surface deformation and residual stress profiles in x and y directions are studied for single and multiple shots at same location. It is found that with multiple shots at same location, peak compressive residual stress and plastically affected depth increase initially and then saturate. Orthogonal experiment design combined with numerical modeling is used to study the effect on laser parameters in [20]. It is found that with increase in size of action zone of laser and pressure pulse duration, the peak compressive stress and plastically affected depth increase. Round spot, high pressure amplitude and duration can induce stress hole at the center which can be eliminated by using overlapping spots. In [21], dynamic response analysis at different intensities reveals that the reverse plastic loading causes stress drop in the center part of

processed region. Using square spot shape prevents the focalization of reverse loading and reduces the stress drop at the center of the spot.

To scan large workpieces, a sequence of laser shocks was required. Complex overlap of successive laser shots resulted in anisotropy of residual stresses. The patterns of compressive and tensile stresses in the processed region were studied by various authors to improve the homogeneity of residual stresses. Hirano *et al* [22] discussed the anisotropic stress generation in the workpiece. A model is developed to study the stress distribution in the laser processed area which is in good terms with experimental results. Sagar *et al* [23] also studied the effect of sequence on tensile stress distributions at edges. They proposed an optimum sequence for shorter patch to induce ideal surface and in-depth stress distributions. Neila *et al* [24] simulated 25 overlapping spots and studied the effect of percentage overlap and LSP strategies on average residual stresses. It is found that with increase in percentage overlap, homogeneity of surface stress increases. Though the path of LSP doesn't affect the global residual stress distribution significantly, it affects the magnitude and gradient of local stresses. Karbalaian *et al* [25] studied the effect of square overlapping laser pulses on 35CD4 steel using ABAQUS/Explicit. It is found that the tensile and compressive residual stresses in x and y directions increase with increase in overlap ratio. 0-20% overlap ratio is suggested to attain a compressive stress of 300MPa in the workpiece for the examined laser parameters. Correa *et al* [26] developed a 3D model of dog-bone shaped specimens to study the effect of edges and pulse sequence on final residual stress distribution. Stress distributions for 3 different strategies are studied to obtain optimum residual stress at the edges which act as stress concentration zones. By correlating experimental and simulation data, it is confirmed that the crack nucleation occurs at maximum tensile stress region. Compressive residual stresses are induced at the edges in strategy 3, where the scanning starts at

the center of the sample and ends at the edge. Correa *et al* [27] investigated stress generation at different stages during zigzag-type area processing. It is found that LSP protects the workpiece more in laser advancing direction. The anisotropy in $\sigma_x$ and $\sigma_y$ is addressed by using random-type scanning pattern.

From the literature, it is found that the amount of residual compressive stress and plastically affected depth depend on laser parameters (laser power density, pulse duration, wavelength, repetition rate spot size and shape), materials, ambient environment, etc. To improve the application of laser shock peening, it is of critical importance to optimize the process by fully understanding the effects of different parameters. Due to recent advancements, lasers with high repetition rate have been developed. The feasibility and effect of high repetition rate lasers in LSP remains unstudied. This research studies the effects of laser repetition rate, spot size and sequence on the final shock peening results by finite element modeling. It also focuses on developing an optimum pattern to induce maximum residual stresses at very high repetition rates.

# CHAPTER 3: NUMERICAL MODEL

## 3.1 Introduction

Since LSP is a fast process, it is difficult to experimentally study the propagation of shock wave and stress generation within the component at each time step. Therefore, a numerical model is needed to study the effect of input parameters and to optimize them to increase peak compressive stresses and plastically affected depth.

The numerical model for LSP typically consists of two steps. In the first step, the laser material interaction is studied to determine the spatial and temporal pressure profiles induced into the sample. Extensive studies have been going on to determine the pressure profiles using models such as two-temperature model, hydrodynamic model etc. In the second step, the calculated pressure is applied as the surface load in the finite element model to obtain final residual stress profile in the material. This research focusses only on the second step since our aim is to study the effect of the laser repetition rate. The temporal pressure profile is borrowed from the conclusion of Ref. [17], where the laser parameters are pulse duration of 10 ns, pulse energy of 3 J and wavelength of 1064 nm, as shown in Figure 3.1. It raises to peak value in 10 ns and then gradually decreases. Based on this, the spatial pressure profile is calculated according to the Gaussian distribution:

$$P(r,t) = P(t)\exp\left(-\frac{r^2}{2R^2}\right) \quad \textbf{(3.1)}$$

$$r = \sqrt{x^2 + y^2} \quad \textbf{(3.2)}$$

where P is the pressure, r is the distance from laser spot center, R is the laser spot radius, and x and y are coordinates of integration point. Figure 3.2 shows the Gaussian spatial distribution of pressure [17, 24, 28, 31, 38, 42].

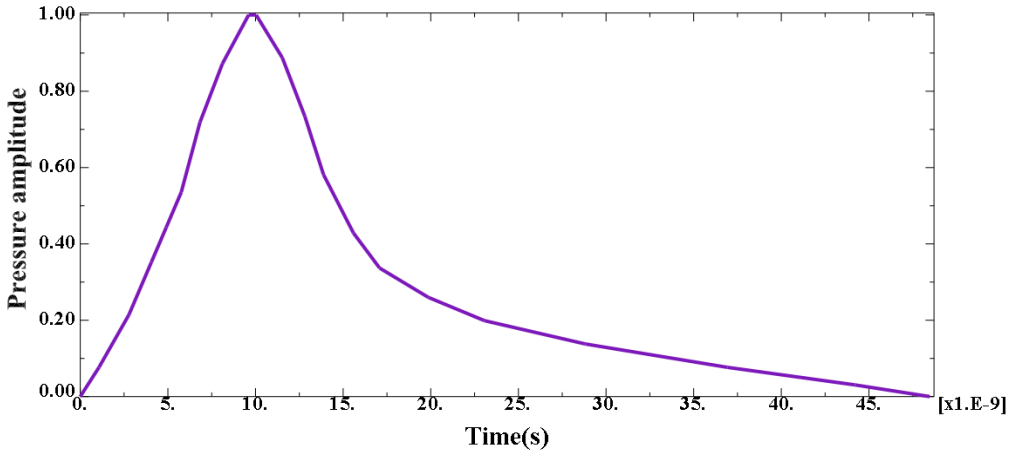


**Figure 3.1: Temporal profile of pressure for a laser with FWHM of 10 ns, pulse energy of 3 J and wave length of 1064 nm.**

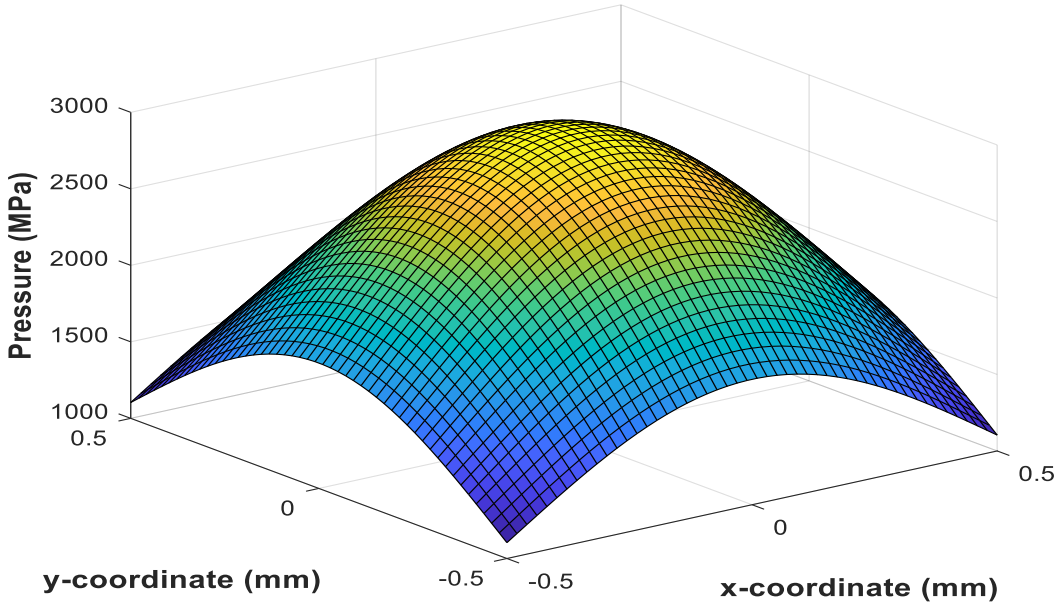


**Figure 3.2: Gaussian spatial distribution of pressure.**

### 3.2 Finite element model

#### 3.2.1 2D model

A 2D axisymmetric computational domain is set up in ABAQUS to simulate the material deformation under the surface pressure load obtained from Section 3.1 [2,7]. It is useful to study the effect of multi-pulse shooting on the same spot. Since the affected area is very small compared to the size of the workpiece, only a small part of the workpiece is modeled. CAX4R (4-node bilinear axisymmetric quadrilateral, reduced integration and hourglass control) elements are used for finite computational domain. Infinite elements (CINAX4) are used to provide quiet boundaries around the finite domain. The size of finite domain is chosen such that the residual stress profile is not affected by the further increase in size of the domain. The size of the mesh is chosen based on mesh sensitivity analysis. Mesh sensitivity analysis is decreasing the size of the mesh till the results become consistent. Table 1 summarizes the mesh sizes used for different spot sizes.

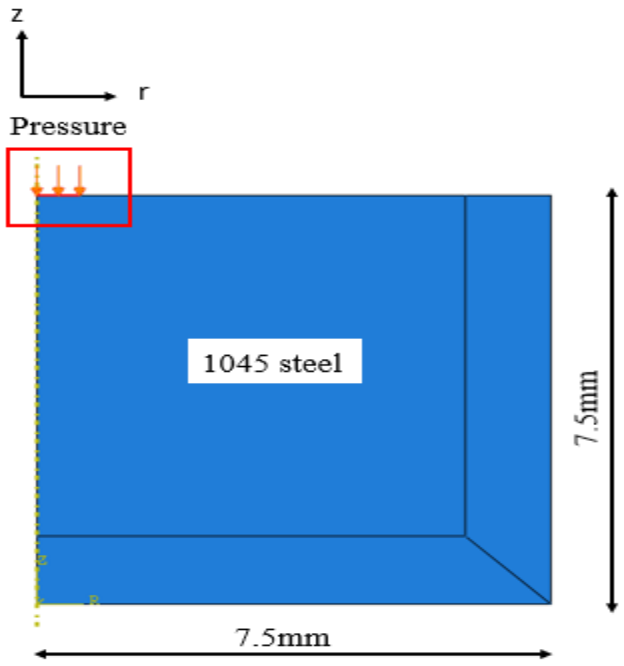


**Figure 3.3: Axisymmetric model set up for 1mm spot diameter.**

**Table 1: Summary of mesh sizes used at various spot sizes**

| Spot size | Mesh size in x-direction | Mesh size in y-direction |
|---|---|---|
| 1mm | 25μm | 10μm |
| 0.1mm | 2.5μm | 2.5μm |
| 0.01mm | 0.25μm | 0.25μm |

A user subroutine *VDLOAD is used to model temporal and spatial variation of pressure on the sample surface [13, 28, 38, 42]. ABAQUS/Explicit algorithm is used to obtain the dynamic material response. In this algorithm, the equation of motion is integrated using Explicit central difference scheme as follows:

$$\ddot{\boldsymbol{u}}^{(i)} = \mathbf{M}^{-1} \cdot (\mathbf{F}^{(i)} - \mathbf{I}^{(i)}) \tag{3.3}$$

$$\dot{\boldsymbol{u}}^{(i+\frac{1}{2})} = \dot{\boldsymbol{u}}^{(i-\frac{1}{2})} + \left(\frac{\Delta t\,(i+1) + \Delta t(i)}{2}\right)\ddot{\boldsymbol{u}}^{(i)} \tag{3.4}$$

$$\boldsymbol{u}^{(i+1)} = \boldsymbol{u}^{(i)} + \Delta t^{(i+1)}\,\dot{\boldsymbol{u}}^{(i+\frac{1}{2})} \tag{3.5}$$

Where $\boldsymbol{u}$ is displacement increment, $\dot{\boldsymbol{u}}$ is velocity, $\ddot{\boldsymbol{u}}$ is acceleration, **M** is diagonal mass matrix, **F** is external force vector, **I** is the internal force vector and *i* represents the time step. The velocity and displacement increment at current time step are calculated from velocity and acceleration from previous time step [32].

Element-by-element estimation method is used for time incrementation because the infinite elements limit the use of global time estimation method. In this method, the stability limit is calculated based on present dilatation wave speed in each element. The stability limit is given by

$$\Delta t \leq \min(\, L_e \sqrt{\frac{\rho}{\lambda+2\mu}}) \quad \textbf{(3.6)}$$

where $L_e$ is the smallest dimension of the element, ρ is the density of the material, λ and μ are Lame's constants for the material [32].

The workpiece is subjected to the shooting of four laser pulses at the same location with different repetition rates. For lower repetition rates where there is no overlap of pressure pulses, each pressure pulse is given in a step with step time equal to repetition rate. At high repetition rates where there is temporal overlap between pressure pulses, the overlapping pressure pulses are specified in a single step. The overlap of pressure pulses is specified using amplitude definition, based on the assumption that the consequence pressure pulses have linear superposition.

### 3.2.2 3D model

A 3D computational domain is set up in ABAQUS to study the LSP over a large area by laser scanning. Since the affected area is very small compared to size of the workpiece, only a small part of work piece is modeled. C3D8R (An 8-node linear brick, reduced integration, hourglass control) elements are used for the finite computational domain. To prevent the effect of wave reflecting at the boundaries on residual stresses, infinite elements (CIN3D8) are used around the finite domain. The size of finite domain is chosen such that further increase in domain size does not affect the residual stresses.

The size of the mesh is chosen based on mesh sensitivity analysis. A mesh size of 50 μm is used in x, y and z directions such that a compromise is obtained among simulation time, size of

output file and the simulation accuracy. 5X5 and 8X8 of laser scanning patterns are studied to reveal the effect of different repetition rates and scanning patters on the residual stress distribution.

A user subroutine *VDLOAD is used to model temporal and spatial variation of pressure. Surface partitions are used to create different patterns on the workpiece. The combination of *VDLOAD and *Step module are used to apply laser shots in a pattern. Figure 3.4 and Figure 3.5 illustrate 3D model and surface partitions. ABAQUS/Explicit algorithm is used to obtain the dynamic material response.

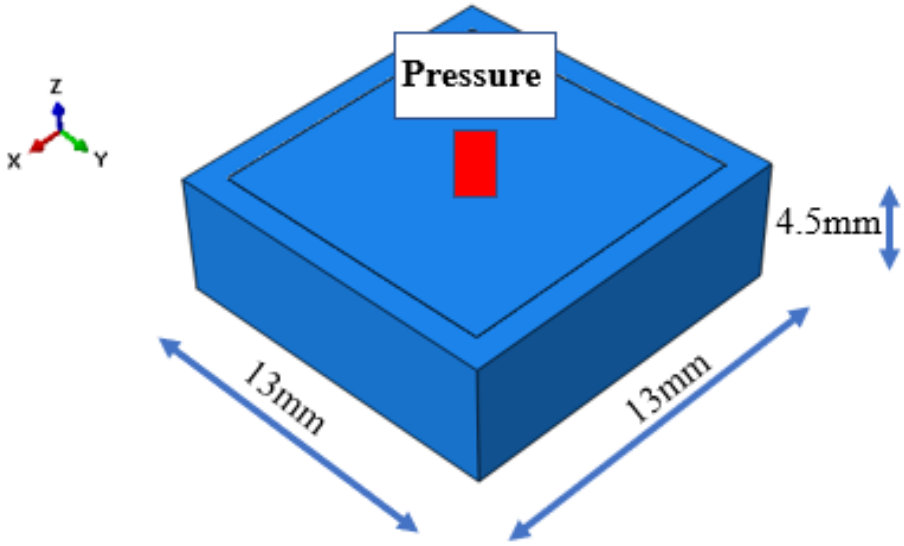


**Figure 3.4: 3D model set up for 1mm spot diameter.**

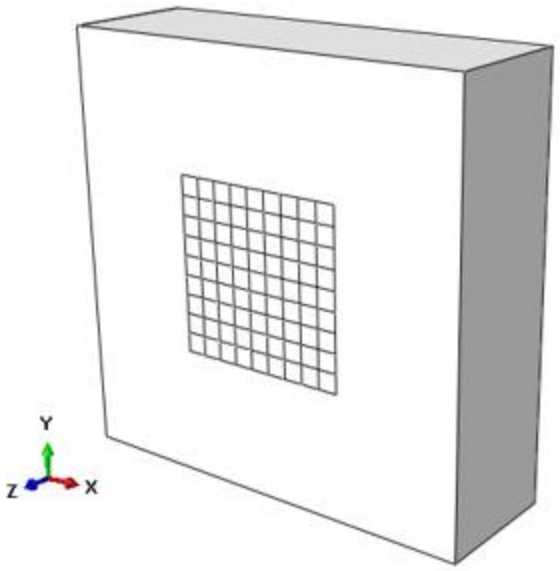


**Figure 3.5: Surface partitions for 8X8 pattern.**

### 3.2.3 Material model

In LSP, the material is strained at high rates exceeding $10^6$ $s^{-1}$. At this high strain rate, the yield strength and elastic modulus of the material change. Hence, a model which accurately captures the elastic-plastic material behavior is required. Amarchinta et al. has compared elastic perfectly plastic (EPP) model, Zerilli-Armstrong (ZA) Model and Johnson-Cook (JC) model in [12] and concluded that the results from JC model are consistent with experimental results. Hence, the elastic-plastic behavior of 1045 steel is modeled using JC equation [8, 10, 12, 13, 15, 16, 24, 27, 31, 33, 36, 37, 42] . The flow stress is calculated as a product of strain hardening term, strain rate dependent term and temperature term [13]. Because of the short time scale, the process is considered as adiabatic and the temperature term is neglected. The equation is given as

$$\sigma = [\, A + B\varepsilon^{n} \,] \, [1 + C \ln \frac{\dot{\varepsilon}}{\dot{\varepsilon}_0} \,] \, [1 - T^{m} \,]$$

where $\sigma$ is flow stress, $\varepsilon$ is strain, $\dot{\varepsilon}$ is strain rate, A is yield stress, B is work hardening modulus, n is work hardening coefficient and C is strain rate sensitivity. The material constants A, B, C and n need to be determined experimentally. The constants for 1045 steel are taken from literature [31,33]. Table 2 gives the mechanical properties of 1045 steel.

**Table 2. Material properties of 1045 steel [31, 33]**

| **Properties** | **Value** |
|---|---|
| Density, | 7580 kg/m$^3$ |
| Youngs modulus, E | 206GPa |
| Poisson's ratio | 0.3 |
| A | 507MPa |
| B | 320MPa |
| C | 0.064 |
| n | 0.28 |

# CHAPTER 4: METHODOLOGY

## 4.1 Benchmark simulation

To validate the numerical model in the current research, a 2D model is replicated using parameters in [9]. The surface stress profile in r direction for a mesh density of 0.5 are compared with FEA data and experimental data from Ref. 9.

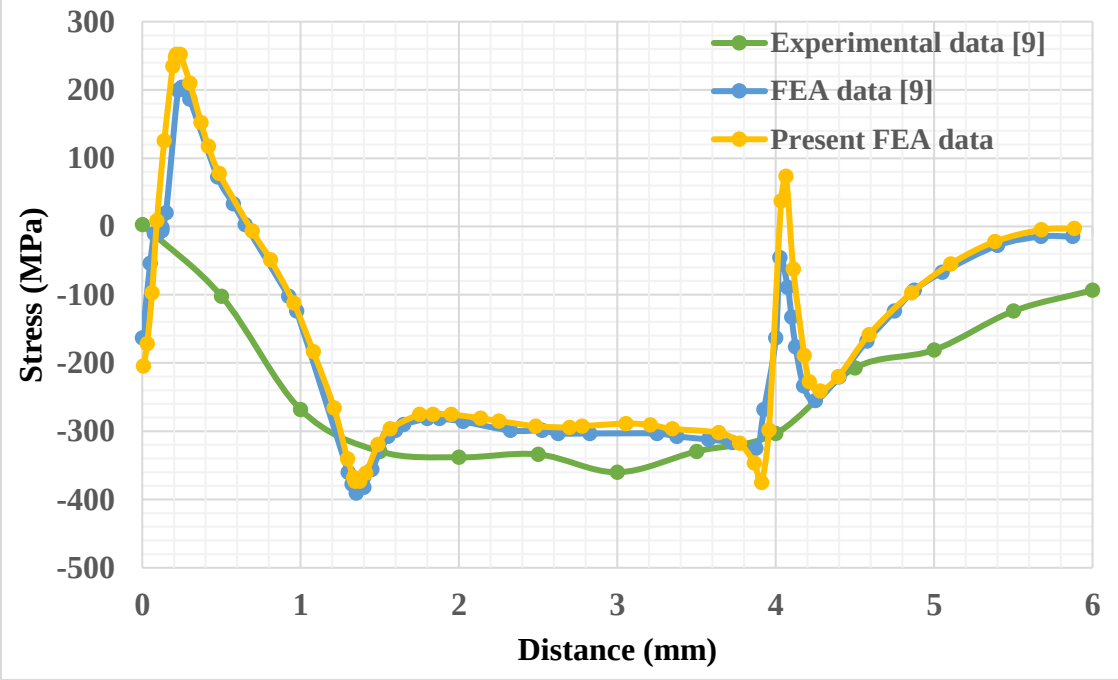


**Figure 4.1: Surface stress profile from benchmark simulation**

Figure 4.1 shows that the developed model is consistent with the numerical model from the literature. The small differences in the residual stress values are attributed to the missing simulation setup parameters like size of time increment and total step time of implicit process.

## 4.2 Repetition rate

Material is subjected to multiple laser shots at the same location to increase peak compressive stress and plastically affected depth [8, 9, 11, 18, 19, 29, 35, 36]. The time interval

between successive laser spots is determined by the repetition rate. Due to recent developments, lasers with very high repetition rates of 100 MHz have been developed, which open new possibilities of LSP by introducing completely different pressure-material interaction dynamics.

The effect of repetition rate is studied at 0.1 MHz, 1 MHz, 10 MHz and 100 MHz for spot diameters of 1 mm, 100 μm and 10 μm. The repetition rate can be characterized into three regimes. It takes about $10^{-5}$ s for the material to relax completely after irradiation of single laser pulse [15]. Therefore, repetition rates below 0.1 MHz can be considered to be the low repetition rate regime, where the material is completely relaxed between two successive pressure pulses. It is only partially relaxed at higher repetition rates. As shown in Figure 3.1, the pressure load introduced by a laser pulse can last for 50 ns, and thus there is no overlap of consecutive pressure pulses for repetition rates lower than 20 MHz. The pressure profile changes due to the overlap of consecutive pulses at repetition rates higher than 20 MHz, which is considered as the high repetition rate regime. For repetition rate of 100 MHz, the peak pressure is 1.6 times of that by a single pressure pulse. The repetition rate regime in between is the moderate regime.

To study the effect of pressure pulse overlap, repetition rates of 20 MHz and 33.3 MHz are used. The pressure pulses are applied one after the other without allowing the material to relax between successive spots at a repetition rate of 20 MHz. The overlap between successive pressure pulses does not change the peak pressure at 33.3 MHz. Repetition rates of 142.9 MHz and 200 MHz are also studied to check for the extent of change in plastically affected depth after 100 MHz.

Figure 4.3 and Figure 4.4 show the overlap of pressure profiles at repetition rates of 33.3MHz and 100MHz respectively. It is assumed that the profile of the incoming pressure wave will not be affected by the former pulse and the material properties remain unchanged.

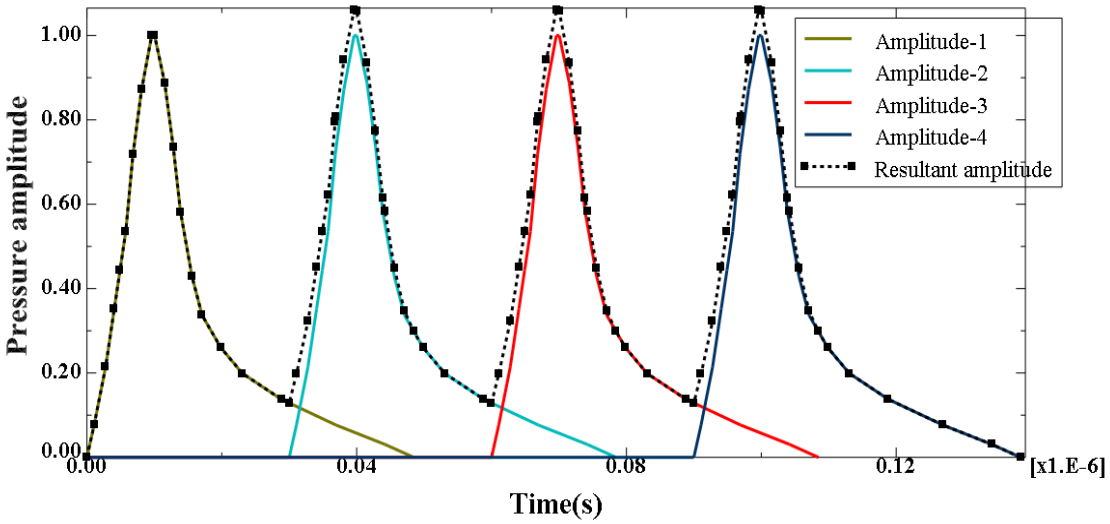


**Figure 4.2: Overlap of pressure profiles at repetition rate of 33.3MHz.**

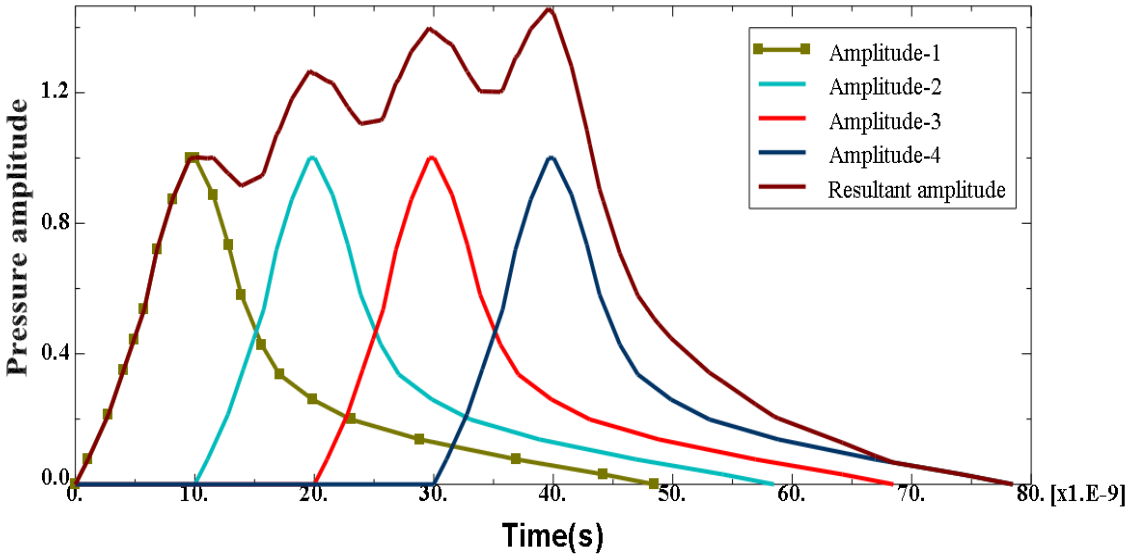


**Figure 4.3: Overlap of pressure profiles at repetition rate of 100MHz.**

### 4.3 Scanning patterns

When treating the workpiece surface over a large area, the scanning pattern is critical to affect the actual residual stress distribution. Therefore, several different scanning patterns are

proposed in this study, and their effects on the surface residual stress distribution are investigated. In sequence 1, laser shots with fixed overlap ratio are applied consecutively in a straight line. The first laser shot in the second row is applied beneath the first spot in the first row; the first spot in the third row is applied beneath first spot in second row and so on. The overlap ratio of successive spots in x and y directions is constant. Figure 4.5 illustrates sequence 1 in which the distance between consecutive rows is D/2.

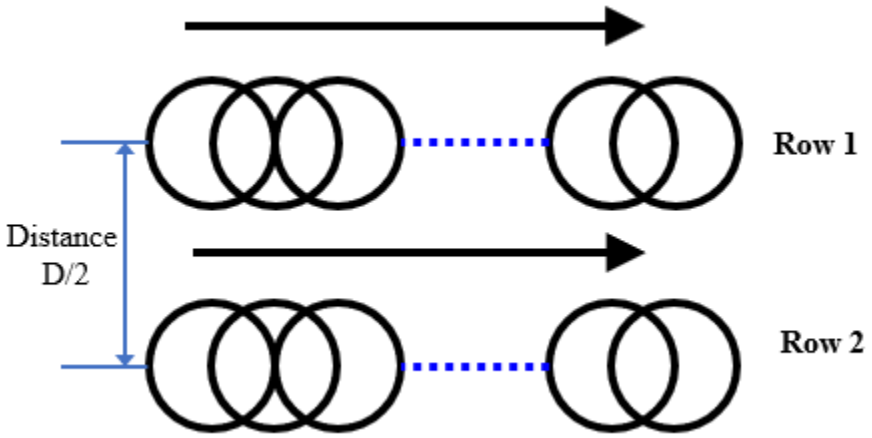


**Figure 4.4: Sequence 1**

Sequence 2 is similar to sequence 1 except the first spot in the second row is applied beneath the last spot in the first row, the first spot in the third row is applied beneath last spot in the second row and so on. The overlap ratio of successive spots is constant in x and y directions. Figure 4.6 illustrates sequence 2 in which the distance between consecutive rows is D/2.

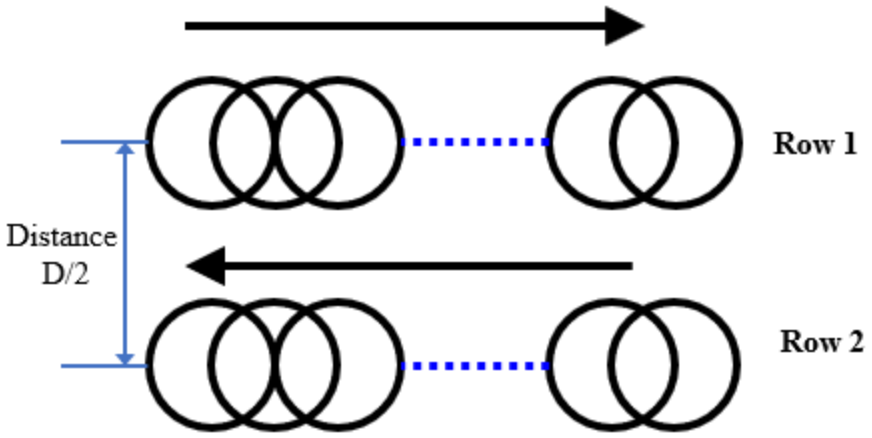


**Figure 4.5: Sequence 2**

In sequence 3, laser shots with fixed overlap ratio are applied consecutively in a straight line. The first laser shot in second row is applied below the first spot in first row with an offset distance equal to the radius of spot. The first spot in third row is applied below the first spot in the second row with the same offset distance and so on. The overlap ratio of successive spots in x and y directions is constant. Figure 4.7 illustrates sequence 3 in which the distance between successive rows is D/2.

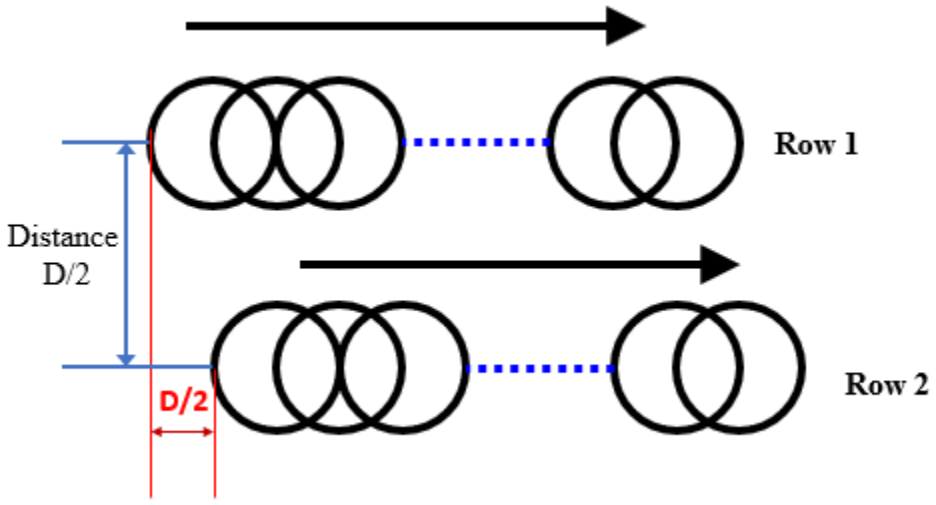


**Figure 4.6: Sequence 3**

Sequence 4 is similar to sequence 3 except the first spot in the second row is applied below the last spot in the first row with an offset distance equal to the radius of spot, the first spot in third row is applied below the last spot in the second row with the same offset distance and so on. Figure 4.8 illustrates sequence 4 in which the distance between successive rows is D/2.

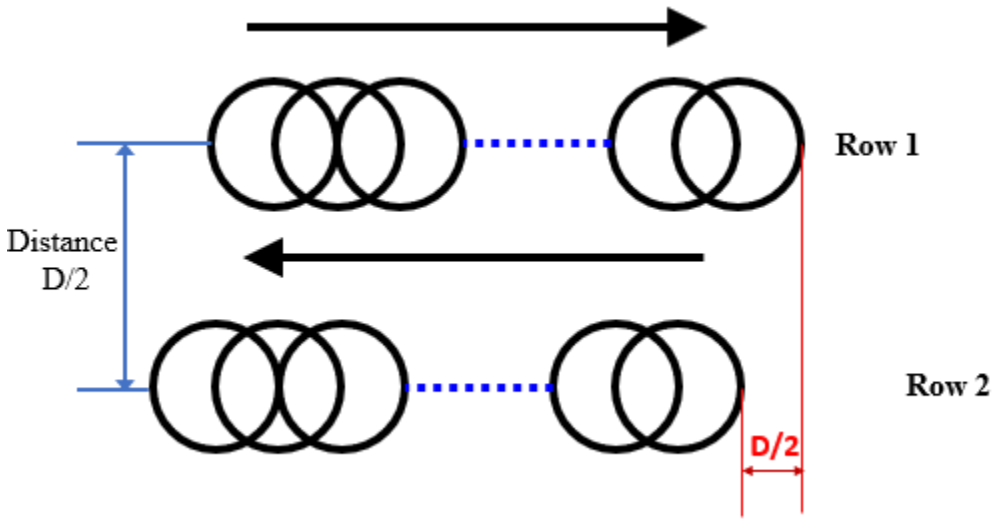


**Figure 4.7: Sequence 4**

Another proposed pattern is the circular scanning pattern. In this sequence, the rings of laser spots are applied consecutively. The overlap ratio between two consecutive spots in a ring and between two spots in consecutive rings is kept constant. Figure 4.9 shows circular pattern. The number in the figure represents the advancement of laser pulses.

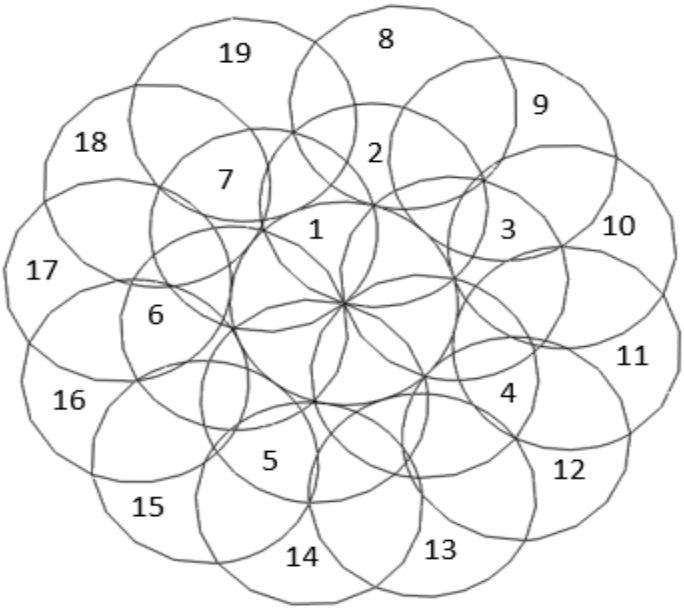


**Figure 4.8: Circular pattern**

In a sequence, the residual stresses generated by a laser spot are affected by the interaction of surrounding laser spots. There will be straight and diagonal overlap *(circular pattern)* of adjacent spots in a pattern. The effect of second laser spot on the residual stresses at the center of the first laser spot is studied at straight and diagonal overlap ($45^o$ angle).

Firstly, the effect of different sequences on the residual stress profiles in x, y and z directions are studied at repetition rate of 0.1 MHz using 5X5 pattern. A circular laser spot of 1 mm with 50% overlap between successive spots is used. The material is completely relaxed between consecutive pulses at this repetition rate. Later, the stress profiles for the sequences are studied at repetition rates of 1 MHz, 10 MHz and 50 MHz. If the workpiece is very large, there will be abundant time gap between adjacent rows. So, the material is allowed to relax for $10^{-5}$ s

after each row of spots for all sequences except for circular sequence. The effect of repetition rate on the sequence is also studied without allowing the material to relax after each row of laser spots.

To eliminate the edge effect caused due to external laser spots, the computational domain is increased to accommodate 8X8 spot patterns. The non-uniformities in S11 (residual stress in x-direction) and S22 (residual stress in y-direction) for sequences 1 and 2 are studied at all repetition rates. To decrease the non-uniformity and increase the minimum residual stress on the workpiece by decreasing the effect of relaxation waves on successive laser pulses, two zigzag patterns are tested.

Figure 4.10 shows the zigzag pattern 1 for sequence 1. The number in the figure represents the advancement of laser pulses. The overlap between two successive pulses is less for this pattern. Although the final pattern is same as sequence 1, the time at which each pulse is irradiated highly differs. The spot centers of 7 and 9 in row 2 are collinear with the spot centers of 1, 3 and 5 in row 1. Similarly, spot centers of 2 and 4 are collinear with the spot centers of 6, 8 and 10 in row 2. Figure 4.11 illustrates zigzag pattern 1 for sequence 2. The number in the figure represents the advancement of laser pulses.

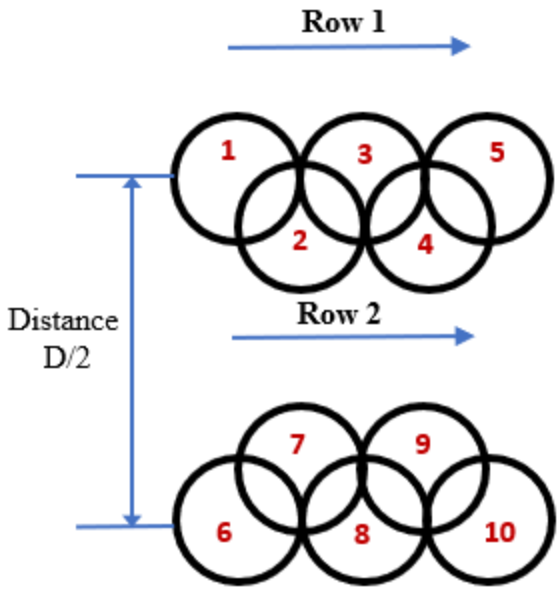


**Figure 4.9: Zigzag pattern 1 for sequence 1.**

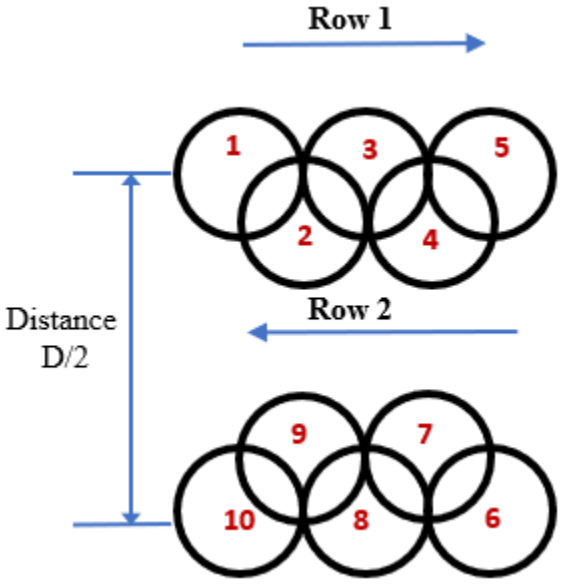


**Figure 4.10: Zigzag pattern 1 for sequence 2.**

Figure 4.12. shows the zigzag pattern 2 for sequence 1. Each row is represented by different color. The successive laser pulses in a row advance in right direction. The final pattern is same as

sequence 1 but the overlap between successive spots is eliminated and the time of irradiation of spots is entirely different.

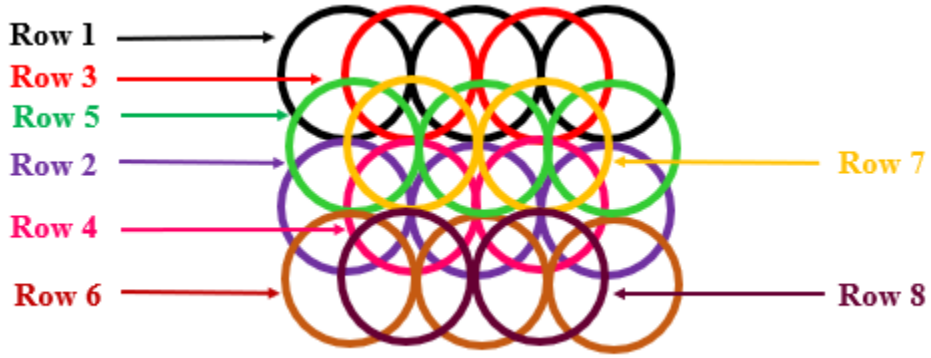


**Figure 4.11: Zigzag pattern 2 for sequence 1.**

The two zigzag patterns are tested at repetition rates of 0.1 MHz, 1 MHz, 10 MHz and 20 MHz. The two zigzag patterns are also tested for sequence 2. Statistical analysis of residual stresses in the center part (1.5 mm X 1.5 mm) of the processed area is performed. Sample mean, range, standard deviation, minimum and maximum values are calculated and analyzed.

# CHAPTER 5: RESULTS AND DISCUSSION

## 5.1 Effect of repetition rate

The surface (along r) and in-depth (along z) distributions (Figure 5.0) of residual stresses are compared at different repetition rates for a spot of diameter 0.1 mm. Figure 5.1 shows that repetition rates below 10 MHz do not have significant impact on in-depth stress distributions. High residual stresses of 820 MPa are induced to a greater depth at high repetition rate of 100 MHz. This is because of the increase in amplitude of the pressure due to overlapping laser pulses at 100 MHz. Figure 5.2 shows that the surface stress profiles remain unaffected for repetition rates lower than 10 MHz. At high repetition rate of 100 MHz, the surface stresses become tensile (600 MPa). This is attributed to the increase in relaxation of surface residual stress due to free degree of freedom in z direction with increase in pressure magnitude (for constant spot size).

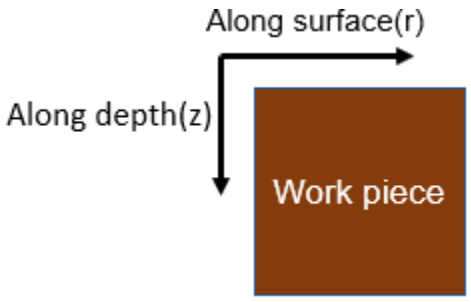


**Figure 5.0: Illustration of surface and in-depth directions**

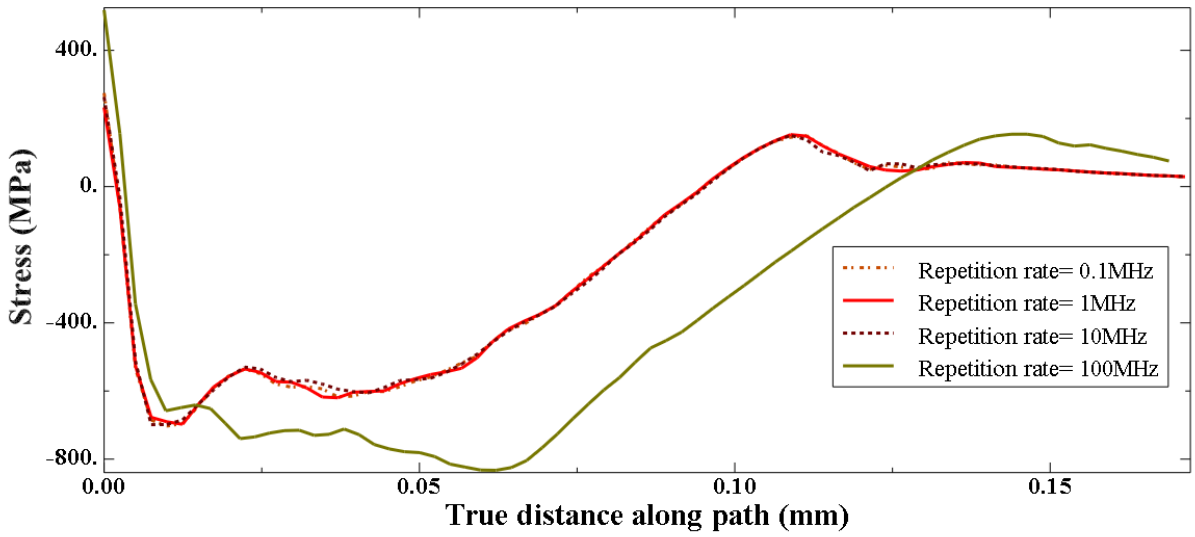


**Figure 5.1: Comparing in-depth residual stress distributions at repetition rates of 0.1 MHz, 1 MHz, 10 MHz and 100 MHz for a spot diameter of 0.1 mm.**

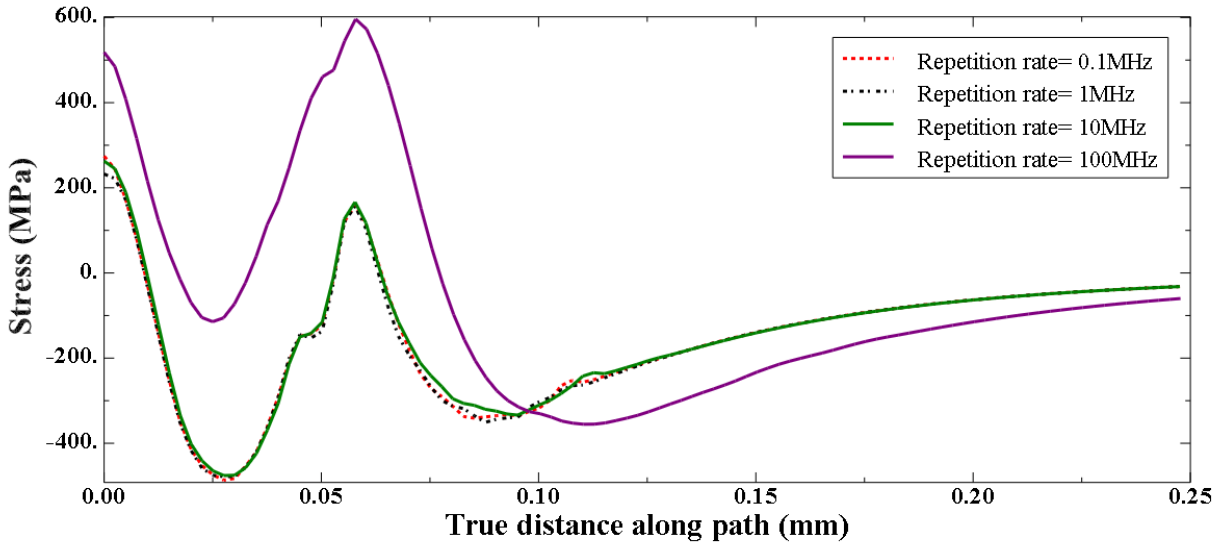


**Figure 5.2: Comparing surface residual stress distributions at repetition rates of 0.1 MHz, 1 MHz, 10 MHz and 100 MHz for a spot diameter of 0.1 mm.**

The effect of repetition rates between 10 MHz-100 MHz and after 100 MHz are studied, considering the rapid increase in peak value and affected depth of compressive stress from 10 MHz

to 100 MHz. Figures 5.3 and 5.4 shows the variation of in-depth and surface stress profiles between repetition rates from 10 MHz to 200 MHz. For repetition rate of 20 MHz, there is no time for relaxation between consecutive pressure pulses and for repetition rate of 33.3 MHz, the overlap between successive pressure pulses does not change the peak pressure and the peak compressive stress. At the repetition rates of 20 MHz and 33.3 MHz, the peak compressive stress is constant but the plastically affected depth decreases compared with the repetition rate of 10 MHz. This is due to decrease in the depth travelled by the incoming pressure wave because of the effect of active relaxation waves in depth (z) direction. The depth and peak compressive stress increase with the increase in repetition rates after 100 MHz due to the increase in peak magnitude of pressure by pulse superposition.

As shown in Figure 5.4, the peak surface tensile stress at the center decreases between repetition rates of 10 MHz and 100 MHz, and then increases after 100 MHz. The tensile stress at the center increases with the increase in peak pressure magnitude. For repetition rates of 20 MHz and 33.3 MHz, the peak magnitude remains the same as the magnitude at 10 MHz but there is no time interval between successive pulses. The continuous pressure pulse decreases the effect of relaxation waves at the center.

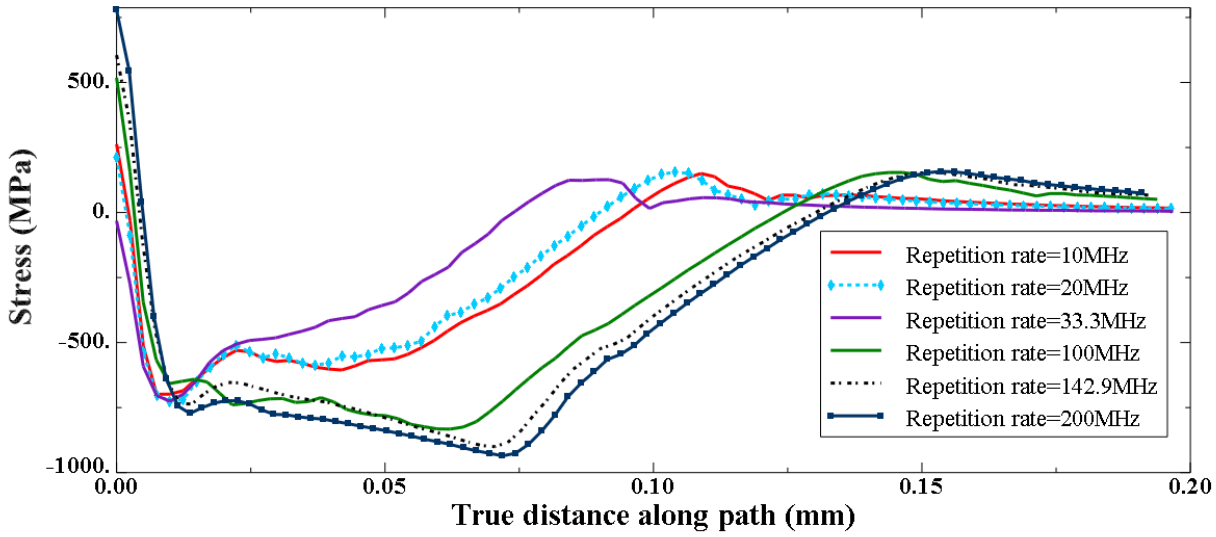


**Figure 5.3: Comparing in-depth residual stress distributions at repetition rates of 33.3 MHz, 50 MHz, 10 MHz, 100 MHz 142.9 MHz and 200 MHz for a spot diameter of 0.1 mm.**

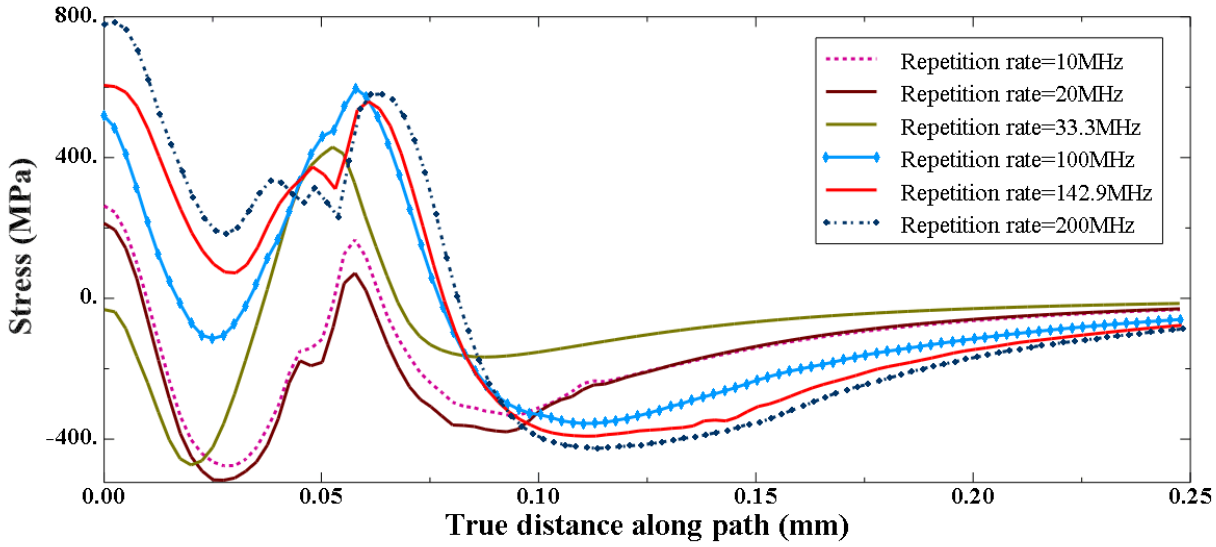


**Figure 5.4: Comparing surface residual stress distributions at repetition rates of 33.3 MHz, 20 MHz, 10 MHz, 100 MHz, 142.9 MHz and 200 MHz for a spot diameter of 0.1 mm.**

The spot diameter is increased to 1mm to study the effect of repetition rate at larger diameters of the pulse. Figure 5.5 and Figure 5.6 show the variation of in-depth and surface stress profiles at various repetition rates for spot diameter of 1 mm. The compressive stress and plastically affected depth are not significantly affected by repetition rates below 10 MHz. At high repetition rate of 100 MHz, the peak compressive stress and plastically affected depth increases abruptly because of the increase in peak magnitude of pressure due to overlapping laser pulses. Surface tensile stresses are absent for larger spots because the strength of the relaxation waves is not sufficient to cause significant reverse straining at repetition rates below 10 MHz. However, at high repetition rate of 100 MHz, the overlapping pressure pulses generate strong relaxation waves which cause tensile stresses at the center of spot.

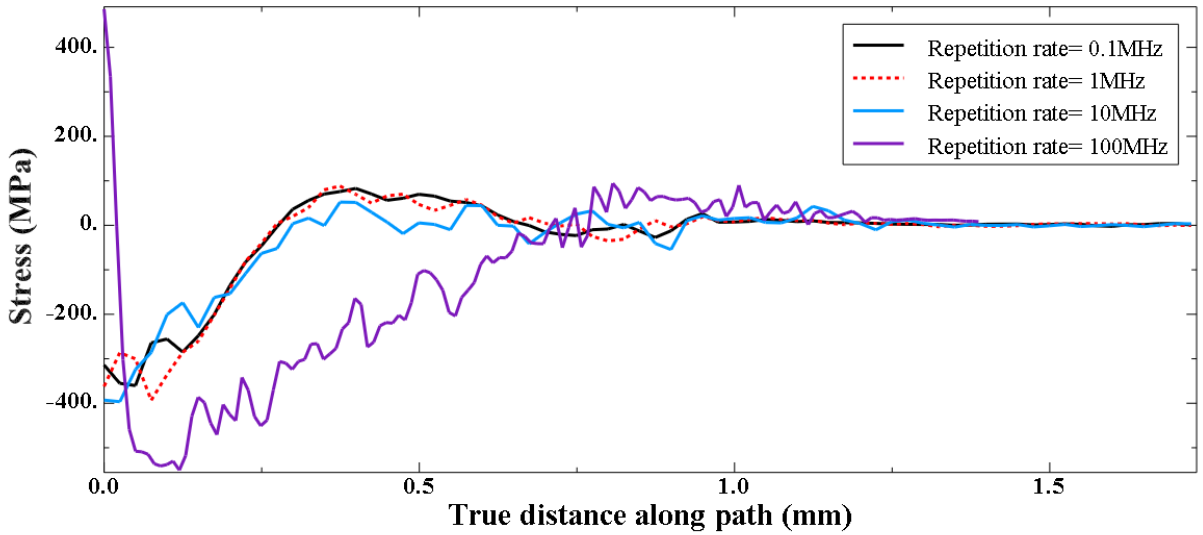


**Figure 5.5: Comparing in-depth residual stress distributions at repetition rates of 0.1 MHz, 1 MHz, 10 MHz and 100 MHz for a spot diameter of 1 mm.**

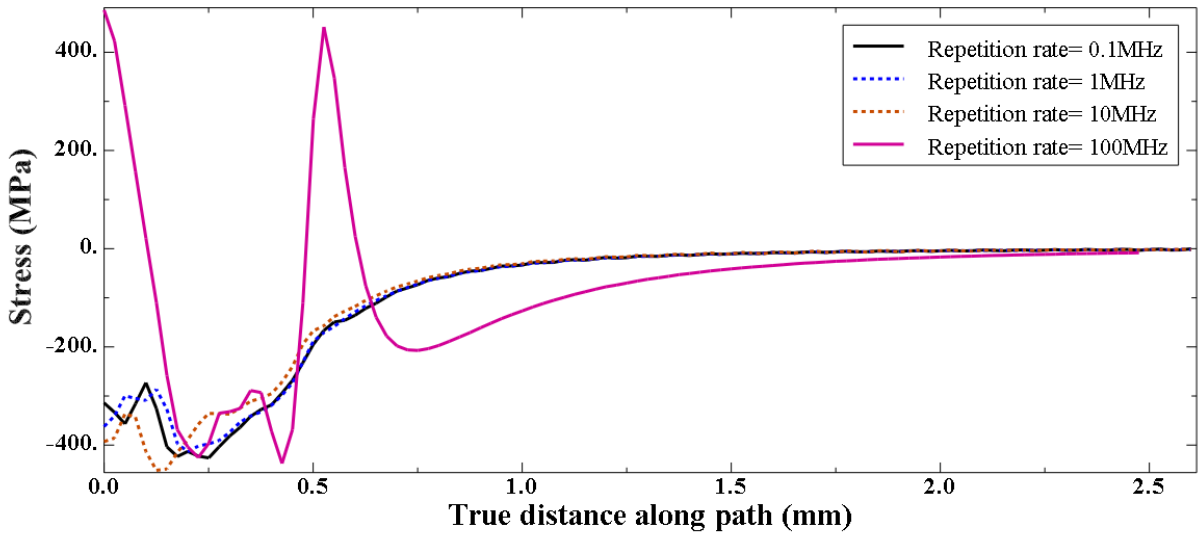


**Figure 5.6: Comparing surface residual stress distributions at repetition rates of 0.1 MHz, 1 MHz, 10 MHz and 100 MHz for a spot diameter of 1 mm.**

The diameter of the spot is decreased to 0.01 mm to study the effect of repetition rate for smaller laser pulses. Figure 5.7 and Figure 5.8 shows the variation of in-depth and surface stress profiles at various repetition rates for spot diameter of 0.01 mm. There is no significant effect of repetition rates below 10 MHz on stress profiles. The peak compressive stress and plastically affected depth are high at high repetition rate of 100 MHz due to overlapping of the pressure pulses. The surface stresses are tensile from r/2 for all repetition rates. The reverse straining has the dominant effect at the boundary of the spot instead of center because of the very small size of the affected area. However, the reverse straining decreases at high repetition rate of 100 MHz. Due to overlapping pressure pulses at 100 MHz and very small size of the spot, the metal is highly deformed affecting the metal outside the spot boundary (600 MPa residual stress outside the spot boundary).

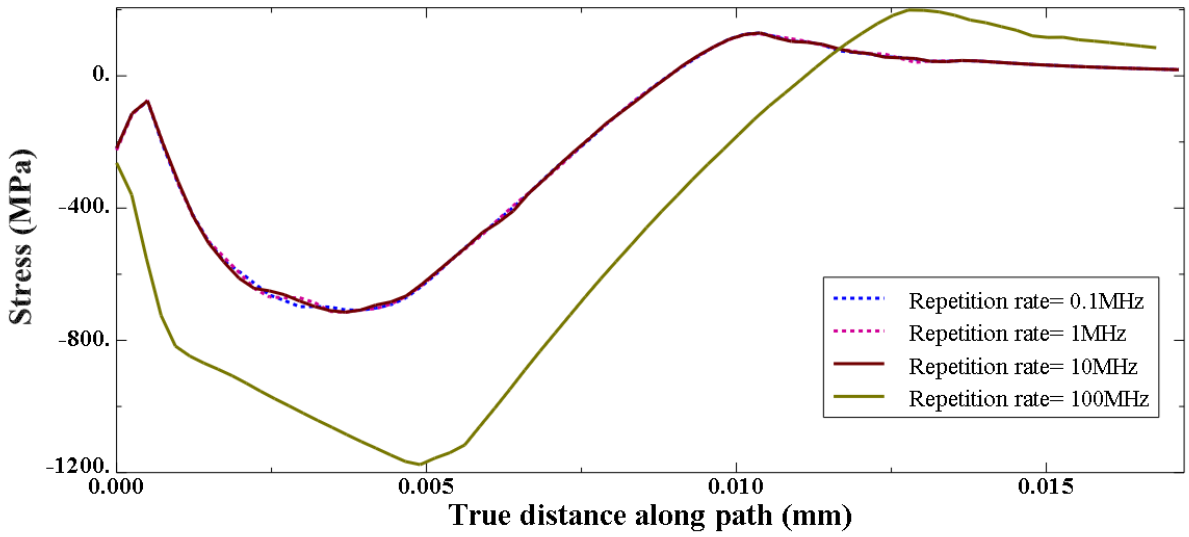


**Figure 5.7: Comparing in-depth residual stress distributions at repetition rates of 0.1 MHz, 1 MHz, 10 MHz and 100 MHz for a spot diameter of 0.01 mm.**

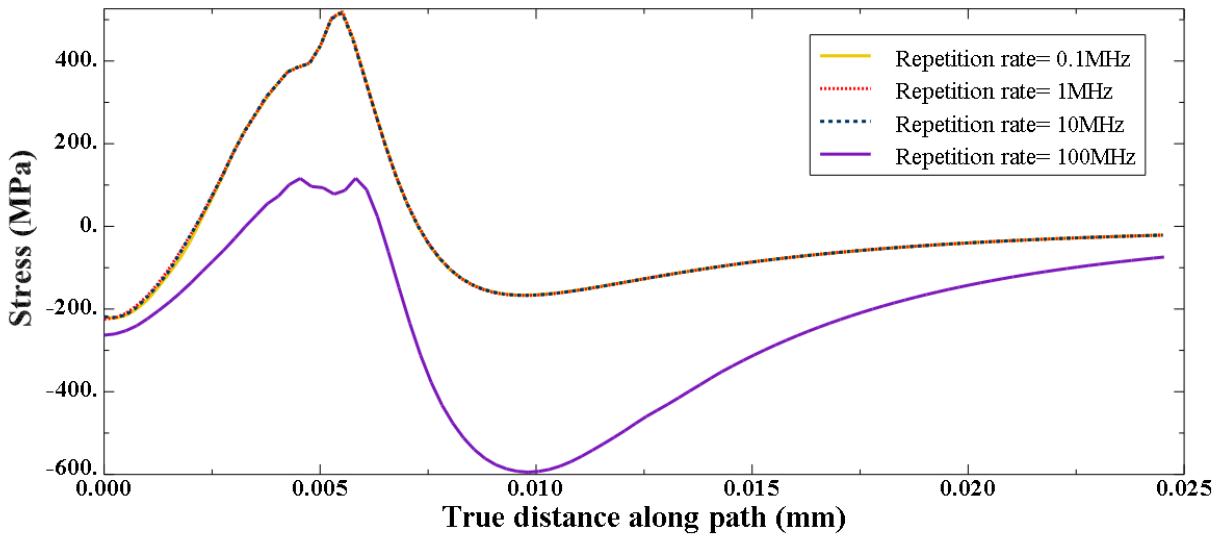


**Figure 5.8: Comparing surface residual stress distributions at repetition rates of 0.1 MHz, 1 MHz, 10 MHz and 100 MHz for a spot diameter of 0.01 mm.**

### 5.2 Effect of spot size at constant repetition rate

The effect of spot size is studied at constant repetition rate to understand the variation of peak compressive stresses. The stress profiles for different spot sizes are plotted along normalized distance. The normalized distance is defined as the ratio of true distance at point to the total distance of the path. Figure 5.9 shows the variation of in-depth profiles with spot size at constant repetition rate of 100 MHz. It should be noticed that the peak laser-induced shock wave is kept the same for all laser diameters. The peak compressive stress is high for small spot diameter of 0.01 mm. With increase in spot size, the peak compressive stress decreases due to planar relaxation of the shock wave. Therefore, small beam diameter is beneficial to induced higher compressive residual stress, but it will be slower to treat large surfaces.

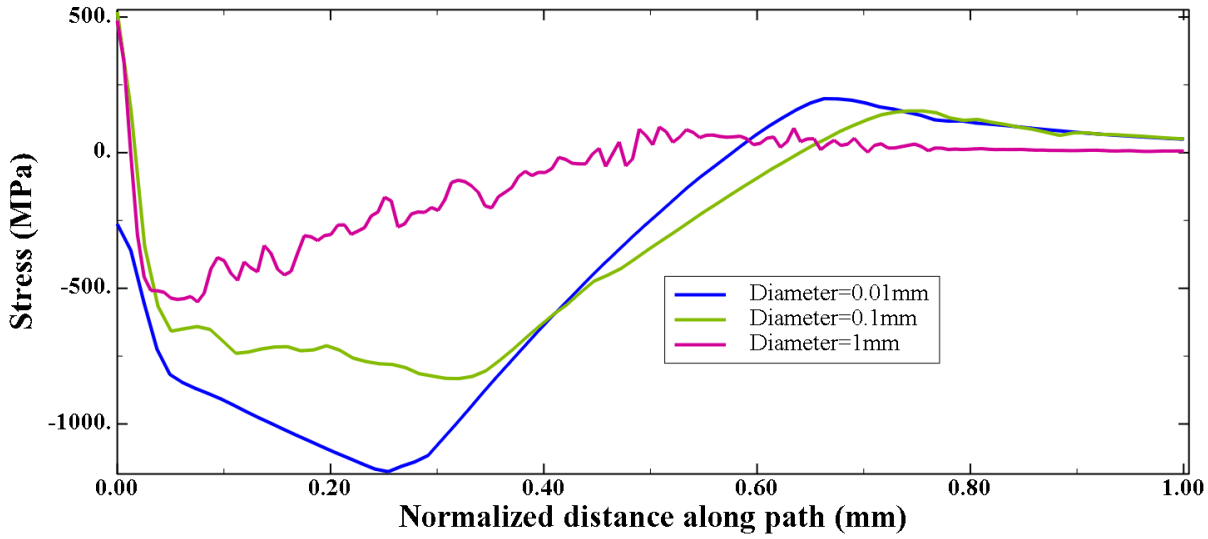


**Figure 5.9: Comparing in-depth residual stress distributions at repetition rate of 100 MHz for a spot diameter of 1 mm, 0.1 mm, 0.01 mm.**

## 5.3 Effect of overlap angle

### 5.3.1 Introduction

A scanning pattern is required to induce residual stresses in large workpieces. It is important to study the effect of different patterns as they influence the uniformity and limits of the induced residual stress. Straight line scanning patterns are the simplest ones. The line of centers of successive spots could be parallel to either x or y axes in straight patterns (sequence 1-4). A different type of patter is that the line of centers for successive spots is diagonal to x-axes (circular pattern). Hence, the change in residual stress at the center of first spot due to overlap angle is initially studied.

### 5.3.2 Straight overlap

Figures 5.10-5.12 illustrate straight overlap and stress patterns. S11 and S22 on the surface decrease at the center of first spot, after application of the second spot. On application of the second spot, the material under pressure will be under compression and the material around the spot will be under tension. Since the first spot will be in tensile region of second spot, the induced compressive stress is relaxed. The stress at center of first spot further decreases if it falls in tensile region of surrounding spots.

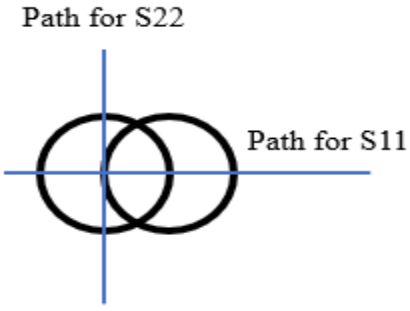


**Figure 5.10: Illustration of straight overlap**

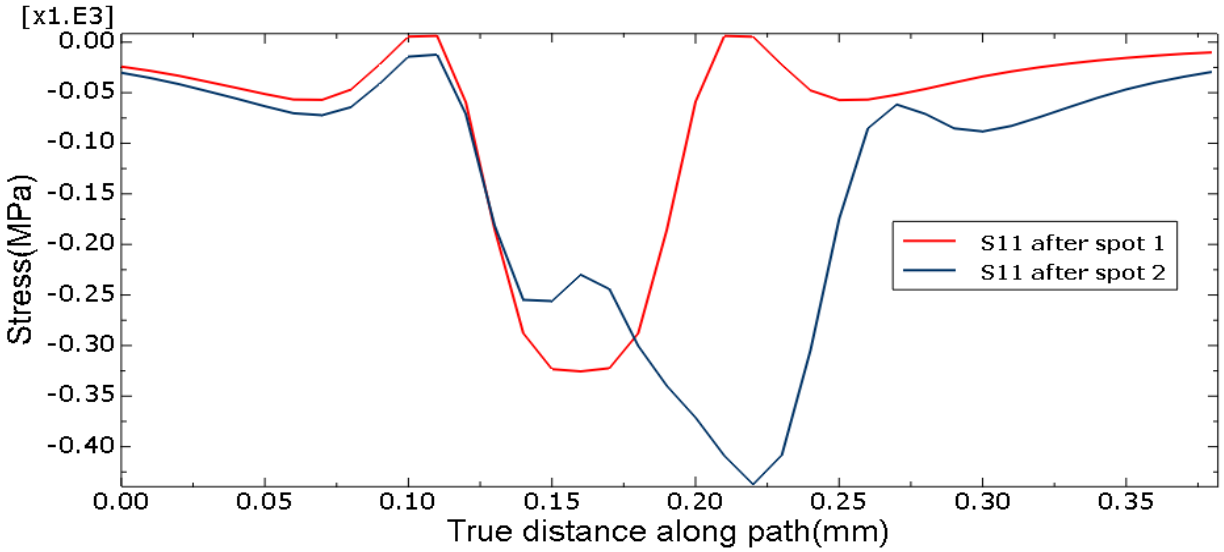


**Figure 5.11: Comparison of S11 after the first and second pulse for straight overlap**

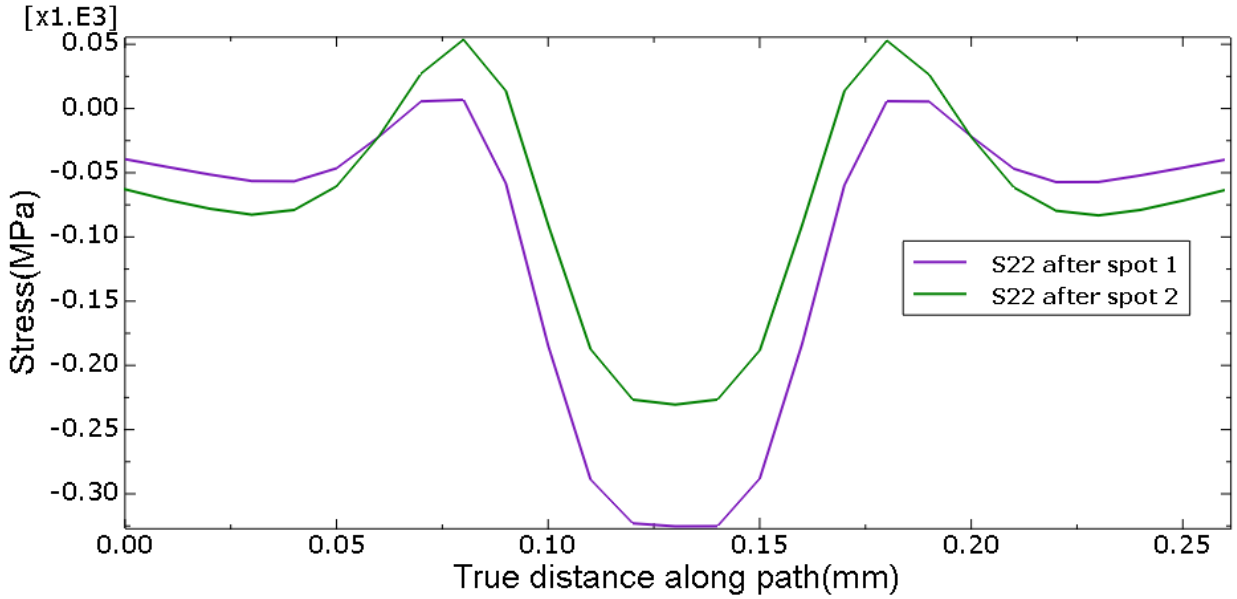


**Figure 5.12: Comparison of S22 after the first and second pulse for straight overlap**

### 5.3.3 Diagonal overlap

Figures 5.13- 5.15 illustrate diagonal overlap and stress patterns. S11 and S22 decrease after application of the second spot. The decrease in stress (100 MPa) is similar to straight overlap

but the stress profiles are different. The distribution of S11 is more uniform when there is diagonal overlap of spots. This is because the center of second spot does not lie on the path.

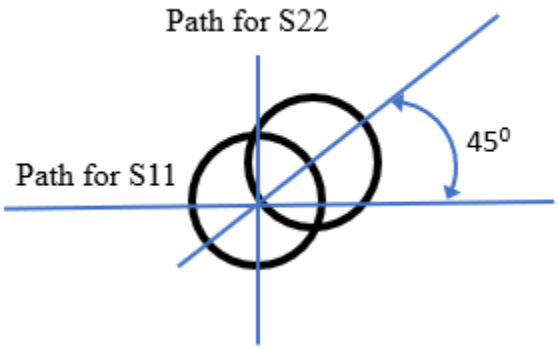


**Figure 5.13: Illustration of diagonal overlap**

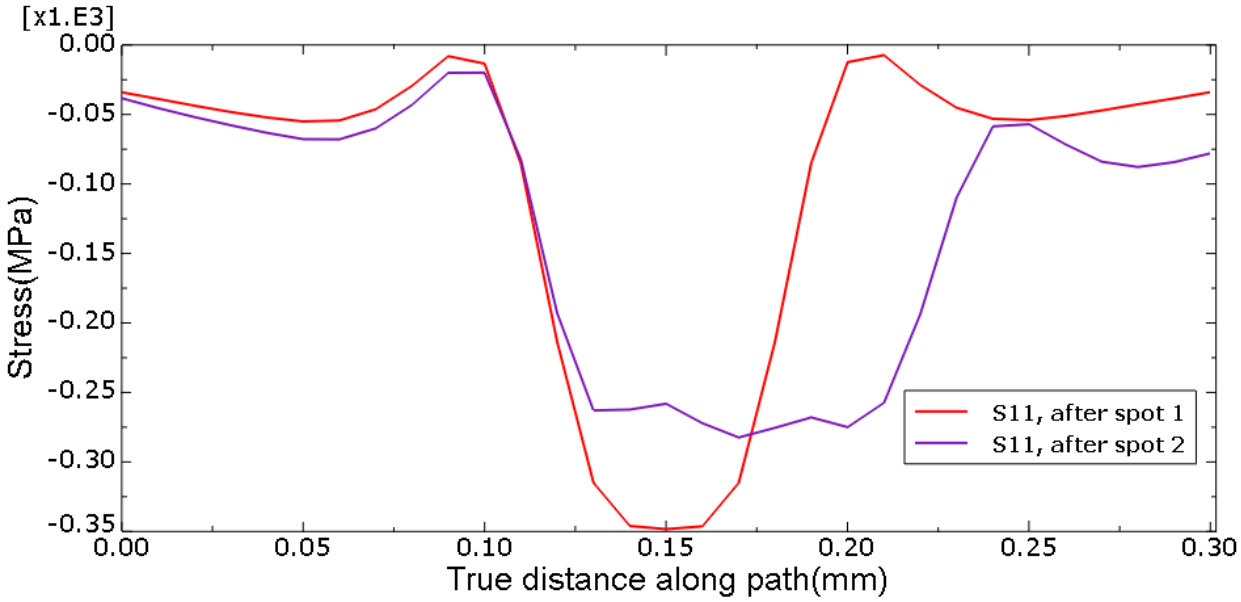


**Figure 5.14: Comparison of S11 after first and second spot for diagonal overlap**

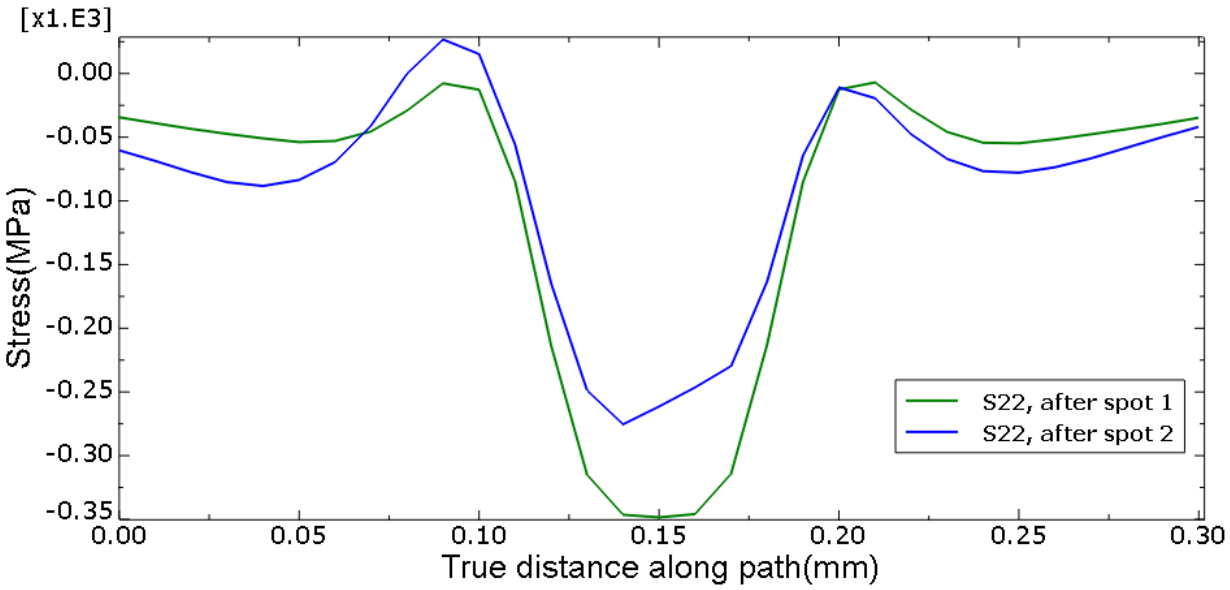


**Figure 5.15: Comparison of S11 after first and second spot for diagonal overlap**

### 5.4 Effect of sequence

The different effects of different overlap manners inspire the design of different scanning patterns. A pattern is comprised of numerous straight and diagonal overlaps between successive laser pulses. The effect of pattern is studied first using 25 pulses for sequence 1 and 2 (described in Section 4.3), 23 pulses for sequences 3 and 4 and 19 pulses for circular pattern at repetition rate of 0.1 MHz. The stress profiles for the 5 patterns are plotted across 4 paths. To eliminate the edge effect, the 1 mm X 1 mm central area of the processed region is only considered to determine limits and non-uniformity of residual stresses.

#### 5.4.1 Paths

In a sequence, there will be complex overlap of successive spots in x and y directions which is repeated. To study the distribution of residual stress, paths are taken such that different

interactions between adjacent spots are covered. Figure 5.16 shows the interaction of spots in x and y directions for sequences 1 and 2.

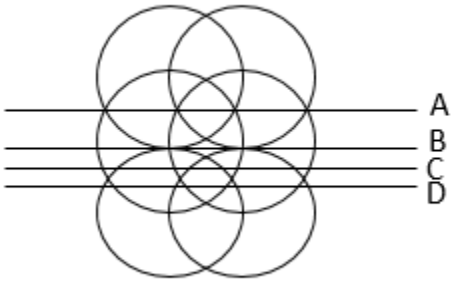


**Figure 5.16: Interaction of adjacent spots for sequence 1 and 2**

Four paths are chosen to study the residual stress distributions. Path b is taken at the center of processed area. Paths a and d are taken on either side of path b at a distance of 0.25 mm. Path c is taken at a distance of 0.125 mm from path b. Figure 5.17 shows different paths at center row of laser shots in processed area of the workpiece. The interaction patterns vary for sequence 3, sequence 4 and circular pattern. But to compare the distributions, residual stresses are studied at the same paths. Paths e, f, g and h are considered in vertical direction to plot S22. Path f passes through the center of processed area. Paths e and h are on either of path f at a distance of 0.25 mm. Path g is taken at a distance of 0.125 mm right from path f.

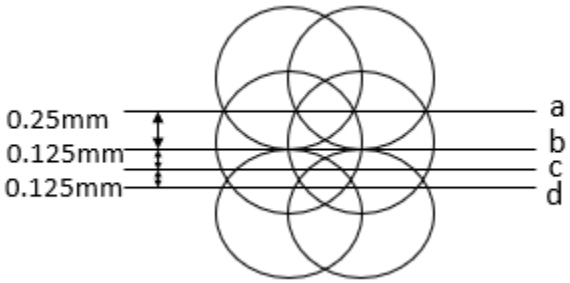

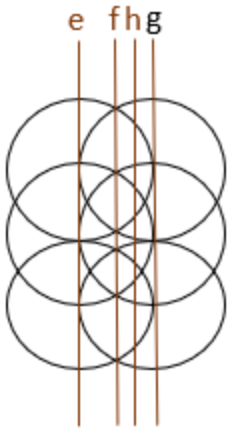


**Figure 5.17: Paths for studying residual stress distribution**

### 5.4.2 Effect of pattern at repetition rate of 0.1MHz

The material is completely relaxed before the subsequent laser spot is applied at a repetition rate of 0.1 MHz. Hence, the residual stresses are affected only by the pattern of laser shock application. Figure 5.18 shows the contour plot for sequence 1 along with the paths. Figures 5.19-5.28 show the surface residual stress profiles (S11 and S22) for all the sequences at a repetition rate of 0.1 MHz. Table 3 summarizes the upper and lower limits and non-uniformity of S11 and S22 for all sequences at a repetition rate of 0.1 MHz.

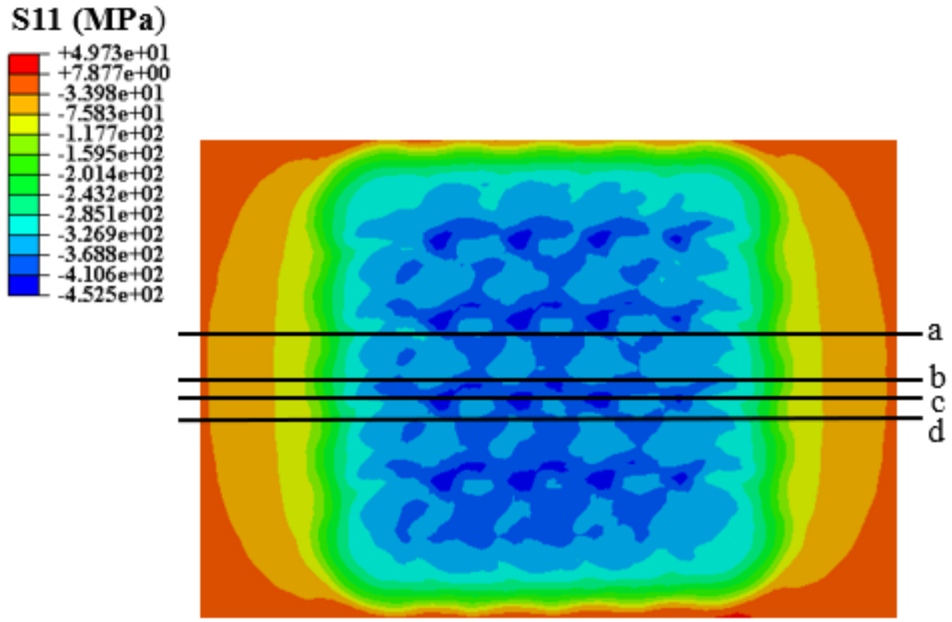


**Figure 5.18: Contour plot (S11) for sequence 1**

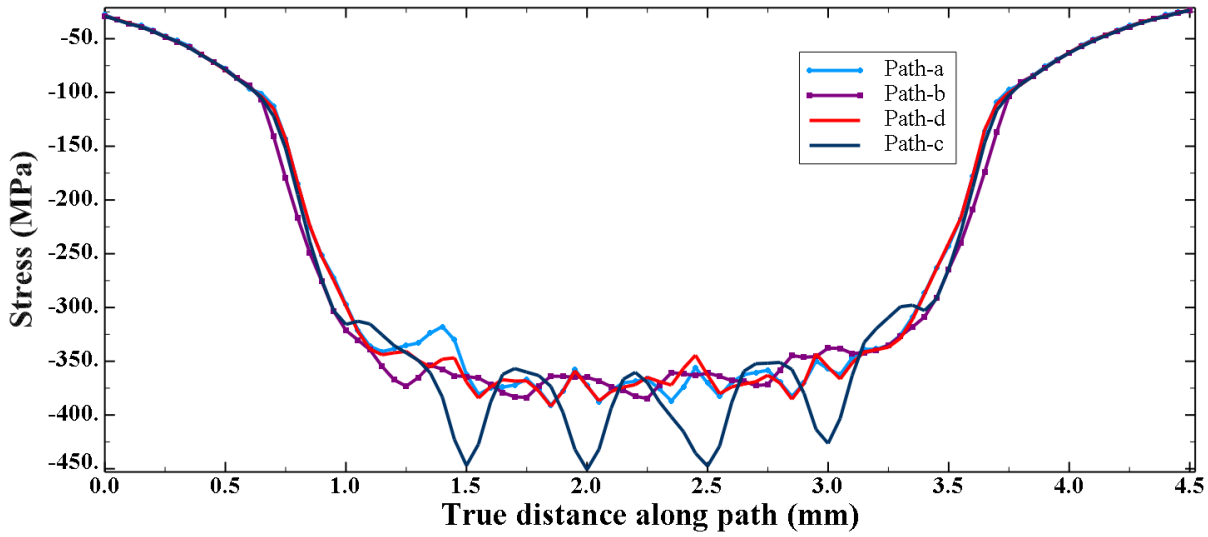


**Figure 5.19: S11 for sequence 1 at repetition rate of 0.1 MHz (5X5)**

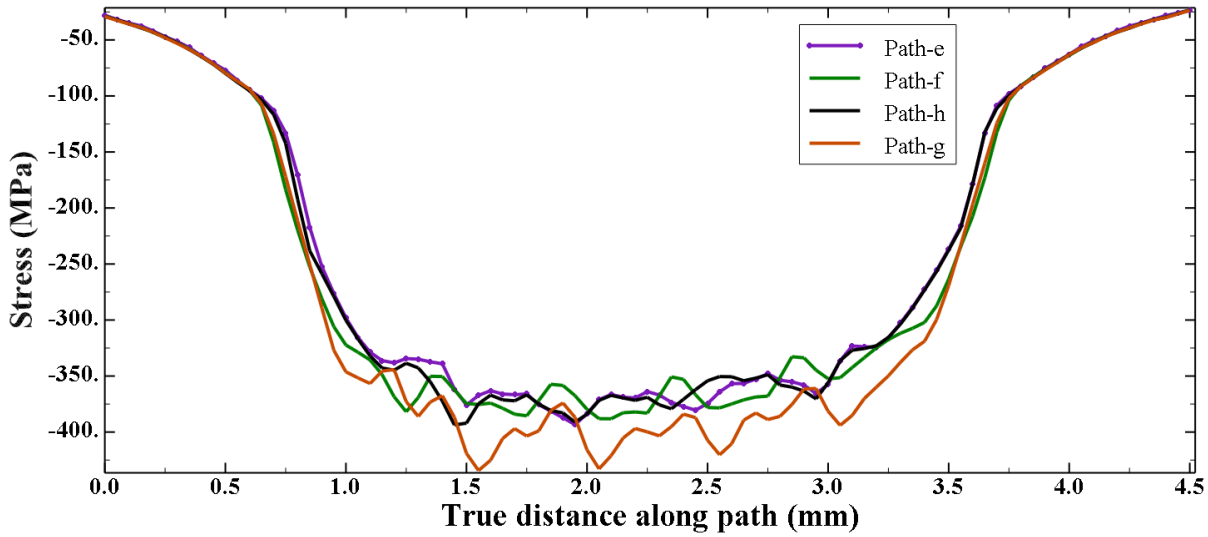


**Figure 5.20: S22 for sequence 1 at repetition rate of 0.1 MHz (5X5)**

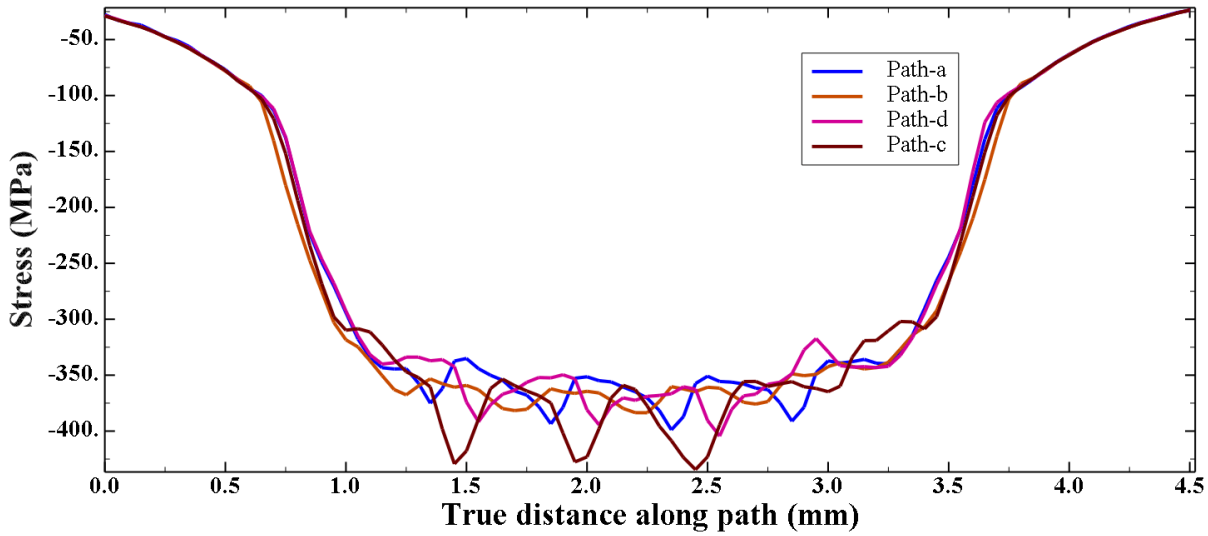


**Figure 5.21: S11 for sequence 2 at repetition rate of 0.1 MHz (5X5)**

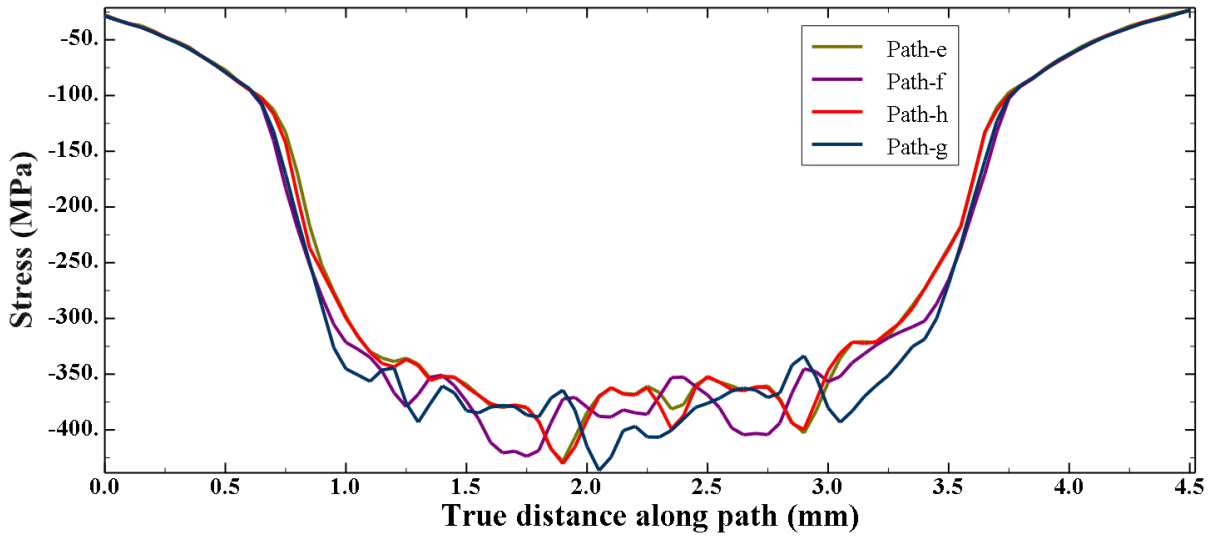


**Figure 5.22: S22 for sequence 2 at repetition rate of 0.1 MHz (5X5)**

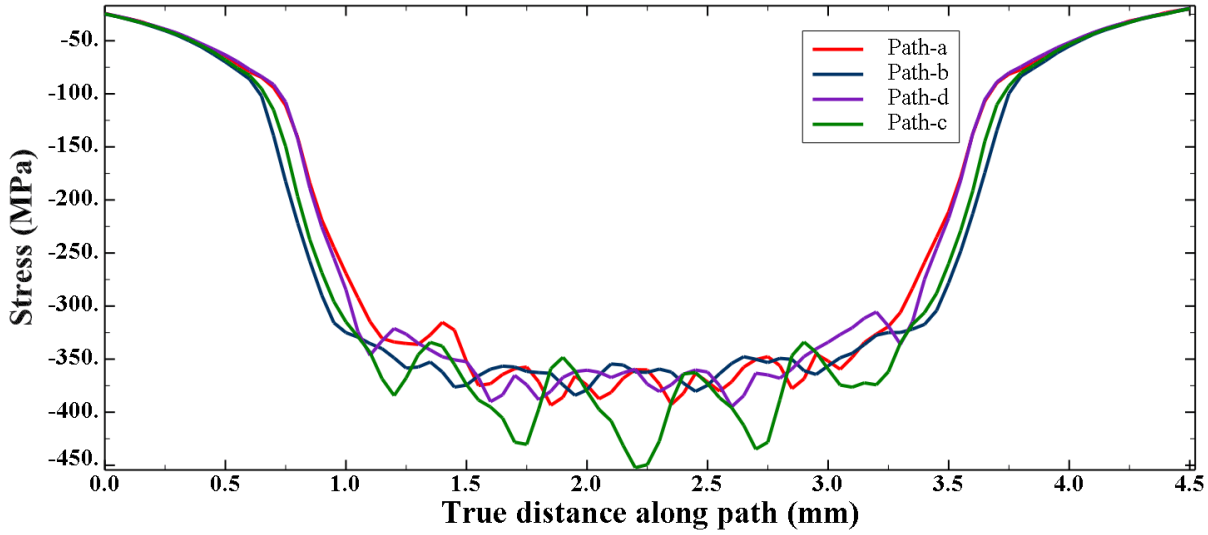


**Figure 5.23: S11 for sequence 3 at repetition rate of 0.1 MHz**

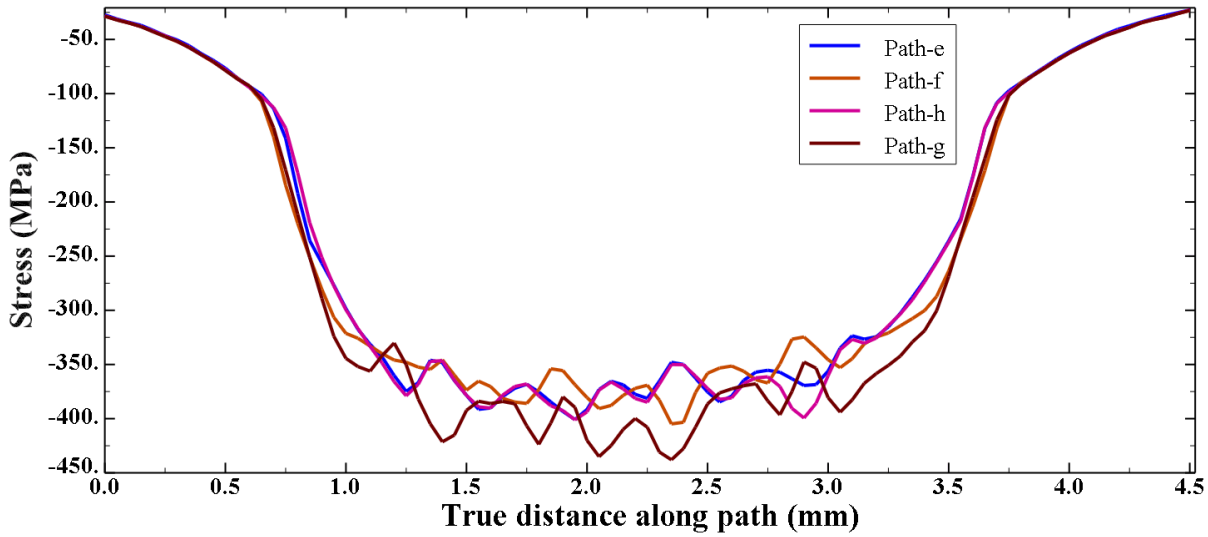


**Figure 5.24: S22 for sequence 3 at repetition rate of 0.1 MHz**

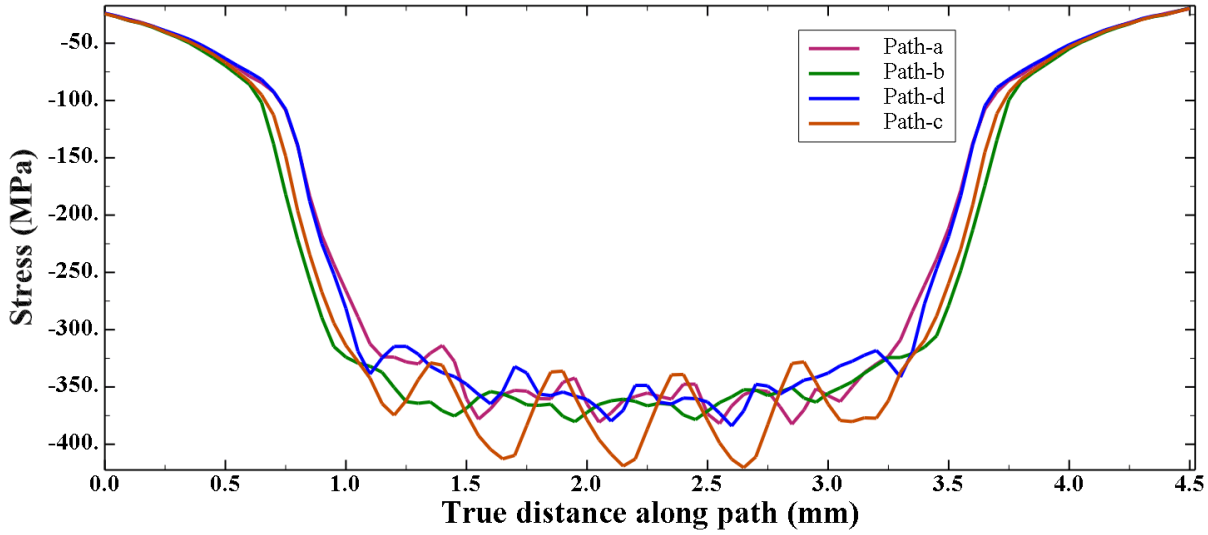


**Figure 5.25: S11 for sequence 4 at repetition rate of 0.1 MHz**

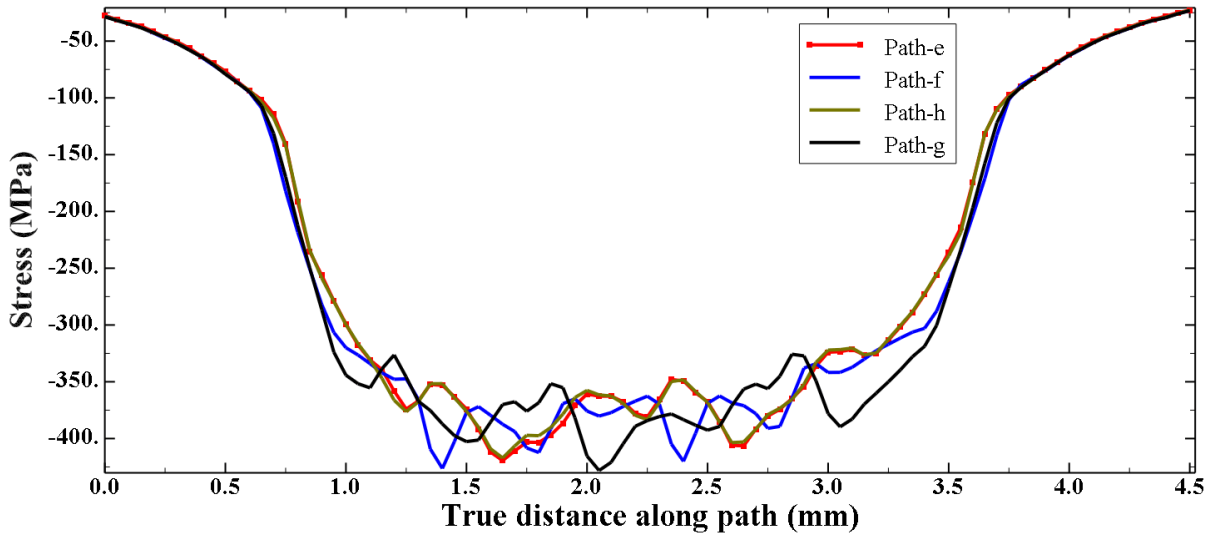


**Figure 5.26: S22 for sequence 4 at repetition rate of 0.1 MHz**

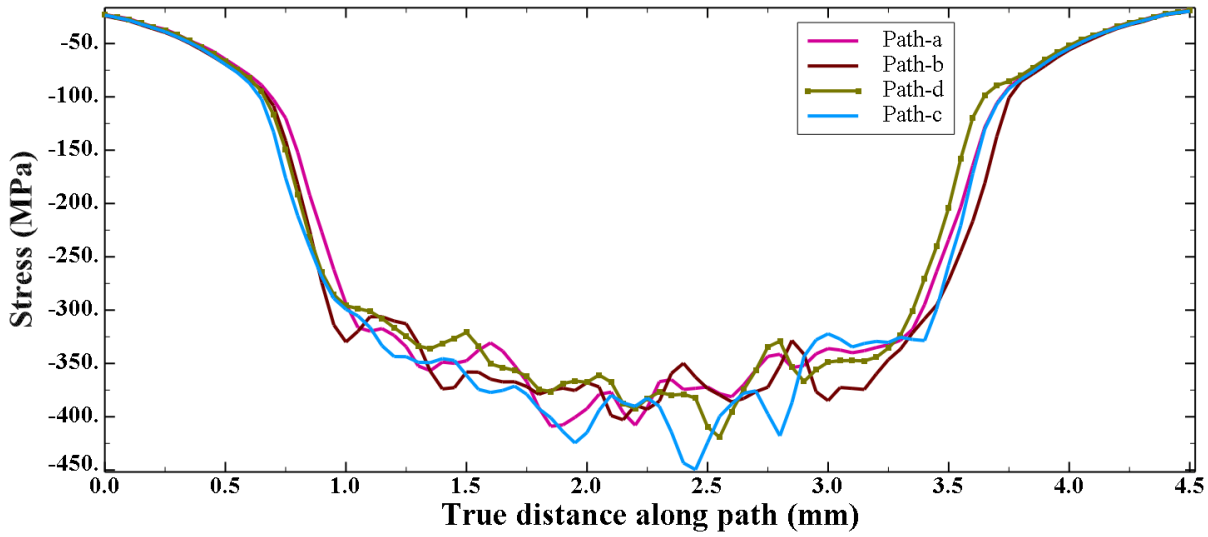


**Figure 5.27: S11 for circular sequence at repetition rate of 0.1 MHz**

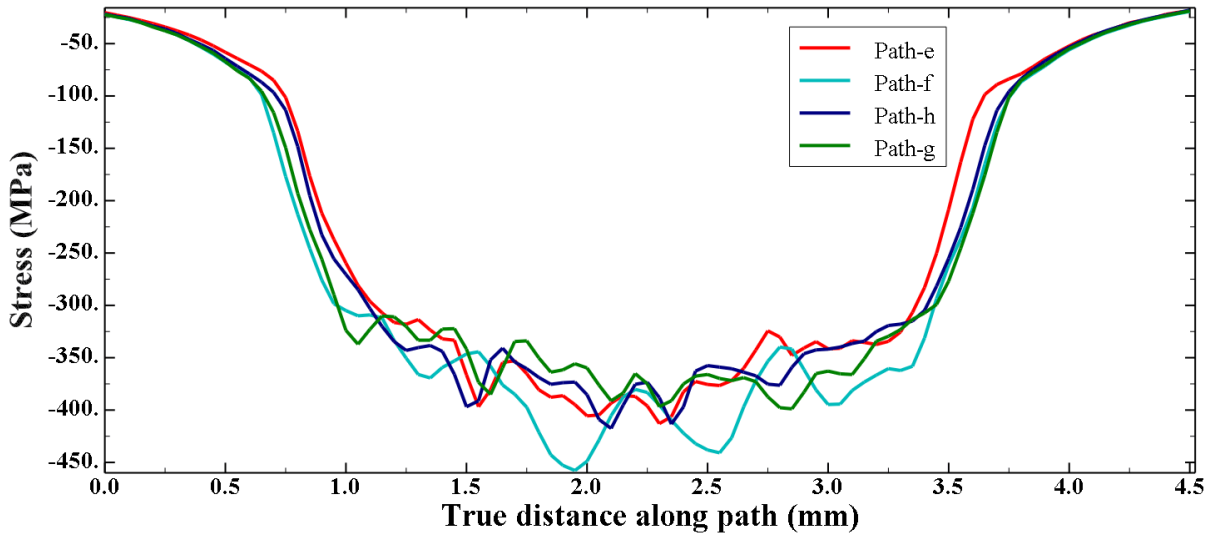


**Figure 5.28: S22 for circular sequence at repetition rate of 0.1 MHz**

**Table 3. S11 and S22 for different sequences at repetition rate of 0.1 MHz**

| Sequence | S11 limits (Range) MPa | S22 limits (Range) MPa |
|---|---|---|
| Sequence 1 | 350-450 (100) | 350-430 (80) |
| Sequence 2 | 350-435 (85) | 350-435 (85) |
| Sequence 3 | 350-450 (100) | 350-435 (85) |
| Sequence 4 | 340-420 (80) | 350-430 (80) |
| circular | 350-450 (100) | 330-450 (120) |

From table 3, the minimum residual stress on the surface is constant for all sequences. The non-uniformity and limits of residual stress in y-direction (S22) is almost the same for sequences 1, 2, 3 and 4 since it is perpendicular to the laser advancement. The non-uniformity in S11 is higher than S22 for sequences 1 and 3. The non-uniformity in S22 is the highest for circular pattern.

The interaction of a laser spot with spots in same row and spots in other row differs significantly giving raise to different limits and non-uniformities to residual stresses in x and y directions. The effect of pattern is not significant at low repetition rates which allow complete relaxation of residual stresses before application of subsequent laser spots. Though, the pattern is affecting the profile, the limits and non-uniformity is not highly affected.

### 5.4.3 Effect of pattern at repetition rate of 1 MHz

The repetition rate is increased to 1 MHz to study the effect of repetition rate on sequence of pulse application. The material is partially relaxed before the subsequent laser spot is applied at a repetition rate of 1 MHz. It is assumed that size of workpiece is very large, and it takes longer time to come back to the first spot of subsequent row in a pattern. So, the material is allowed to relax completely for time period of $10^{-5}$ s after each row of laser spots. The relaxation time is not given after each ring of spots in circular pattern. Figures 5.29 and 5.30 show the variation of surface residual stress profiles (S11 and S22) for sequence 1 at different paths at a repetition rate of 1 MHz. Table 4 summarizes the upper and lower limits and non-uniformity of S11 and S22 for all sequences at a repetition rate of 1 MHz.

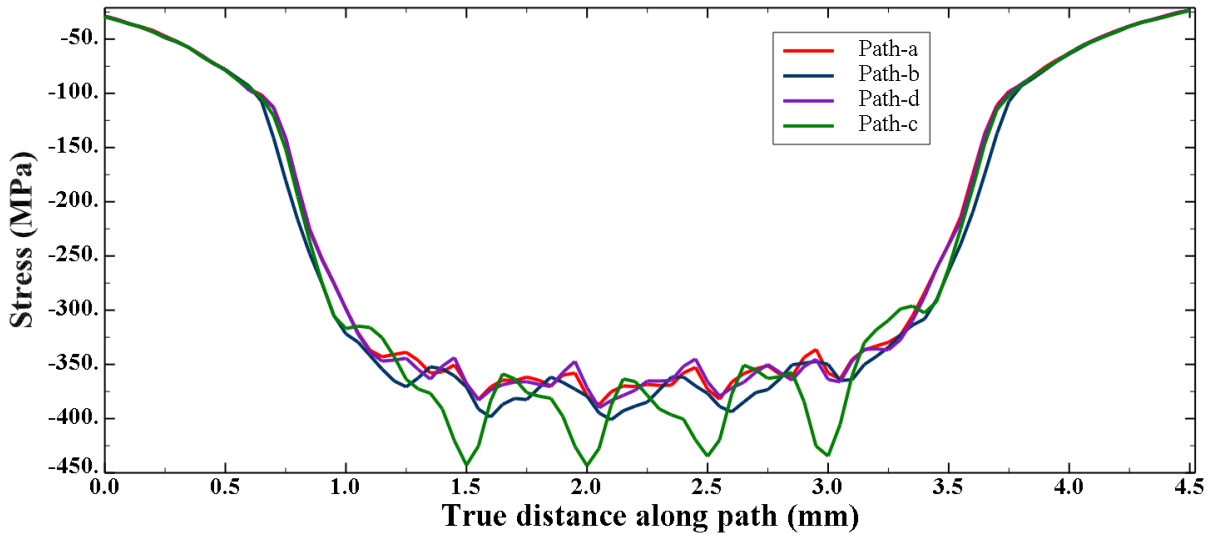


**Figure 5.29: Comparison of S11 for sequence 1 at repetition rate of 1 MHz**

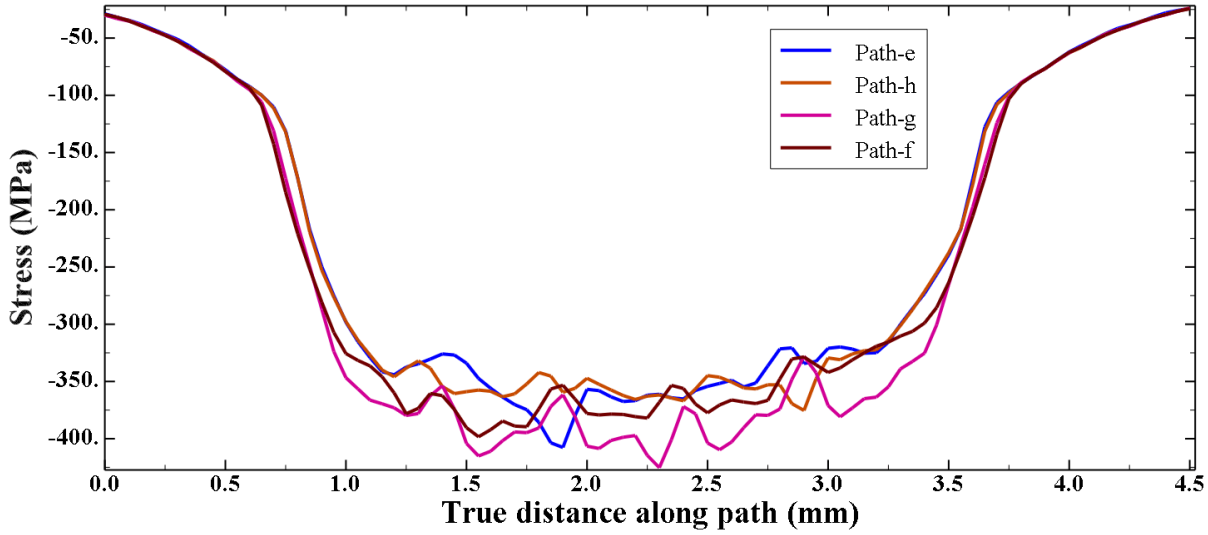


**Figure 5.30: Comparison of S22 for sequence 1 at repetition rate of 1 MHz**

**Table 4. Comparing limits of S11 and S22 for different sequences at repetition rate of 1 MHz**

| Sequence | S11 limits (Range) MPa | S22 limits (Range) MPa |
|---|---|---|
| Sequence 1 | 345-445 (100) | 340-425 (85) |
| Sequence 2 | 340-430 (90) | 355-430 (75) |
| Sequence 3 | 355-430 (75) | 350-430 (80) |
| Sequence 4 | 340-410 (70) | 345-435 (90) |
| circular | 345-460 (115) | 330-460 (130) |

From table 4, the non-uniformity in x and y directions for circular pattern has increased slightly. For all other patterns, the non-uniformity in S11 and S22 does not change significantly. The stress relaxation slightly affects the limits of S11 and S22 for all the patterns. There is no significant difference in stress profiles among patterns except for the circular pattern. At low repetition rates below 0.1 MHz, the reduce in stress at a location will be only due to tensile stresses of surrounding pulses. But at high repetition rates above 0.1 MHz, the stress drop is attributed to the interaction of relaxation waves with incoming pressure pulses and tensile region of surrounding pulses. The high non-uniformity for the circular pattern is attributed to the stress drop at the center pulse because of the immediate irradiation of 6 pulses in the second ring. The active relaxation waves at the center affects the 6 incoming pressure pulses. For sequences 1-4, predominant stress drops at a pulse location occurs only because of immediate pulses in a row. By the time the pulses in the next row are irradiated, the material is completely relaxed at the previous row eliminating the stress drop due to interaction of relaxation waves with incoming pressure pulse.

### 5.4.4 Effect of pattern at repetition rate of 10 MHz

The material is partially relaxed before the subsequent laser spot is applied at a repetition rate of 10 MHz. The material can relax completely for a period of $10^{-5}$ s after each row of laser spots for sequences 1, 2, 3 and 4. It is not allowed to relax for circular pattern. Figures 5.31 and 5.32 show the variation of surface residual stress profiles (S11 and S22) for sequence 1 at different paths at a repetition rate of 10 MHz. Table 5 summarizes the upper and lower limits and non-uniformity of S11 and S22 for all sequences at a repetition rate of 10 MHz.

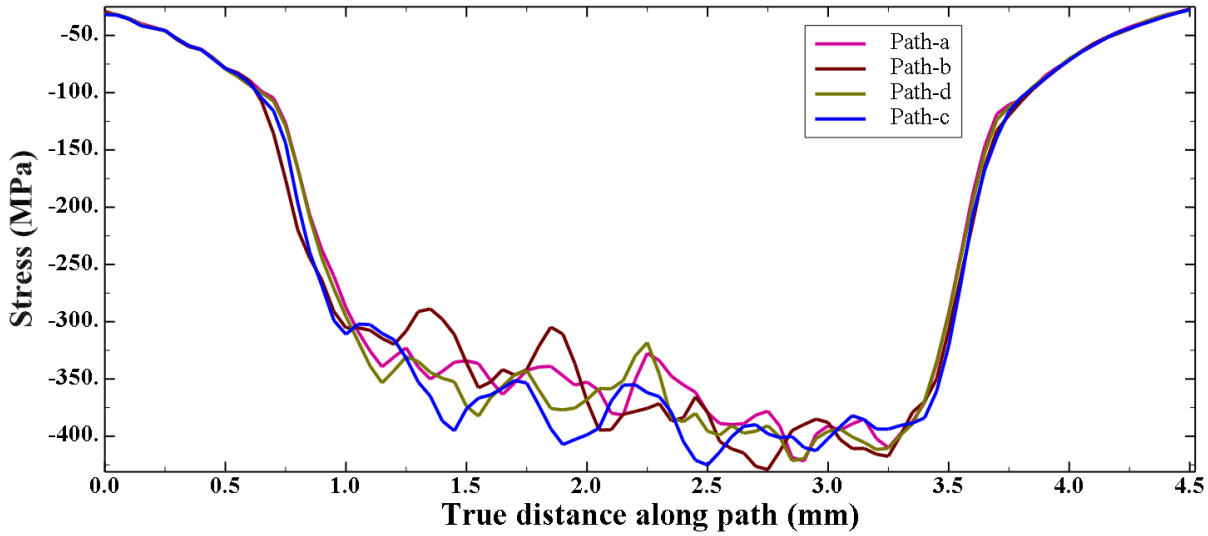


**Figure 5.31: Comparison of S11 for sequence 1 at repetition rate of 10 MHz**

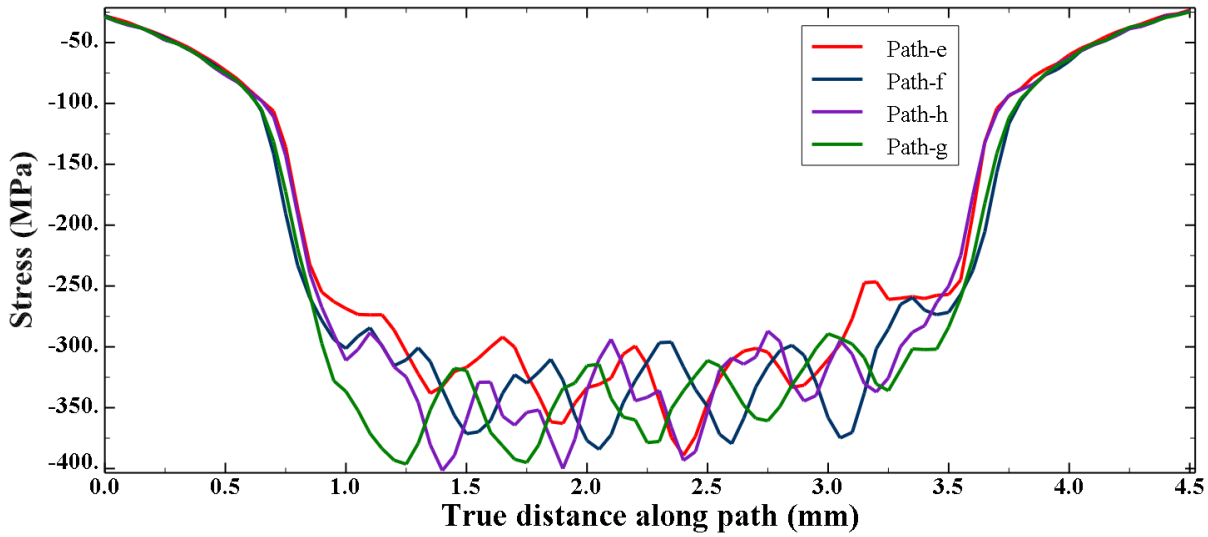


**Figure 5.32: Comparison of S22 for sequence 1 at repetition rate of 10 MHz**

**Table 5. Comparing limits of S11 and S22 for different sequences at repetition rate of 10 MHz**

| Sequence | S11 limits (Range) MPa | S22 limits (Range) MPa |
|---|---|---|
| Sequence 1 | 315-425(110) | 290-400(110) |
| Sequence 2 | 340-425(85) | 310-410(100) |
| Sequence 3 | 325-425(100) | 300-405(105) |
| Sequence 4 | 320-400(80) | 310-400(90) |
| circular | 215-360(145) | 250-365(115) |

Since the scan path is x-direction and the material is allowed to relax after each row, the non-uniformity in y-direction has increased for all patterns. The lower and upper limits of residual stresses for all patterns have decreased because of the active relaxation waves affecting incoming

pressure pulses. The effect of active relaxation waves increases because of the decrease in time gap between successive pulses. The stress profiles are different but there is not significant difference in limits and non-uniformity among patterns 1-4. The non-uniformity is the highest for circular pattern. This is because of the relaxation of residual stresses at the center pulse due to 6 immediate pulses in the second ring giving raise to high non-uniformity in x and y directions.

### 5.4.4 Effect of pattern at repetition rate of 20 MHz

At 20 MHz, immediately after the pressure becomes zero at a spot, the successive spot is applied in the pattern. So, strong relaxation waves are active in and around the new laser spot. The material is allowed to relax completely for time period of $10^{-5}$ s after each row of laser for sequences 1-4. It is not allowed to relax for circular pattern. Figures 5.33 and 5.34 show the variation of surface residual stress profiles (S11 and S22) for sequence 1 at different paths at a repetition rate of 20 MHz. Table 6 summarizes the upper and lower limits and non-uniformity of S11 and S22 for all sequences at a repetition rate of 20 MHz.

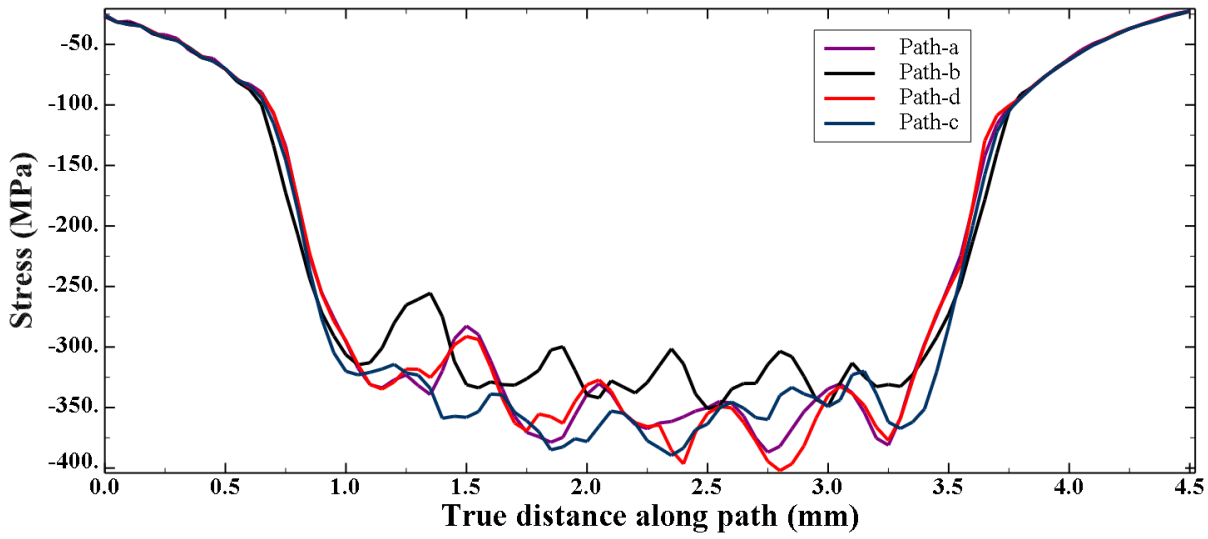


**Figure 5.33: Comparison of S11 for sequence 1 at repetition rate of 20 MHz**

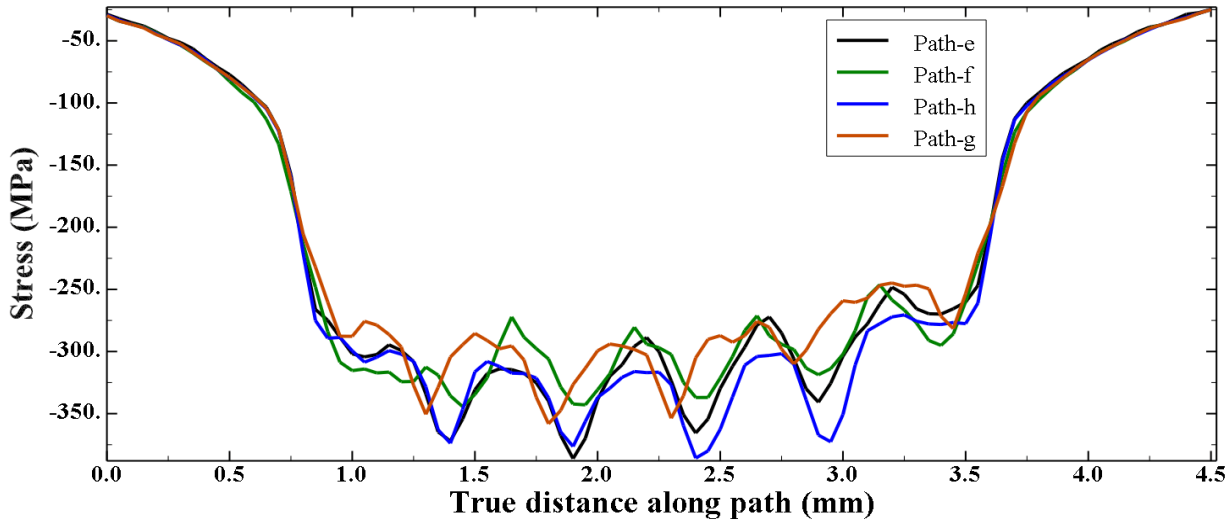


**Figure 5.34: Comparison of S22 for sequence 1 at repetition rate of 20 MHz**

**Table 6. Comparing limits of S11 and S22 for different sequences at repetition rate of 20 MHz**

| Sequence | S11 limits (Range) MPa | S22 limits (Range) MPa |
|---|---|---|
| Sequence 1 | 300-400(100) | 270-385(115) |
| Sequence 2 | 300-405(105) | 280-380(100) |
| Sequence 3 | 280-385(105) | 245-390(145) |
| Sequence 4 | 290-410(120) | 260-390(130) |
| circular | 225-370(145) | 145-390(245) |

The effect of relaxation waves on incoming pressure pulses further increases. The non-uniformity in S11 and S22 has greatly increased and limits of residual stresses have decreased for all patterns due to the active relaxation waves. The stress profiles are different but there is not

significant difference in limits and non-uniformity among patterns 1-4. The non-uniformity is highest for circular pattern because of the 6 pulses in the second ring.

From the stress profiles at different repetition rates, it can be concluded that with increase in repetition rate, the residual stress decreases and non-uniformity in S11 and S22 increases. Hence, to use high repetition rate lasers, an optimized sequence is needed which is not affected by repetition rate.

### 5.4.5 Residual stress distributions without relaxation after each row

In order to design an optimum sequence, the feasibility of using 5X5 patterns is tested. If the whole workpiece is scanned using 5X5 patterns, relaxation time after each row of laser spots is not given. The sequences 1, 2, 3 and 4 are checked at repetition rate of 20 MHz. Figure 5.35 and 5.36 shows the variation of residual stresses in x and y directions respectively at the center of sequence.

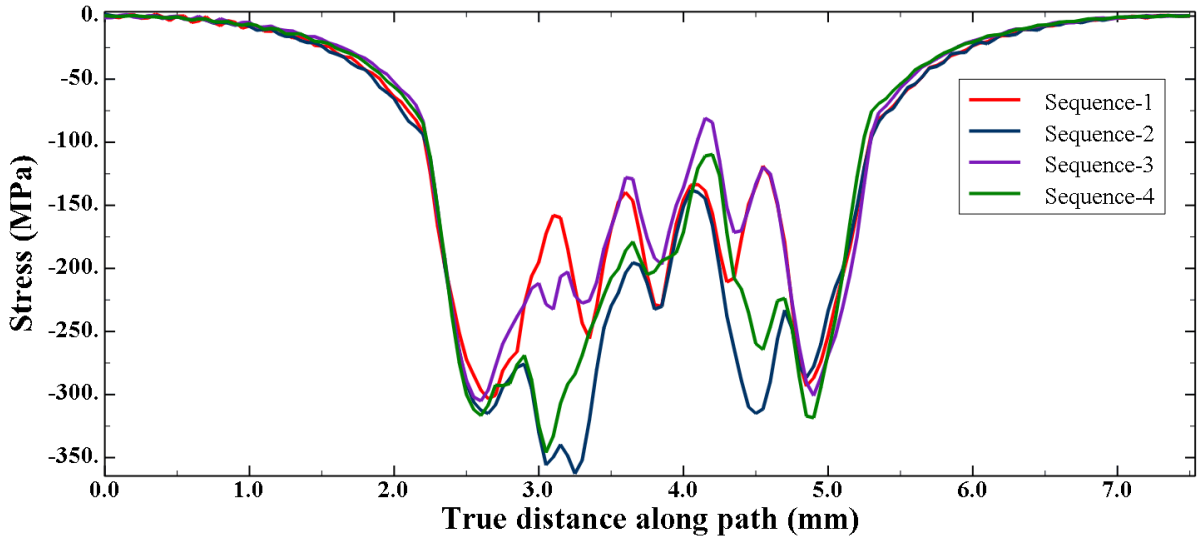


**Figure 5.35: Distribution of S11 at repetition rate of 20 MHz for different sequences without relaxation after each row**

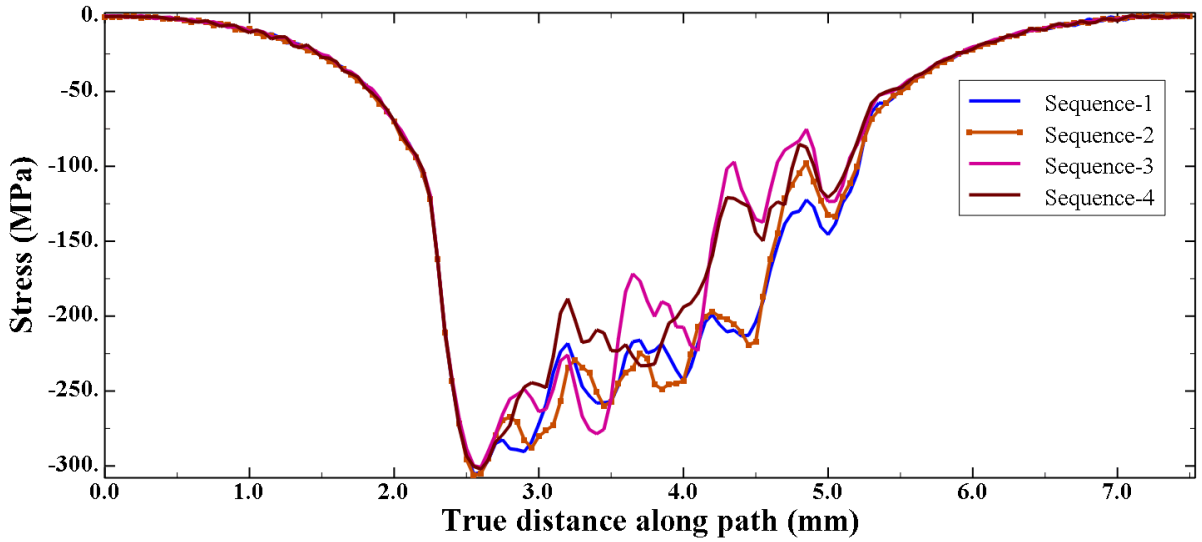


**Figure 5.36: Distribution of S22 at repetition rate of 20 MHz for different sequences without relaxation after each row**

From Figure 5.35 and 5.36, the non-uniformity increases compared to non-uniformity of sequences 1-4 at repetition rate of 20 MHz, and the residual stress decreases highly due to the interaction of active relaxation waves and incoming pressure pulse. Hence, the scanning of workpiece using 5X5 patterns is not beneficial at high repetition rates.

### 5.5 8X8 pattern

To overcome the edge effect on the calculated residual stresses, 8X8 patterns are studied. The residual stress distributions are analyzed in the central part (1.5 mm X 1.5 mm) of processed area. The distributions are taken along 5 paths in x- direction and 5 paths in y-direction. Figure 5.37 and Figure 5.38 show paths along which residual stresses are plotted in x and y directions respectively. The distance between successive paths is 0.125 mm. Path c and h pass through the center of the processed area.

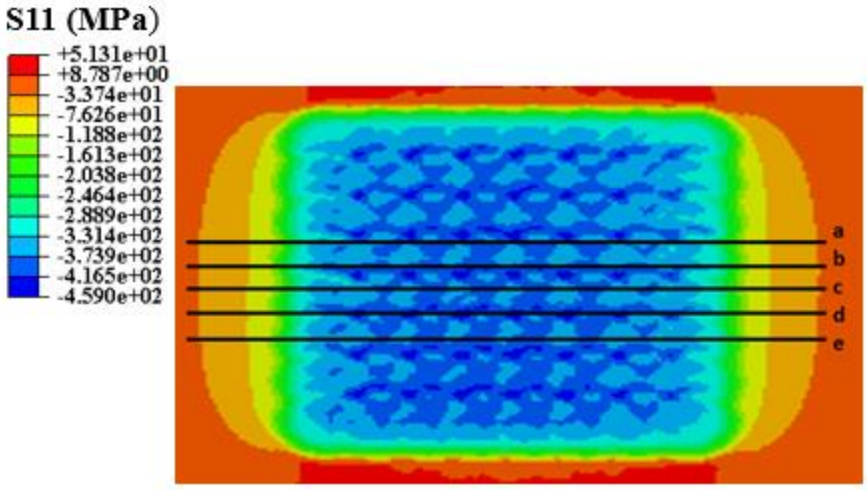


**Figure 5.37: Paths along which S11 is plotted**

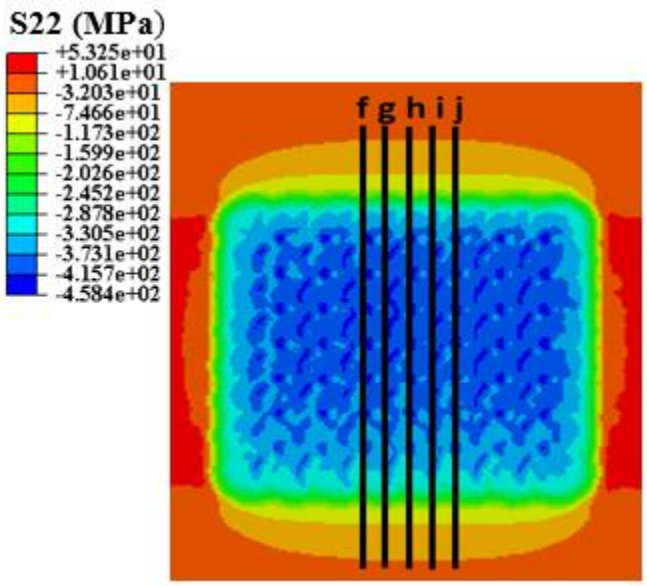


**Figure 5.38: Paths along which S22 is plotted**

Figures 5.39-5.46 show the distributions of S11 and S22 for sequence 1 at repetition rates of 0.1 MHz, 1 MHz, 10 MHz, 20 MHz respectively. Figures 5.47-5.54 show the distributions of S11 and S22 for zigzag pattern 1 at repetition rates of 0.1 MHz, 1 MHz, 10 MHz, 20 MHz respectively. Figures 5.55-5.62 show the distributions of S11 and S22 for zigzag pattern 2 at

repetition rates of 0.1 MHz, 1 MHz, 10 MHz, 20 MHz respectively. Table 7 summarizes the maximum, minimum, average, range and standard deviation of residual stresses induced at different repetition rates for sequence 1 and two zig zag patterns of sequence 1 in the center (1.5 mm X 1.5 mm) area.

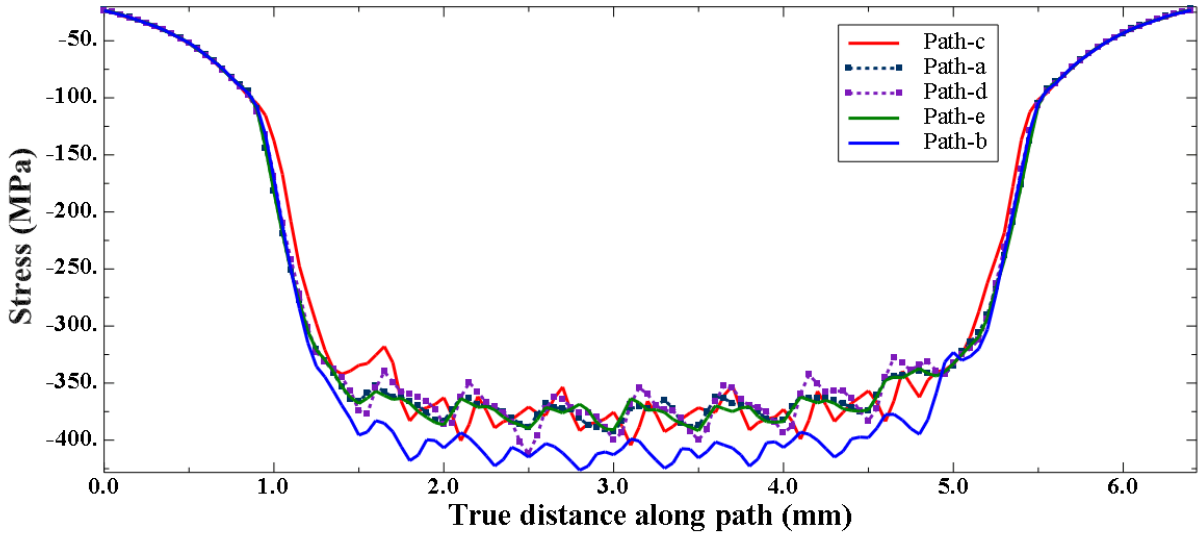


**Figure 5.39: S11 for sequence 1 at repetition rate of 0.1 MHz (8X8)**

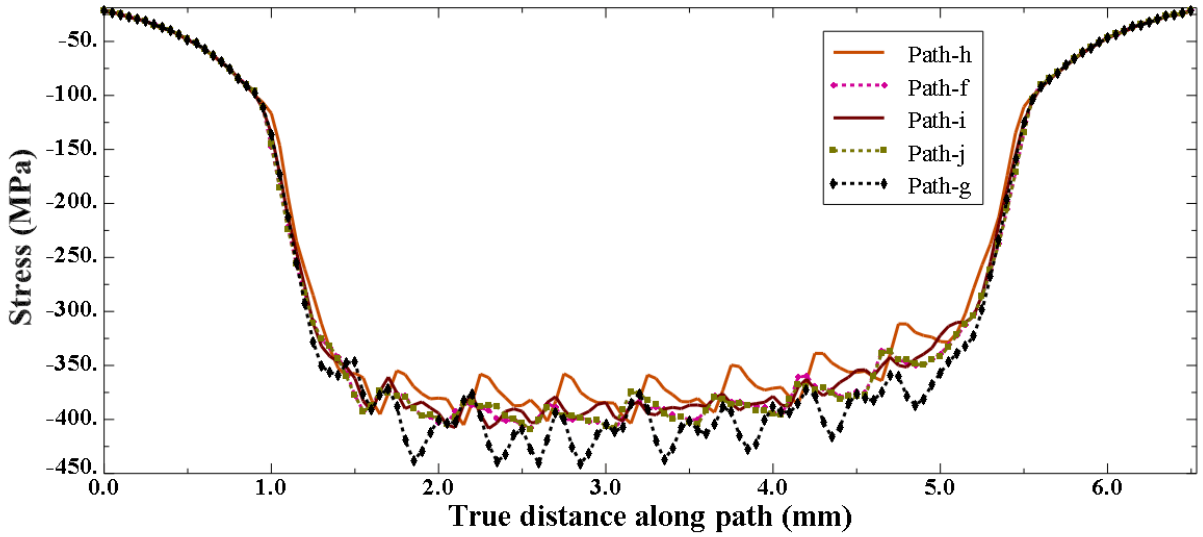


**Figure 5.40: S22 for sequence 1 at repetition rate of 0.1 MHz (8X8)**

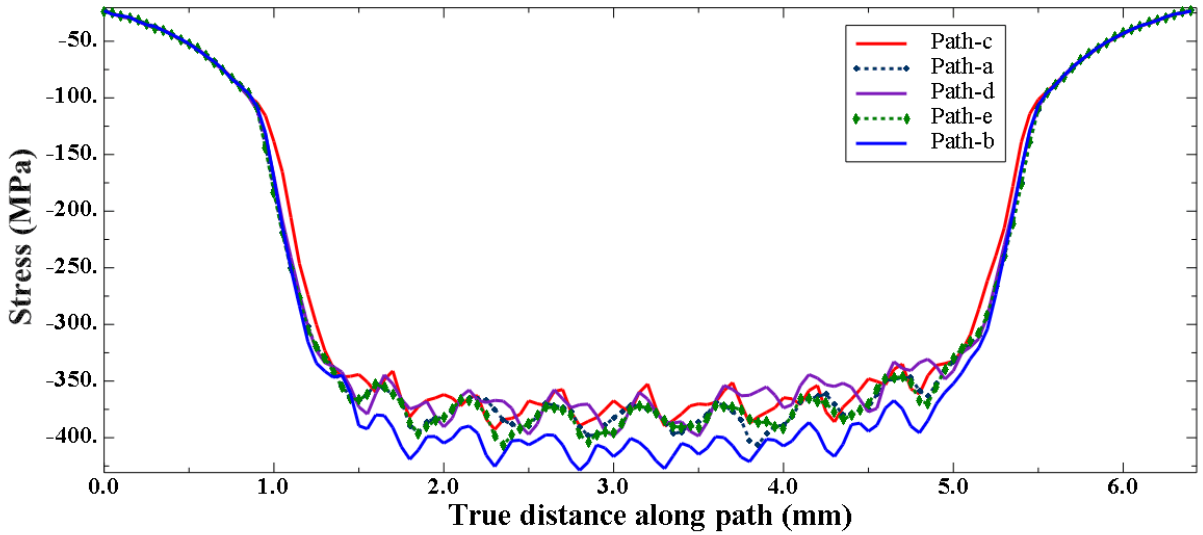


**Figure 5.41: S11 for sequence 1 at repetition rate of 1 MHz (8X8)**

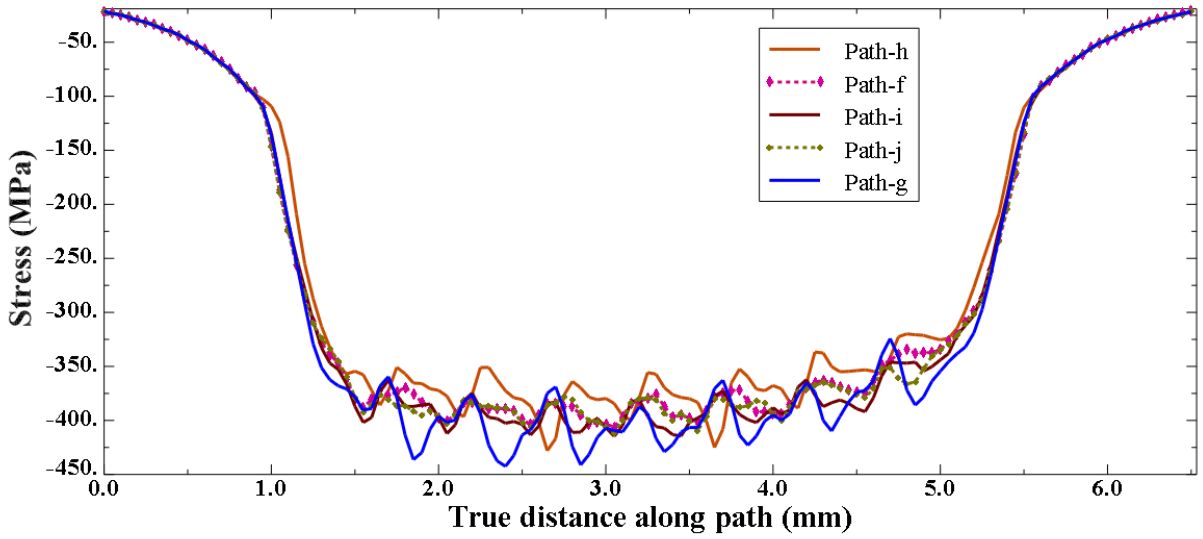


**Figure 5.42: S22 for sequence 1 at repetition rate of 1 MHz (8X8)**

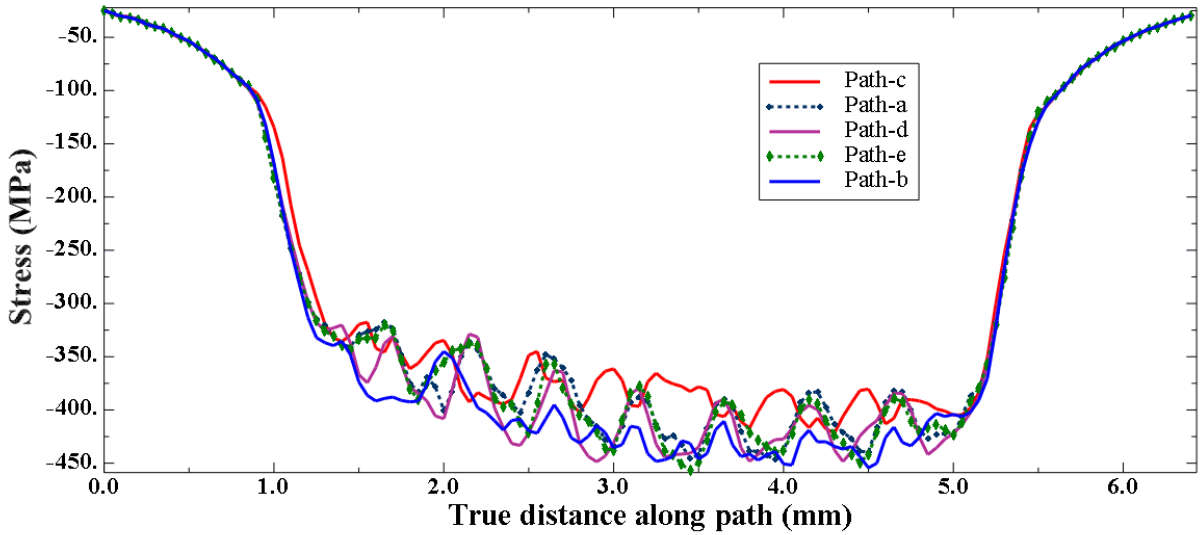


**Figure 5.43: S11 for sequence 1 at repetition rate of 10 MHz (8X8)**

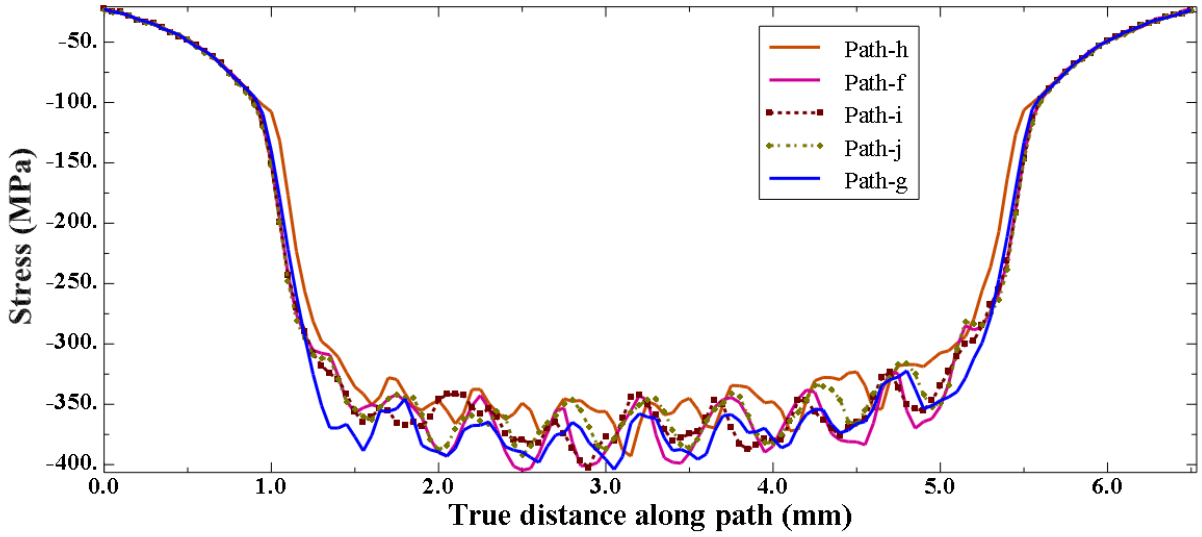


**Figure 5.44: S22 for sequence 1 at repetition rate of 10 MHz (8X8)**

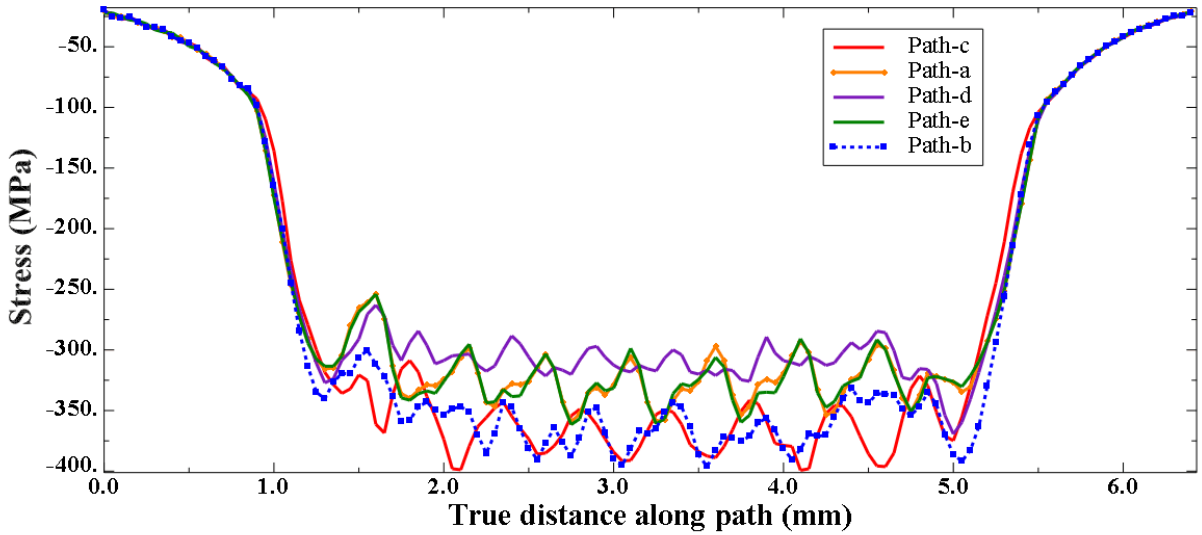


**Figure 5.45: S11 for sequence 1 at repetition rate of 20 MHz (8X8)**

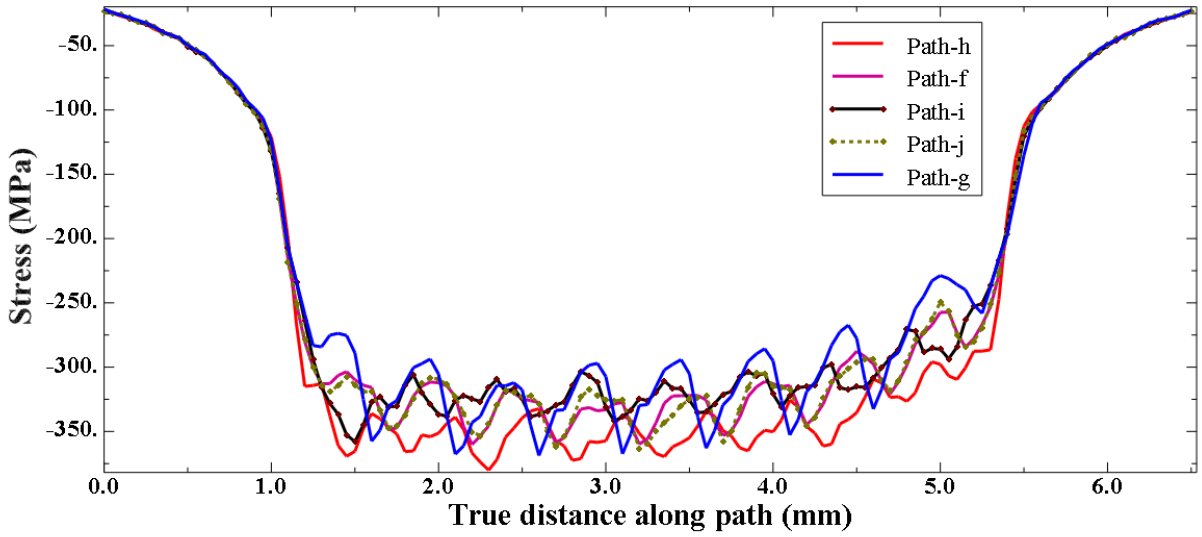


**Figure 5.46: S22 for sequence 1 at repetition rate of 20 MHz (8X8)**

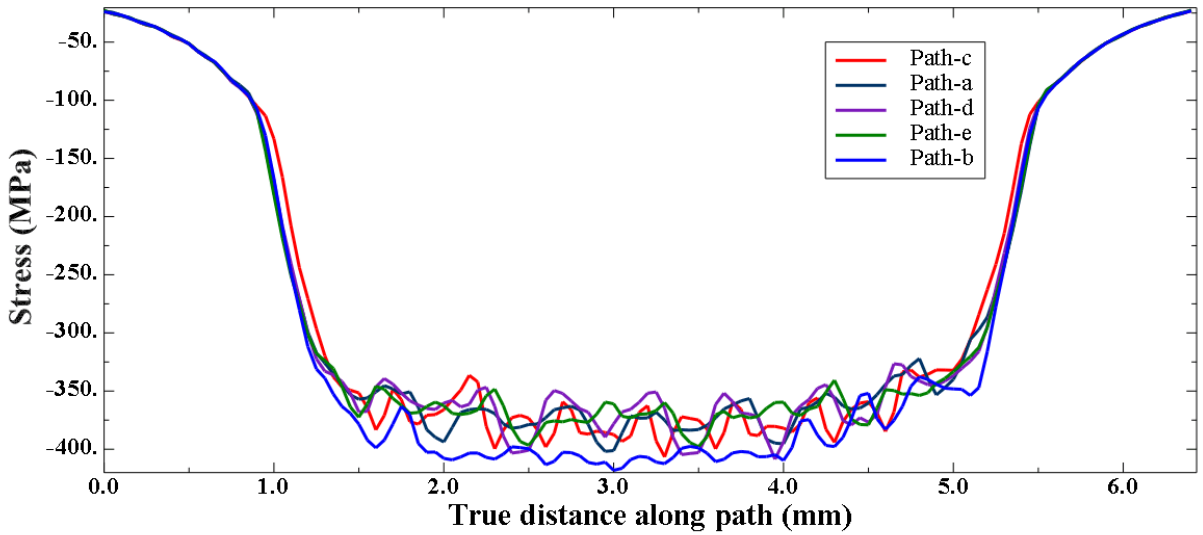


**Figure 5.47: S11 zigzag pattern 1 for sequence 1 at repetition rate of 0.1 MHz**

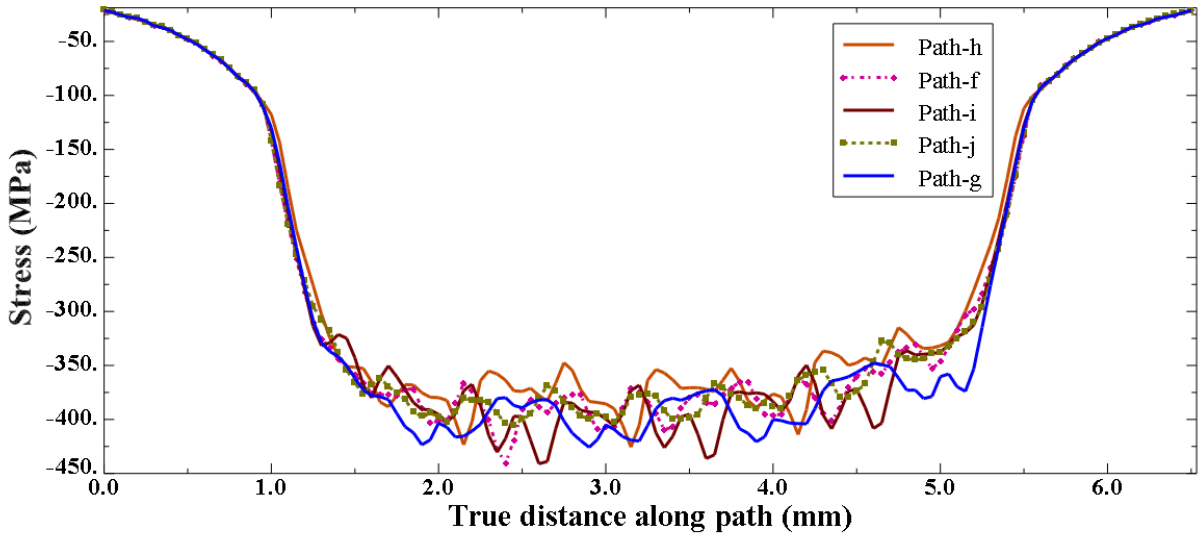


**Figure 5.48: S22 in zigzag pattern 1 for sequence 1 at repetition rate of 0.1 MHz**

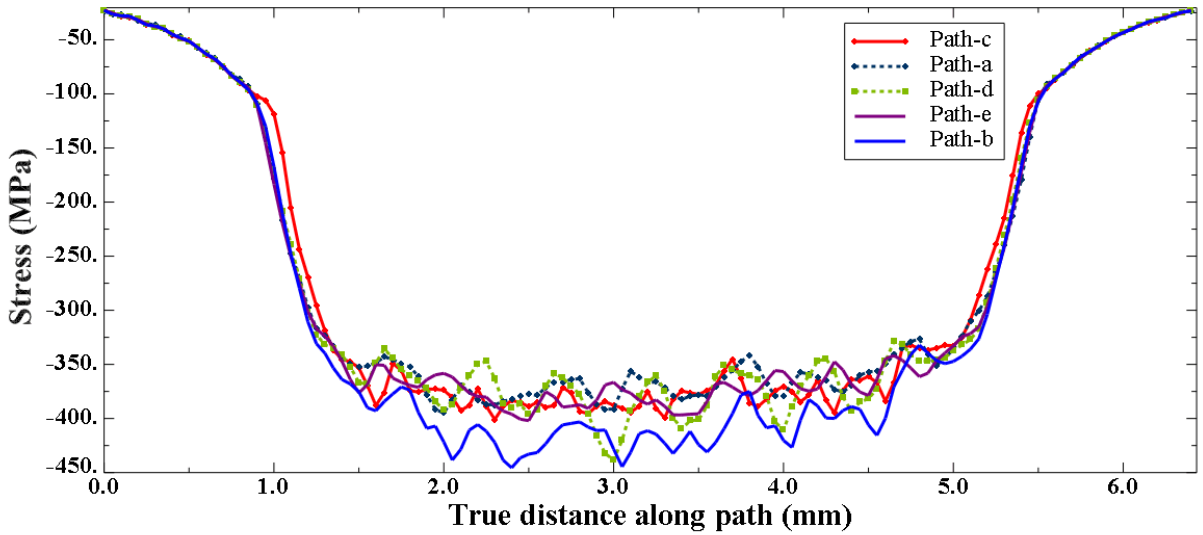


**Figure 5.49: S11 in zigzag pattern 1 for sequence 1 at repetition rate of 1 MHz**

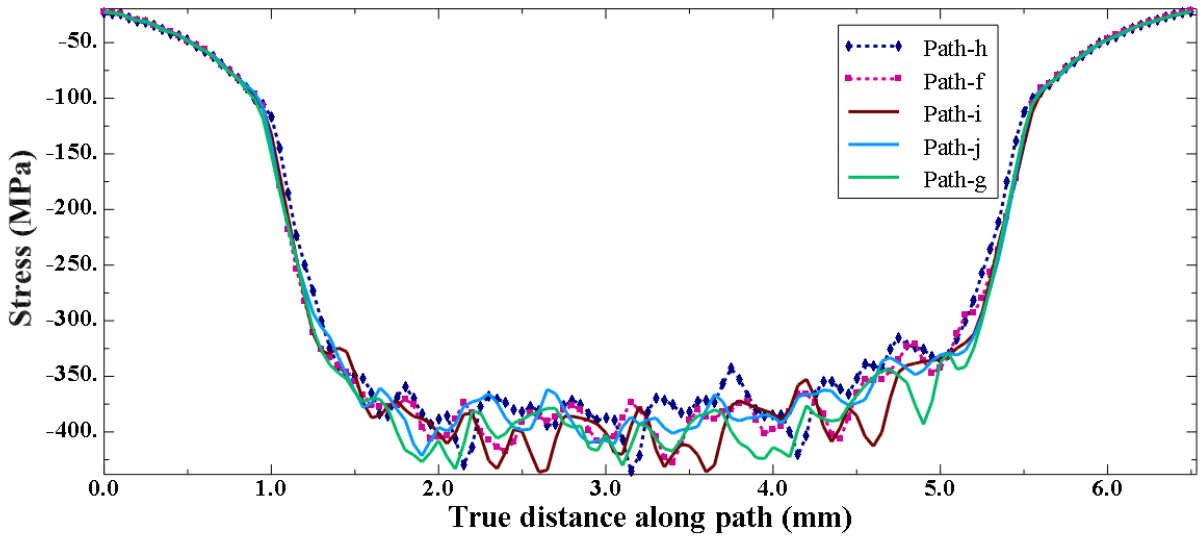


**Figure 5.50: S22 in zigzag pattern 1 for sequence 1 at repetition rate of 1 MHz**

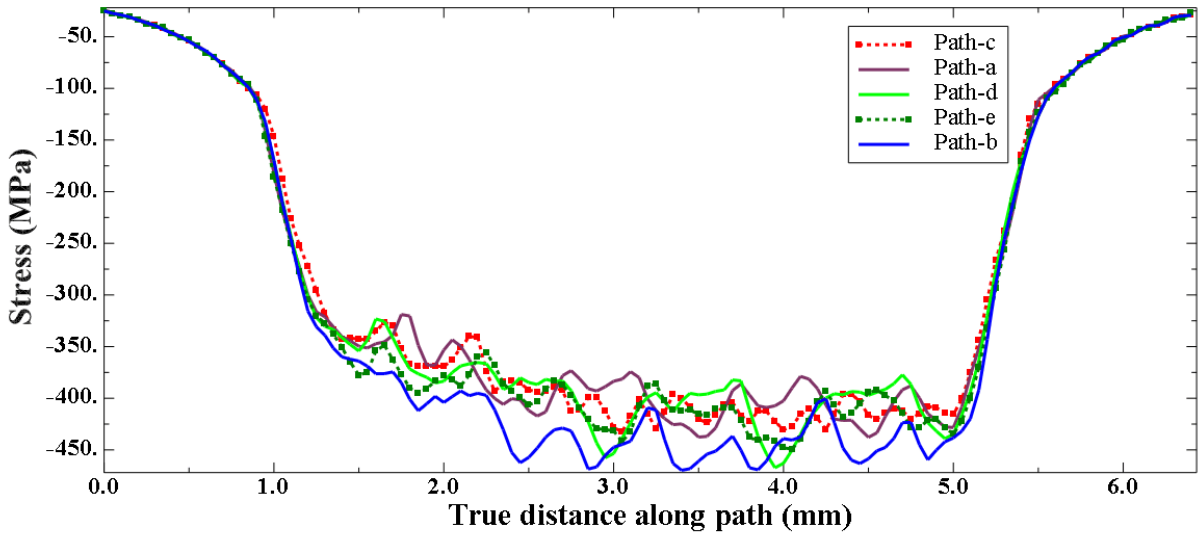


**Figure 5.51: S11 in zigzag pattern 1 for sequence 1 at repetition rate of 10 MHz**

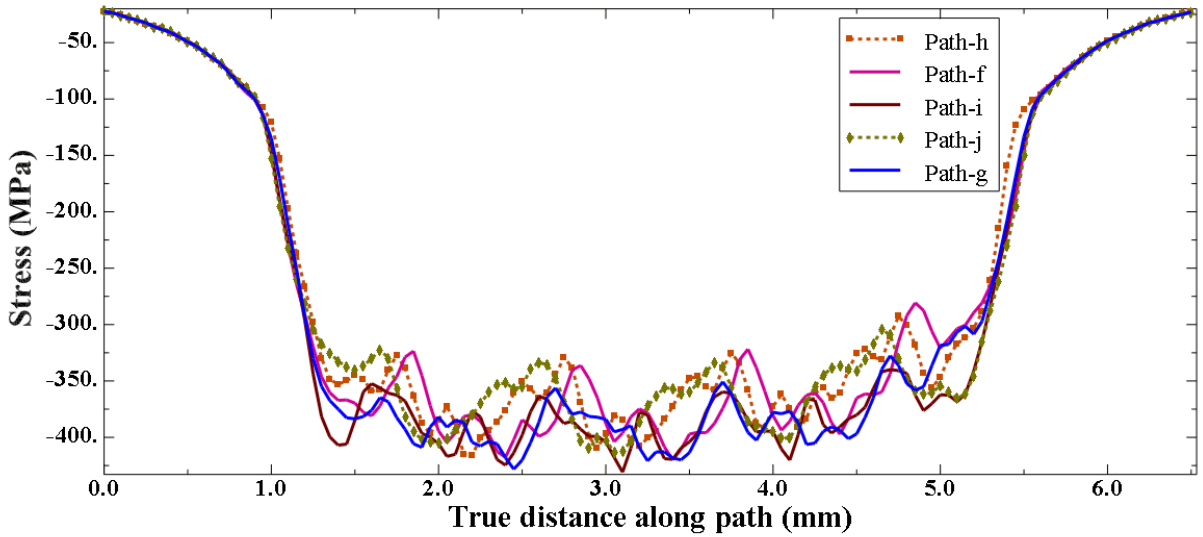


**Figure 5.52: S22 in zigzag pattern 1 for sequence 1 at repetition rate of 10 MHz**

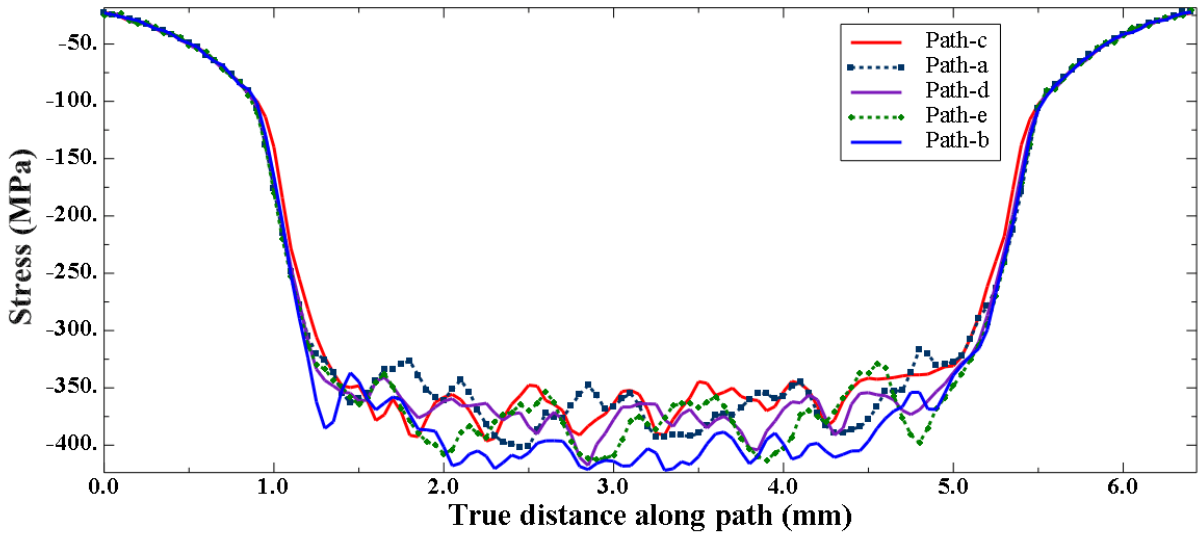


**Figure 5.53: S11 in zigzag pattern 1 for sequence 1 at repetition rate of 20 MHz**

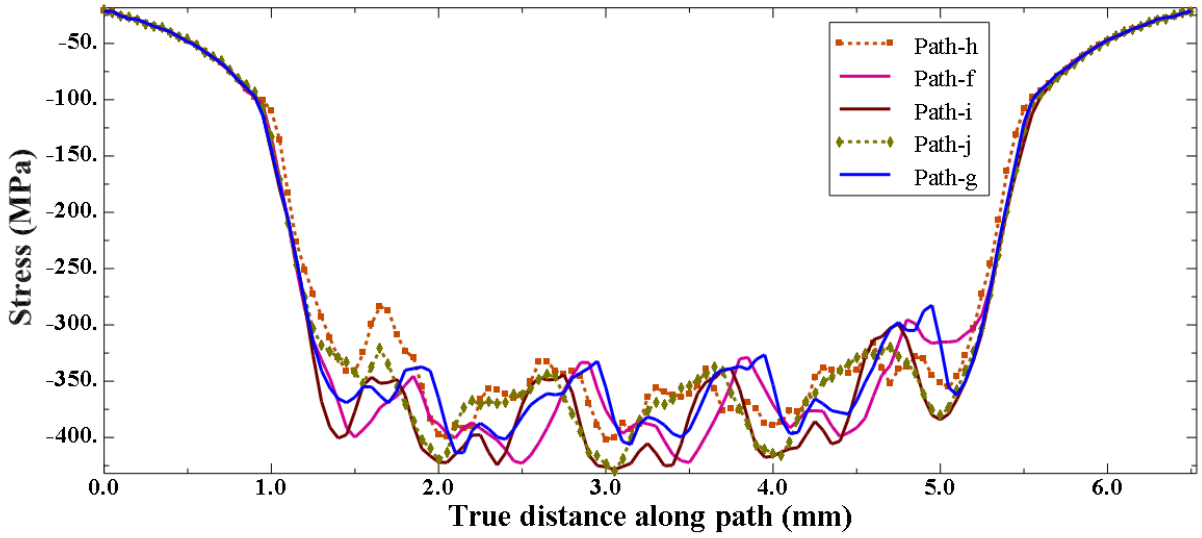


**Figure 5.54: S22 in zigzag pattern 1 for sequence 1 at repetition rate of 20 MHz**

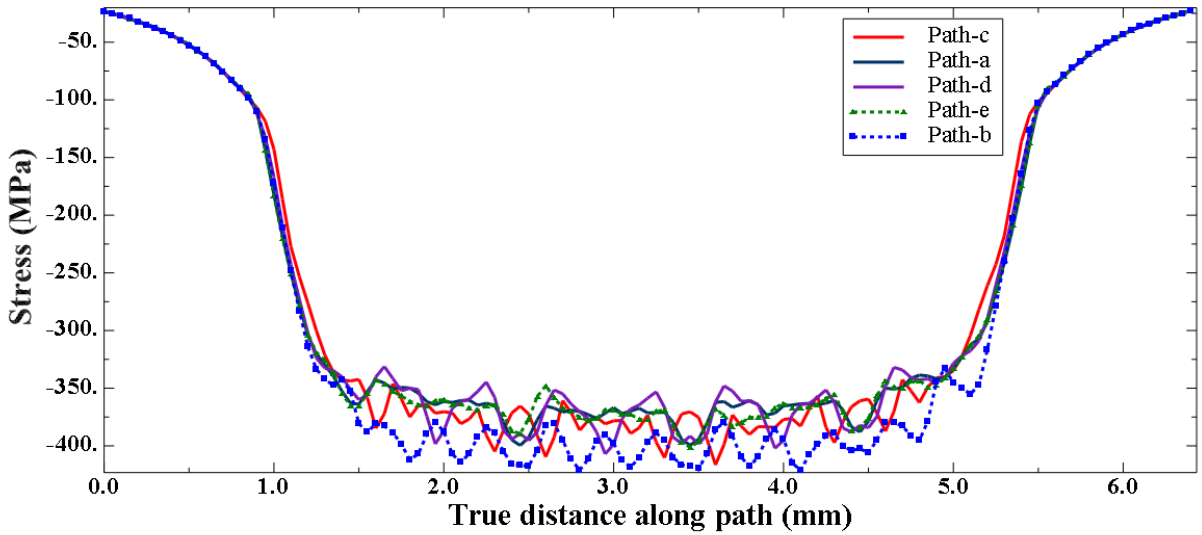


**Figure 5.55: S11 in zigzag pattern 2 for sequence 1 at repetition rate of 0.1 MHz**

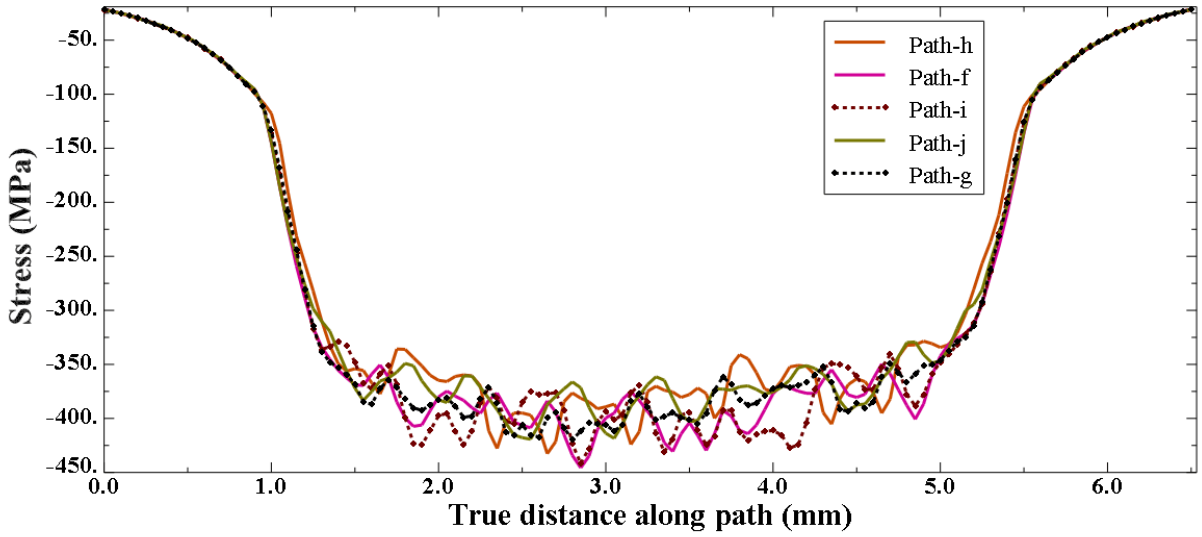


**Figure 5.56: S22 in zigzag pattern 2 for sequence 1 at repetition rate of 0.1 MHz**

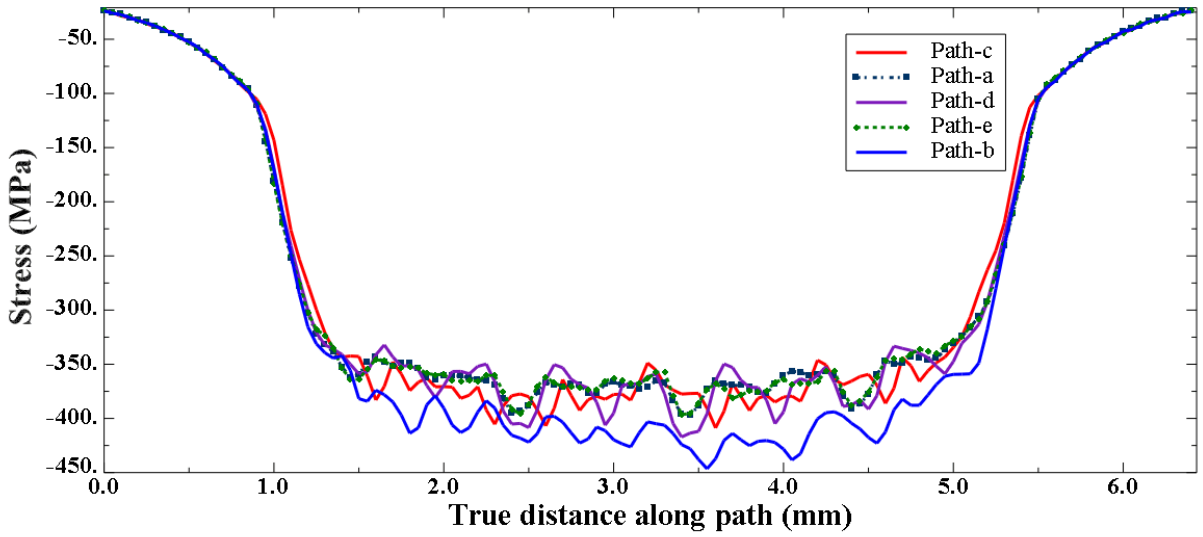


**Figure 5.57: S11 in zigzag pattern 2 for sequence 1 at repetition rate of 1 MHz**

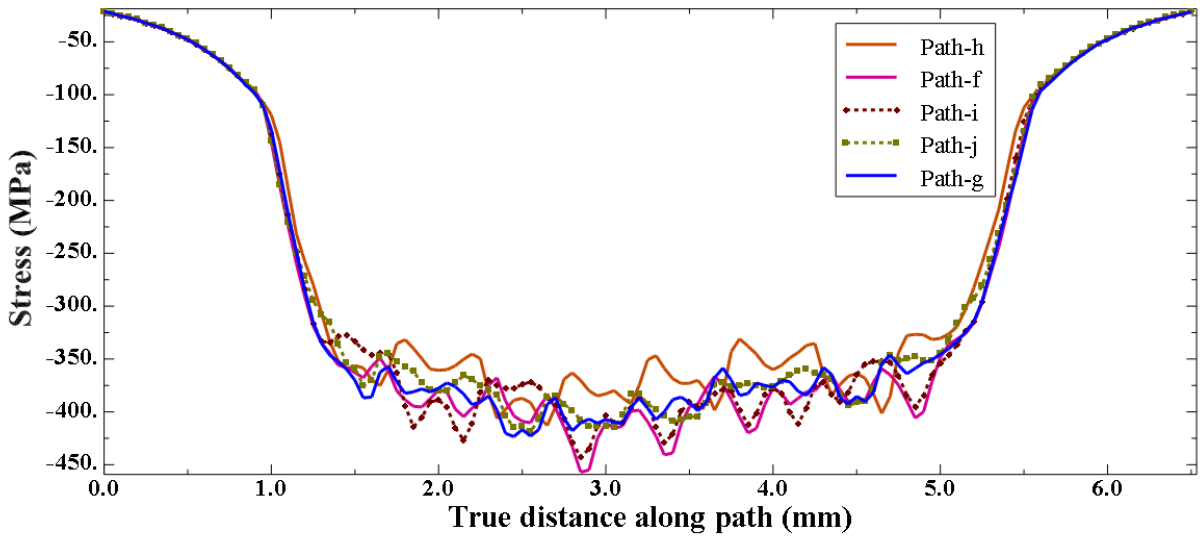


**Figure 5.58: S22 in zigzag pattern 2 for sequence 1 at repetition rate of 1 MHz**

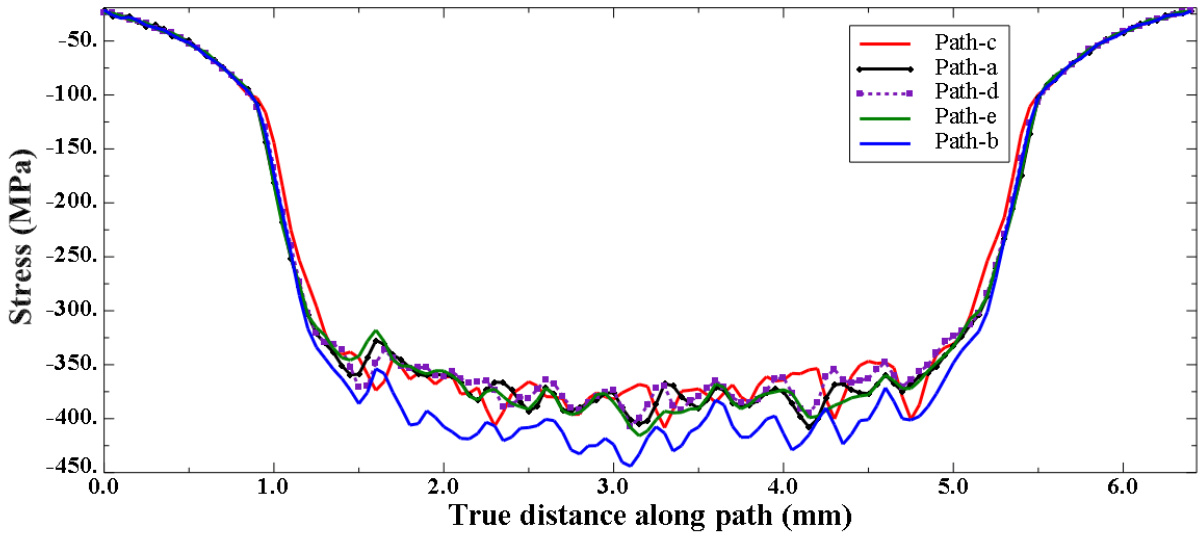


**Figure 5.59: S11 in zigzag pattern 2 for sequence 1 at repetition rate of 10 MHz**

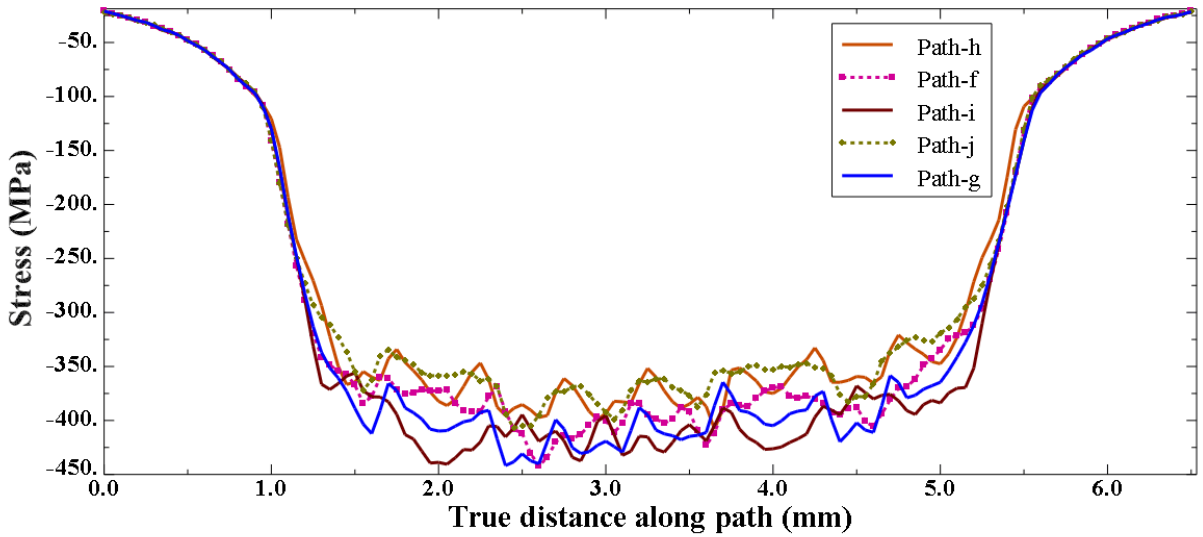


**Figure 5.60: S22 in zigzag pattern 2 for sequence 1 at repetition rate of 10 MHz**

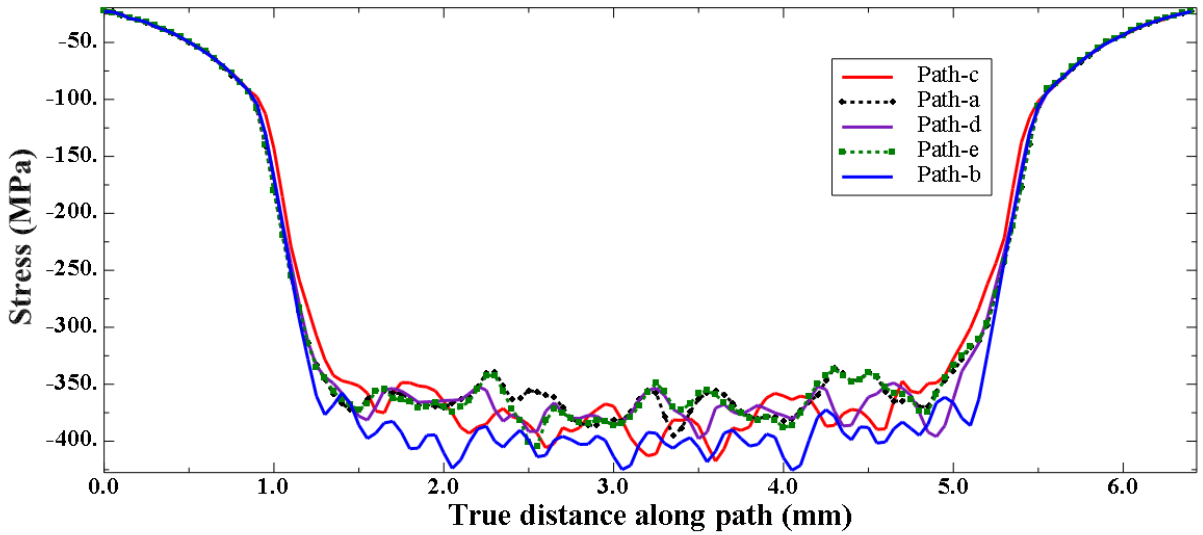


**Figure 5.61: S11 in zigzag pattern 2 for sequence 1 at repetition rate of 20 MHz**

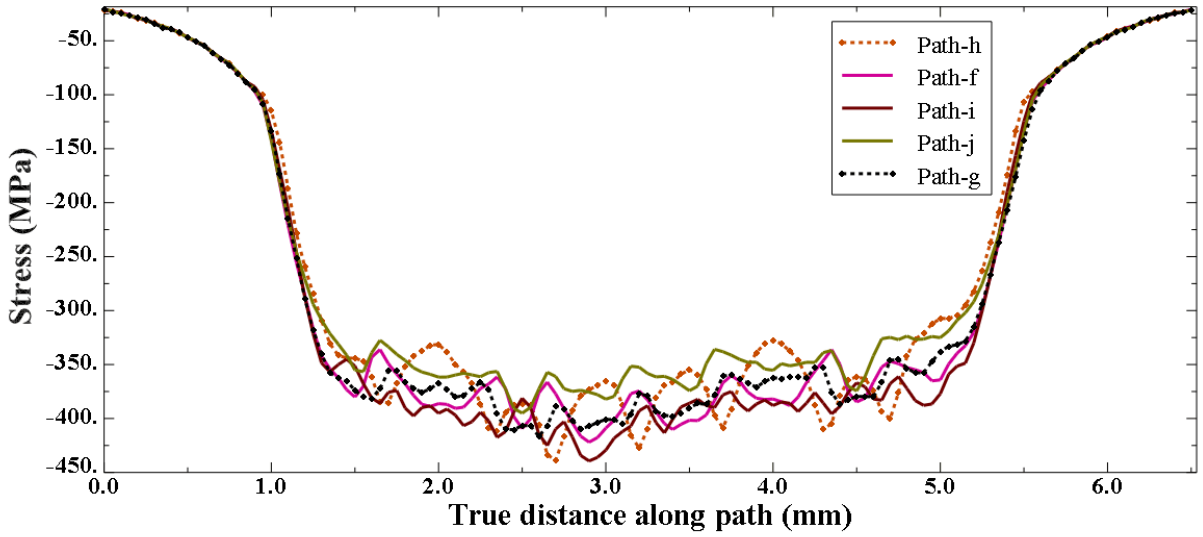


**Figure 5.62: S22 in zigzag pattern 2 for sequence 1 at repetition rate of 20 MHz**

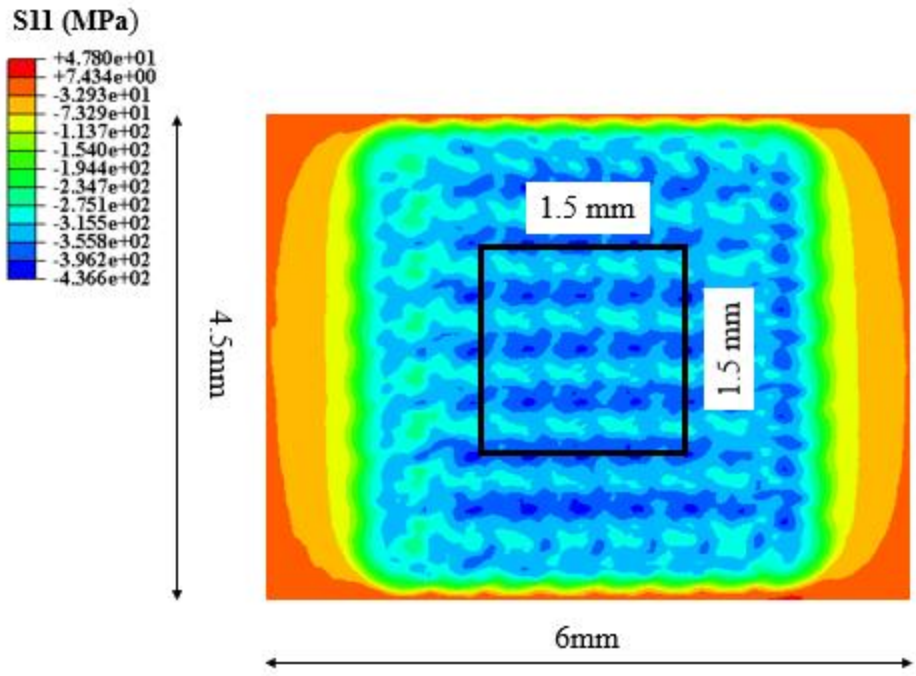


**Figure 5.63: Contour plot (S11) for sequence 1 at repetition rate of 20 MHz**

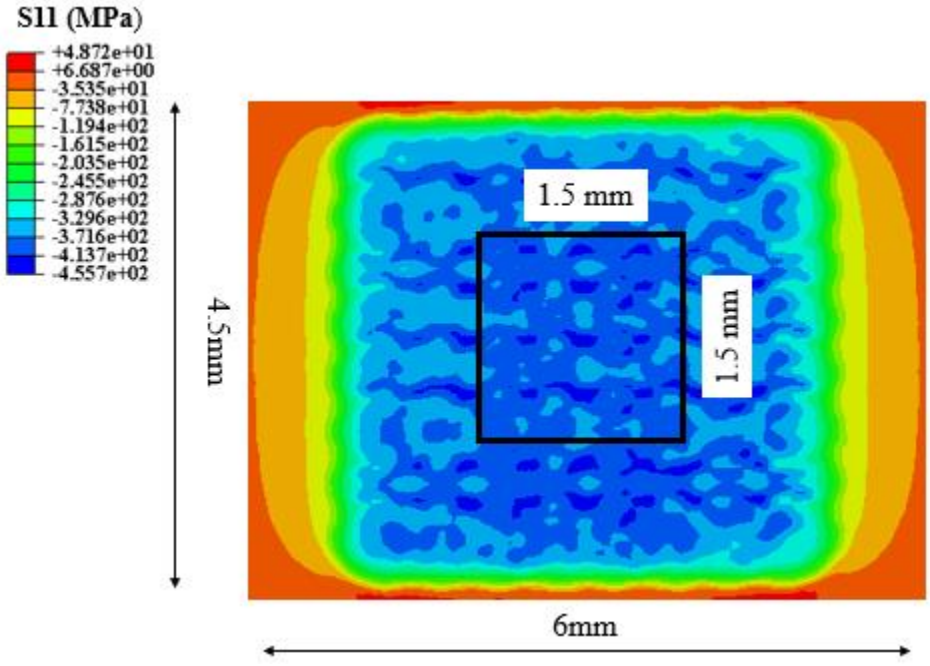


**Figure 5.64: Contour plot (S11) for zigzag pattern 2 at repetition rate of 20 MHz**

**Table 7: Summary of residual stresses for sequence 1, zigzag pattern 1 and zigzag pattern 2**

| Sequence | Repetition rate (MHz) | S11 (MPa) | | | | | S22 (MPa) | | | | |
|---|---|---|---|---|---|---|---|---|---|---|---|
| | | Minimum value | Maximum value | Range | Mean | Standard deviation | Minimum value | Maximum value | Range | Mean | Standard deviation |
| Sequence 1 | 0.1 | 329.51 | 473.46 | 143.95 | 386.48 | 21.25 | 324.23 | 483.01 | 158.77 | 394.00 | 21.37 |
| | 1 | 341.78 | 463.06 | 121.28 | 386.14 | 21.07 | 340.40 | 473.82 | 133.42 | 393.52 | 20.93 |
| | 10 | 330.95 | 466.85 | 135.90 | 410.63 | 25.85 | 315.56 | 429.75 | 114.19 | 369.74 | 21.08 |
| | 20 | 283.58 | 417.24 | 133.66 | 345.65 | 28.74 | 280.94 | 396.89 | 115.95 | 338.09 | 24.97 |
| Zigzag 1 | 0.1 | 334.08 | 457.88 | 123.80 | 382.22 | 19.29 | 338.89 | 454.99 | 116.10 | 389.76 | 18.71 |

| | | | | | | | | | | | |
|---|---|---|---|---|---|---|---|---|---|---|---|
| | 1 | 332.77 | 463.74 | 130.96 | 383.96 | 20.56 | 330.55 | 474.04 | 143.49 | 392.24 | 20.89 |
| | 10 | 334.60 | 473.26 | 138.65 | 406.97 | 25.07 | 312.25 | 454.88 | 142.62 | 380.01 | 23.71 |
| | 20 | 315.15 | 446.41 | 131.25 | 375.78 | 23.20 | 315.54 | 455.52 | 139.98 | 375.61 | 26.89 |
| Zigzag 2 | 0.1 | 342.43 | 456.75 | 114.32 | 388.91 | 22.98 | 340.95 | 460.23 | 119.29 | 395.53 | 21.66 |
| | 1 | 344.62 | 478.96 | 134.35 | 390.03 | 23.27 | 331.00 | 461.87 | 130.87 | 396.82 | 23.34 |
| | 10 | 343.53 | 469.36 | 125.83 | 391.80 | 22.13 | 327.28 | 462.81 | 135.52 | 390.43 | 25.19 |
| | 20 | 339.40 | 450.36 | 110.96 | 387.14 | 18.91 | 327.85 | 454.11 | 126.25 | 388.46 | 20.46 |

The limits of compressive stress changes for 8X8 pattern because of the elimination of edge effect. Mean represents the average value of the residual stress in the area of the sample under consideration. Standard deviation represents how far the residual stress in the area are from the mean residual stress. High standard deviation represents high non-uniformity of residual stress.

For sequence 1, the mean of residual stresses is high and standard deviation is low at lower repetition rates of 0.1 MHz and 1 MHz. The difference between mean and standard deviation of S11 and S22 is less. At repetition rate of 10 MHz, the mean and non-uniformity of S11 is high. This can be attributed to constructive interaction of relaxation waves with incoming pressure wave between consecutive pulses in a row. The minimum value of S11 and S22 is very less at high repetition rate of 20 MHz. The mean value of residual stress is less, and the non-uniformity is high. There is notable difference between mean and standard deviation of residual stresses in x and y directions (S11 and S22). High non-uniformity in S11 can be attributed to the destructive interaction of relaxation waves with the incoming pressure wave between consecutive pulses in a row. The non-uniformity in S22 is high because the scan path is in x-direction.

For zig-zag pattern 1, the mean of residual stress is similar to the mean for sequence 1 at low repetition rates of 0.1 MHz and 1 MHz. The mean of residual stress at high repetition rates of 10 MHz and 20 MHz is higher than mean for sequence 1. But the non-uniformity is high at all repetition rates because the scanning path is not confined to one direction. Though the pulses advances in x- direction, the immediate pulses are irradiated at an angle of $45^0$.

For zig-zag pattern 2, the non-uniformity in S22 is higher than S11. But the change in non-uniformity, minimum and mean of residual stress with respect to repetition rate is not significant. For sequence 1, there is 40.83 MPa decrease in mean of S11 between repetition rates of 0.1 MHz and 20 MHz. But there is only 1.77 MPa decrease in mean for zigzag pattern 2. This is because of

the elimination of effect of relaxation waves between successive spots. Figures 5.63- 5.64 shows the distribution of S11 for sequence 1 and zigzag pattern 2 at repetition rate of 20 MHz. It can be seen that the uniformity in distribution is predominant for zigzag pattern 2.

Figures 5.65- 5.68 show the distributions of S11 and S22 for sequence 2 at repetition rates of 10 MHz and 20 MHz. Figures 5.69-5.72 show the distributions of S11 and S22 for zigzag pattern 1 at repetition rates of 10 MHz and 20 MHz. Figures 5.73-5.76 show the distributions of S11 and S22 for zigzag pattern 2 at repetition rates of 10 MHz and 20 MHz. Table 8 summarizes the maximum, minimum, average, range and standard deviation of residual stresses induced at different repetition rates for sequence 2 and two zig zag patterns of sequence 2 in the center (1.5 mm X 1.5 mm) area.

.

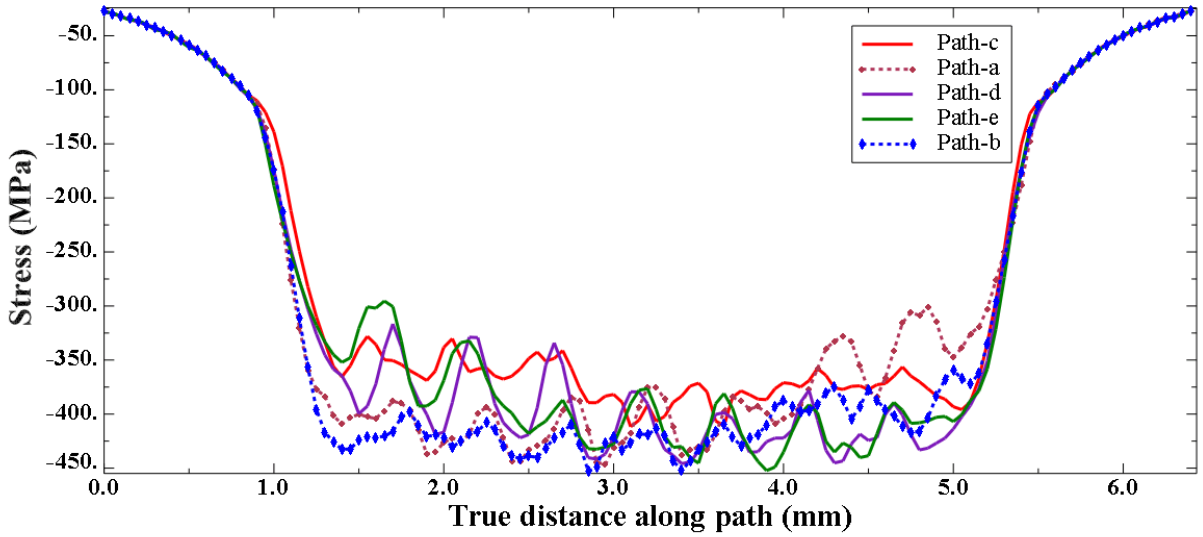


**Figure 5.65: S11 for sequence 2 at repetition rate of 10 MHz (8X8)**

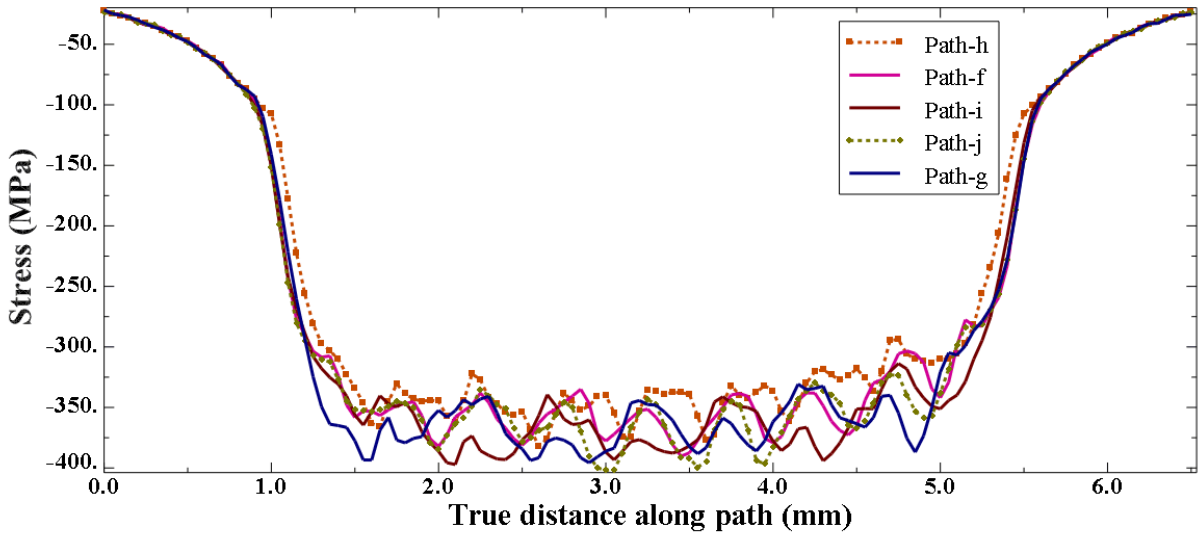


**Figure 5.66: S22 for sequence 2 at repetition rate of 10 MHz (8X8)**

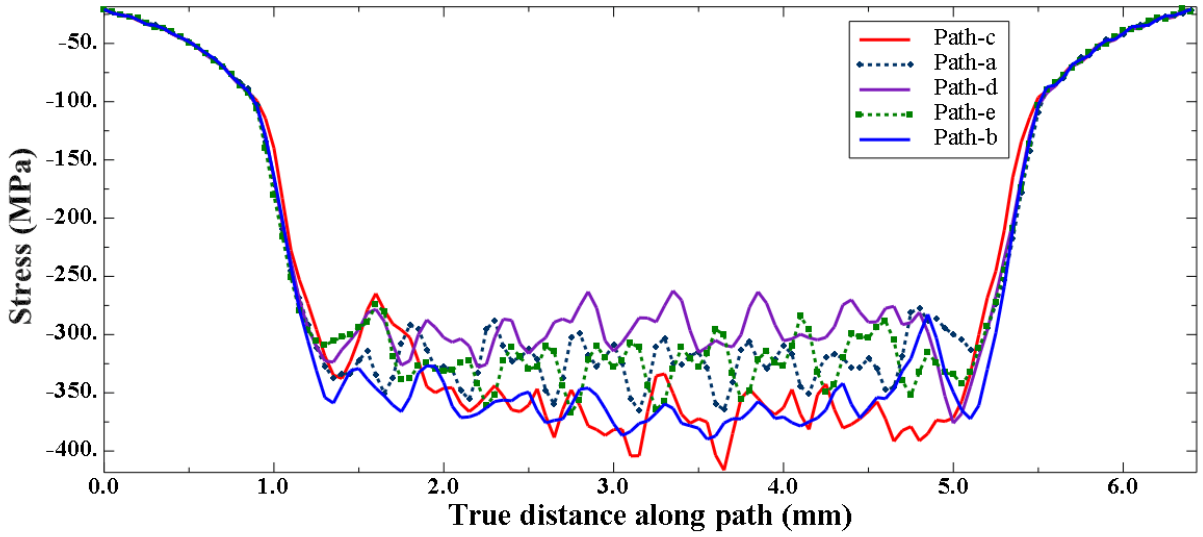


**Figure 5.67: S11 for sequence 2 at repetition rate of 20 MHz (8X8)**

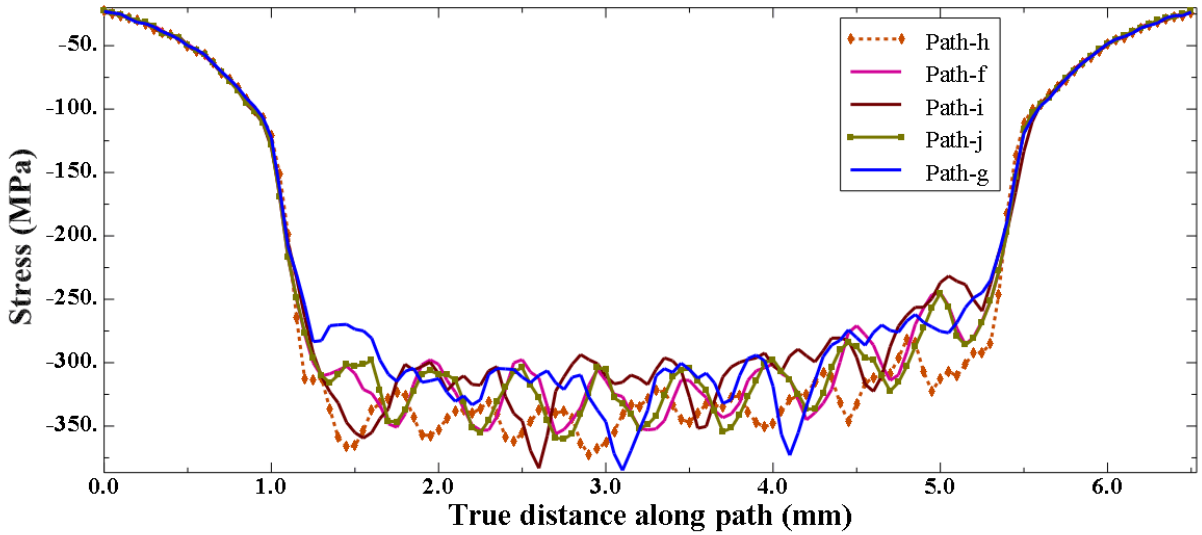


**Figure 5.68: S22 for sequence 2 at repetition rate of 20 MHz (8X8)**

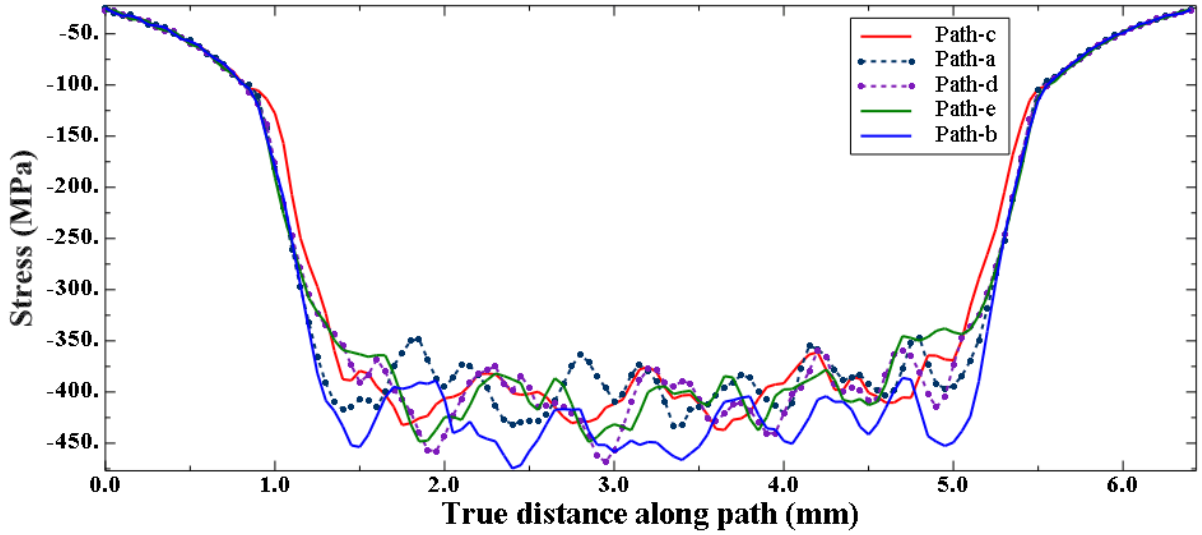


**Figure 5.69: S11 in zigzag pattern 1 for sequence 2 at repetition rate of 10 MHz**

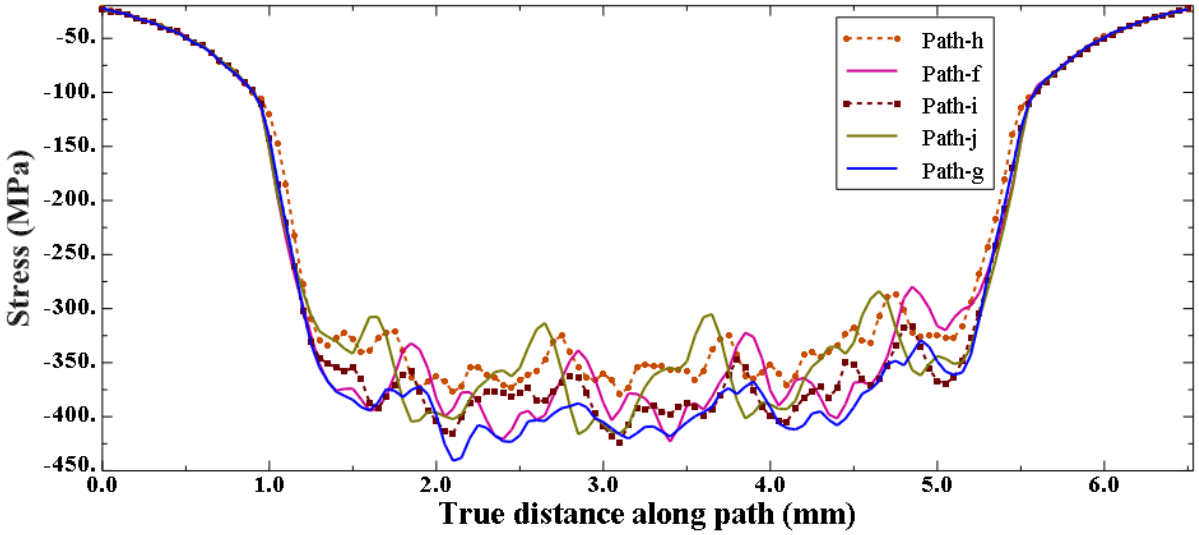


**Figure 5.70: S22 in zigzag pattern 1 for sequence 2 at repetition rate of 10 MHz**

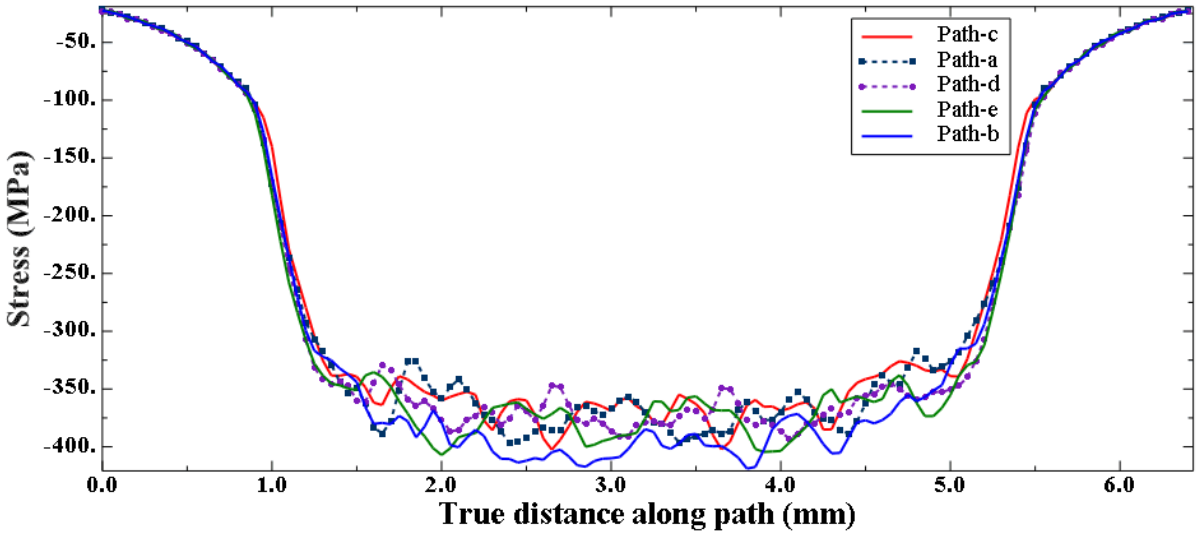


**Figure 5.71: S11 in zigzag pattern 1 for sequence 2 at repetition rate of 20 MHz**

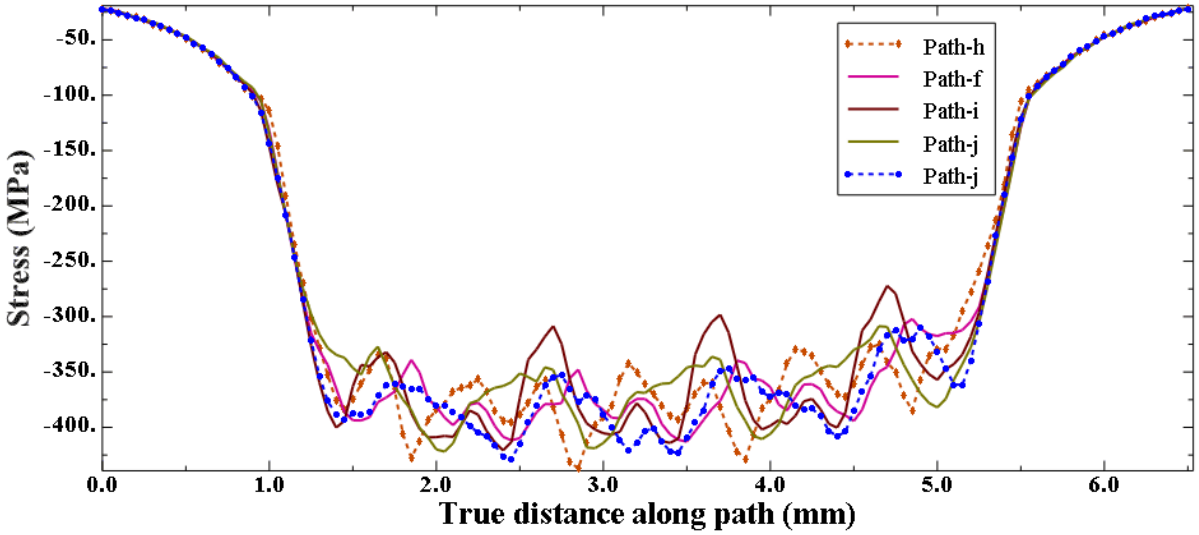


**Figure 5.72: S22 in zigzag pattern 1 for sequence 2 at repetition rate of 20 MHz**

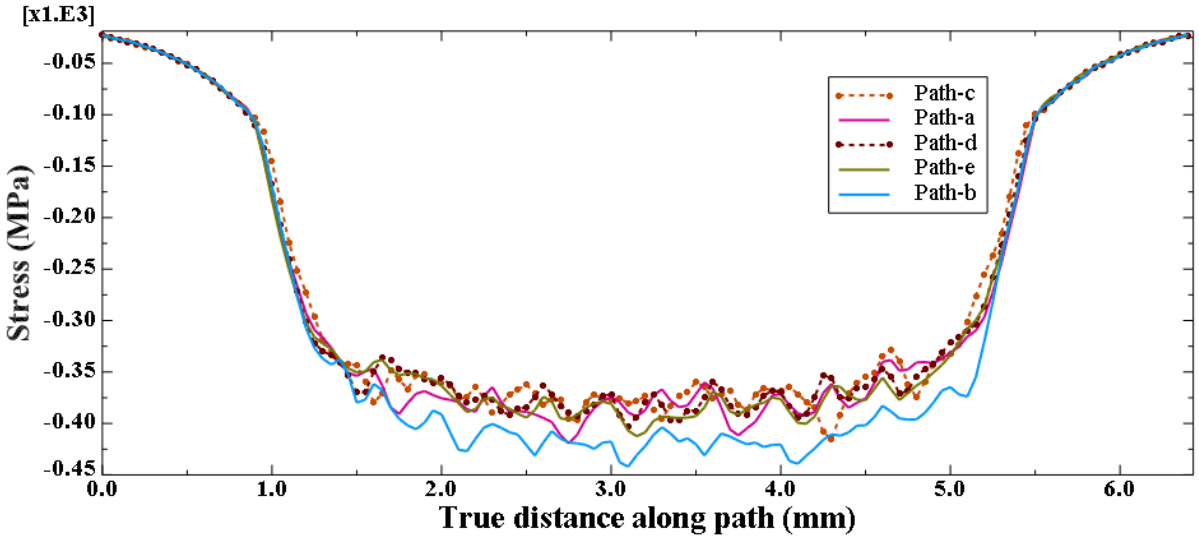


**Figure 5.73: S11 in zigzag pattern 2 for sequence 2 at repetition rate of 10 MHz**

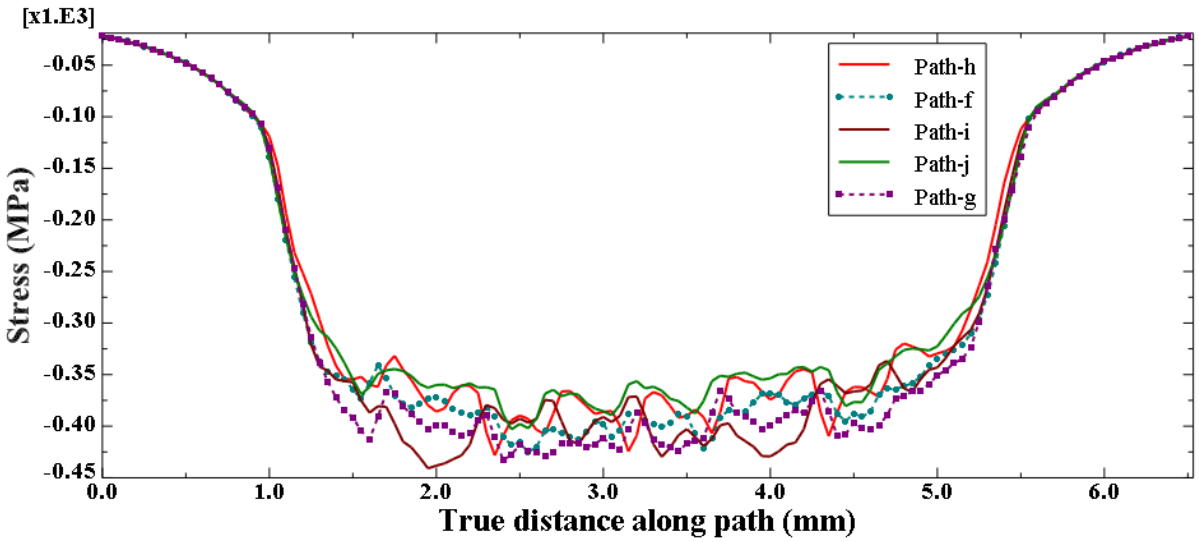


**Figure 5.74: S22 in zigzag pattern 2 for sequence 2 at repetition rate of 10 MHz**

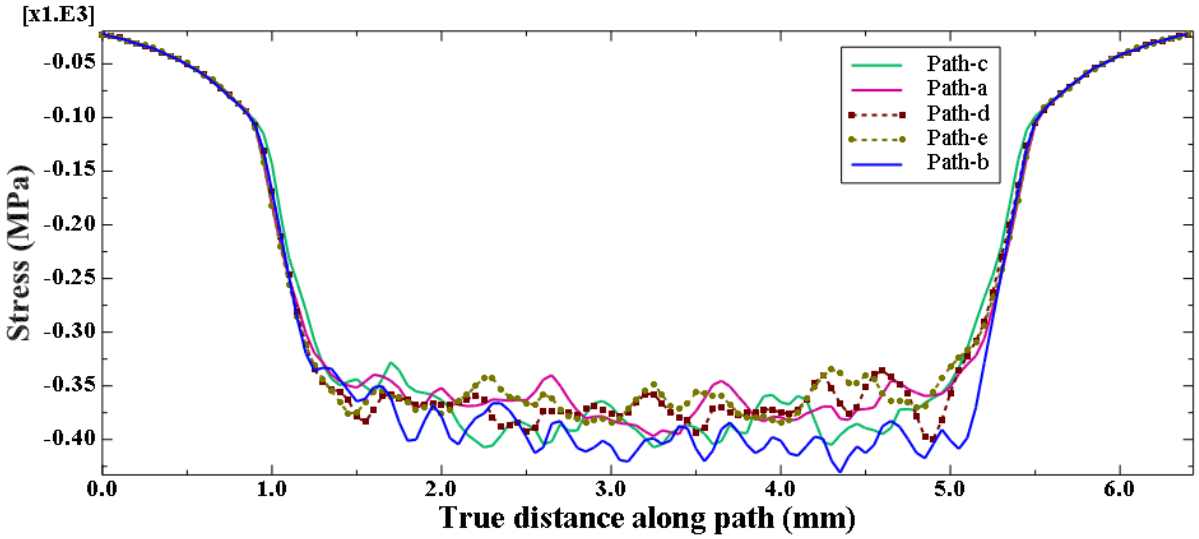


**Figure 5.75: S11 in zigzag pattern 2 for sequence 2 at repetition rate of 20 MHz**

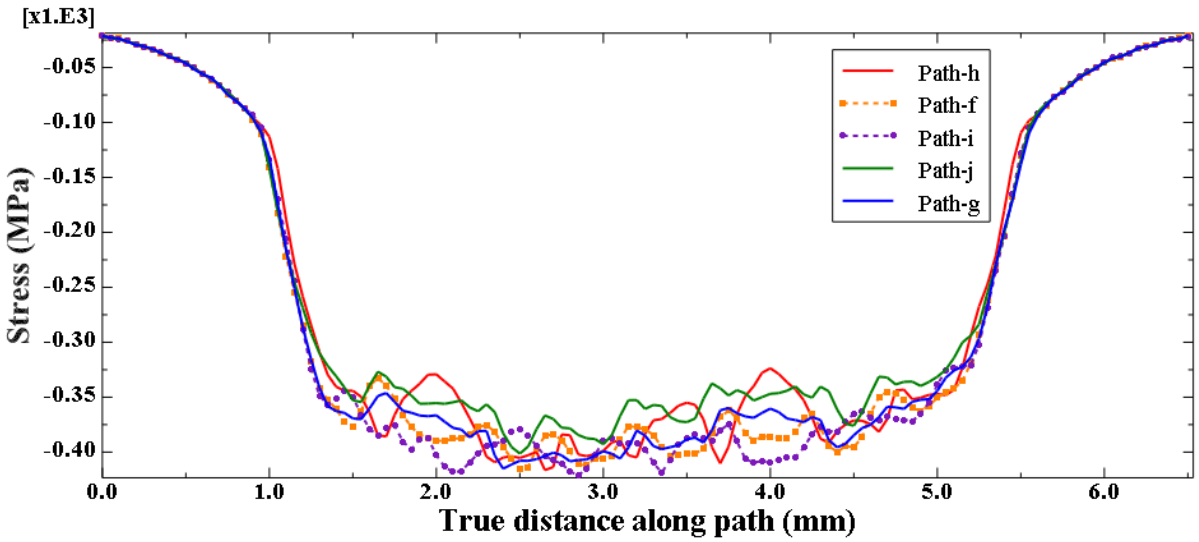


**Figure 5.76: S22 in zigzag pattern 2 for sequence 2 at repetition rate of 20 MHz**

**Table 8: Summary of residual stresses for sequence 2, zigzag pattern 1 and zigzag pattern 2**

| Sequence | Repetition rate (MHz) | S11 (MPa) | | | | | S22 (MPa) | | | | |
|---|---|---|---|---|---|---|---|---|---|---|---|
| | | Minimum value | Maximum value | Range | Mean | Standard deviation | Minimum value | Maximum value | Range | Mean | Standard deviation |
| Sequence 2 | 0.1 | 344.18 | 466.86 | 122.67 | 383.30 | 19.29 | 358.27 | 441.98 | 83.70 | 391.05 | 18.97 |
| | 1 | 337.84 | 467.56 | 129.73 | 382.04 | 20.84 | 348.34 | 456.57 | 108.23 | 389.83 | 18.54 |
| | 10 | 300.99 | 471.48 | 170.49 | 403.47 | 26.71 | 290.51 | 420.00 | 129.49 | 361.68 | 21.27 |
| | 20 | 260.87 | 416.42 | 155.55 | 338.22 | 31.90 | 268.35 | 394.49 | 126.13 | 328.39 | 25.49 |
| Zigzag 1 | 0.1 | 344.12 | 474.18 | 130.06 | 383.39 | 19.69 | 337.10 | 454.12 | 117.02 | 388.09 | 19.27 |

| | | | | | | | | | | | |
|---|---|---|---|---|---|---|---|---|---|---|---|
| | 1 | 334.79 | 463.40 | 128.62 | 385.07 | 21.19 | 339.46 | 461.53 | 122.08 | 390.88 | 20.00 |
| | 10 | 337.19 | 471.36 | 134.17 | 406.21 | 23.23 | 305.10 | 455.92 | 150.82 | 379.38 | 26.20 |
| | 20 | 323.42 | 442.97 | 119.55 | 377.49 | 19.66 | 298.25 | 437.13 | 138.88 | 377.91 | 24.67 |
| Zigzag 2 | 0.1 | 344.09 | 456.33 | 112.24 | 388.41 | 22.74 | 345.09 | 473.55 | 128.46 | 395.12 | 21.59 |
| | 1 | 342.06 | 466.10 | 124.05 | 389.61 | 22.69 | 334.99 | 463.88 | 128.89 | 396.14 | 22.07 |
| | 10 | 340.46 | 467.51 | 127.05 | 392.81 | 21.04 | 320.51 | 466.90 | 146.40 | 392.17 | 25.49 |
| | 20 | 334.83 | 449.60 | 114.77 | 385.35 | 19.47 | 323.68 | 456.90 | 133.22 | 387.33 | 20.78 |

The results for sequence 2 is similar to the results for sequence 1. At lower repetition rates of 0.1 MHz and 1 MHz, the mean of residual stresses (S11 and S22) is high and the standard deviation is low for sequence 2. At high repetition rate of 20 MHz, the minimum and mean of residual stress are low and the non-uniformity is very high due to interaction of active relaxation waves with incoming pressure waves. For zigzag pattern 1 of sequence 2, the mean, minimum and non-uniformity of residual stress are high at all repetition rates compared to sequence 2 because the scanning path is not confined to x-direction. For zigzag pattern 2 of sequence 2, the change in non-uniformity, minimum and mean of residual stress with respect to repetition rate is not significant because of the elimination of effect of relaxation waves.

# CHAPTER 6: CONCLUSIONS AND FUTURE WORK

## 6.1 Conclusions

In this study, the effects of repetition rate, spot size, and scanning pattern of LSP are investigated by numerical analysis. It is revealed that at low repetition rates, where the interval between successive pulses is longer than the material relaxation time, the effect of repetition rate on residual stress distribution is negligible. For repetition rates with less overlap between successive pulses, the peak compressive stress remains the same as the value at lower repetition rates, but the plastically affected depth decreases because of the interaction between the relaxation wave and the incoming pressure pulse. At very high repetition rates (>100 MHz), where the time interval between successive pulses is even shorter than the shock duration, the interaction of metal with shock wave is significantly different, leading to a different residual stress profile. Stronger residual stress with deeper distribution are obtained compared with longer repetition rate cases.

The effect of repetition rate on the residual stress in-depth distribution at different spot sizes is also studied. Deeper distributions with high residual stress are obtained at different spot sizes at high repetition rates. However, the peak compressive stress decreases with increase in spot size. At lower repetition rate, the surface tensile residual stresses are high for smaller spot size. At very high repetition rates, due to stronger pressures acting on very small area, the surface tensile stresses for smaller spot decreases and high compressive stresses are induced outside the spot boundary.

The profile of the surface stress distribution and the peak value changes with the type and amount of overlap between the successive spots. The sequence of application of laser spots changes the profile of residual stress distribution but the limits are not notably affected. With the

increase in repetition rate, the upper and lower limits of residual stress decrease and the non-uniformity increases. The non-uniformity is highest for circular pattern. Processing the large work piece using 5X5 patterns at high repetition rates is not beneficial.

To improve the residual stress uniformity at high repetition rate, two zig zag patterns are proposed. Though zig zag pattern 1 does not affect the mean residual stress, the non-uniformity is high. The residual stress in zigzag pattern 2 is not affected by repetition rate. The non-uniformity is high compared to sequence 1 and 2. But the change in non-uniformity with repetition rate is insignificant. Hence, high repetition rate lasers can be used to induce uniform residual stresses in large workpieces using zigzag pattern 2.

### 6.2 Future work recommendation

At high repetition rates, it is important to study the change in material properties after irradiation of first spot as it determines the profile of further incoming pressure pulses. A 3D model which considers overlap between pressure pulses and change of spot location simultaneously needs to be designed to study effect of repetition rates greater than 20 MHz.

The current study only studies the effect of repetition rate by assuming the pulse energy remains the same for all repetition rate. However, for real laser machines, the pulse energy will be inversely proportional to the repetition rate when it is very high, since the laser average power is constant. Therefore, further analysis considering this fact should be conducted to evaluate the results of LSP at high repetition rate in the future. Experimental study is needed to validate the modeling results and confirm the conclusions.

Nanosecond laser LSP is limited due to the demand of the protective coating and the confining medium, which makes the set-up complicated. The recent studies have proved the

potency of using femtosecond lasers for shock peening, where both the protective layer and confining medium can be removed due to the extremely high pressure and low surface damage by femtosecond lasers. Therefore, the use of femtosecond lasers with high repetition rates can be studied further.

## REFERENCES


[1] https://www.shotpeener.com/library/pdf/2010002.pdf

[2] https://www.cwst.co.uk/services/controlled-shot-peening/

[3] http://www.empowering-technologies.com/news.php

[4] https://www.mnes-us.com/nuclear-services/water-jet-peening

[5] http://exactech.co.jp/uk/products/hip/emerging-technologies/low-plasticity-burnishing

[6] https://www.lsptechnologies.com/how-laser-peening-works.php

[7] Braisted, W., & Brockman, R. (1999). Finite element simulation of laser shock peening. *International Journal of Fatigue*, *21*(7), 719-724.

[8] Peyre, P., Sollier, A., Chaieb, I., Berthe, L., Bartnicki, E., Braham, C., & Fabbro, R. (2003). FEM simulation of residual stresses induced by laser peening. *The European Physical Journal-Applied Physics*, *23*(2), 83-88.

[9] Ding, K., & Ye, L. (2006). Simulation of multiple laser shock peening of a 35CD4 steel alloy. *Journal of Materials Processing Technology*, *178*(1-3), 162-169.

[10] Peyre, P., Chaieb, I., & Braham, C. (2007). FEM calculation of residual stresses induced by laser shock processing in stainless steels. *Modelling and simulation in materials science and engineering*, *15*(3), 205.

[11] Ding, K. (2003). Three-dimensional dynamic finite element analysis of multiple laser shock peening processes. *Surface Engineering*, *19*(5), 351-358.

[12] Amarchinta, H. K., Grandhi, R. V., Langer, K., & Stargel, D. S. (2008). Material model validation for laser shock peening process simulation. *Modelling and simulation in materials science and engineering*, *17*(1), 015010.

[13] Voothaluru, R., & Liu, C. R. (2010, January). Finite Element Analysis of the Effect of Overlapping Impacts of Laser Shock Peening Within Annealed AISI 1053 Steel. In *ASME 2010 International Manufacturing Science and Engineering Conference* (pp. 221-228). American Society of Mechanical Engineers.

[14] Zhang, X. C., Zhang, Y. K., Lu, J. Z., Xuan, F. Z., Wang, Z. D., & Tu, S. T. (2010). Improvement of fatigue life of Ti–6Al–4V alloy by laser shock peening. *Materials Science and Engineering: A*, *527*(15), 3411-3415.

[15] Singh, G., Grandhi, R. V., & Stargel, D. S. (2011). Modeling and parameter design of a laser shock peening process. *International Journal for Computational Methods in Engineering Science and Mechanics*, *12*(5), 233-253.

[16] Brockman, R. A., Braisted, W. R., Olson, S. E., Tenaglia, R. D., Clauer, A. H., Langer, K., & Shepard, M. J. (2012). Prediction and characterization of residual stresses from laser shock peening. *International Journal of Fatigue*, *36*(1), 96-108.

[17] Luo, K. Y., Lu, J. Z., Wang, Q. W., Luo, M., Qi, H., & Zhou, J. Z. (2013). Residual stress distribution of Ti-6Al-4V alloy under different ns-LSP processing parameters. *Applied Surface Science*, *285*, 607-615.

[18] Wei, X. L., & Ling, X. (2014). Numerical modeling of residual stress induced by laser shock processing. *Applied Surface Science*, *301*, 557-563.

[19] Hu, Y., Yao, Z., & Hu, J. (2006). 3-D FEM simulation of laser shock processing. *Surface and Coatings Technology*, *201*(3-4), 1426-1435.

[20] Hu, Y. X., Yao, Z. Q., Wang, F., & Hu, J. (2007). Study on residual stress of laser shock processing based on numerical simulation and orthogonal experimental design. *Surface Engineering*, *23*(6), 470-478.

[21] Hu, Y., Gong, C., Yao, Z., & Hu, J. (2009). Investigation on the non-homogeneity of residual stress field induced by laser shock peening. *Surface and Coatings Technology*, *203*(23), 3503-3508.

[22] Hirano, K., Sugihashi, A., Imai, H., & Hamada, N. (2006). Mecanism of anisotropic stress generation in laser peening processs. In *Proceedings of Icaleo'2006 conference (Miami, USA)*.

[23] Bhamare, S., Ramakrishnan, G., Mannava, S. R., Langer, K., Vasudevan, V. K., & Qian, D. (2013). Simulation-based optimization of laser shock peening process for improved bending fatigue life of Ti–6Al–2Sn–4Zr–2Mo alloy. *Surface and Coatings Technology*, *232*, 464-474.

[24] Hfaiedh, N., Peyre, P., Song, H., Popa, I., Ji, V., & Vignal, V. (2015). Finite element analysis of laser shock peening of 2050-T8 aluminum alloy. *International Journal of Fatigue*, *70*, 480-489.

[25] Karbalaian, H. R., Yousefi-Koma, A., Karimpour, M., & Mohtasebi, S. S. (2015). Investigation on the Effect of Overlapping Laser Pulses in Laser Shock Peening with Finite Element Method. *Procedia Materials Science*, *11*, 454-458.

[26] Wu, X., Huang, C., Wang, X., & Song, H. (2011). A new effective method to estimate the effect of laser shock peening. *International Journal of Impact Engineering*, *38*(5), 322-329.

[27] Correa, C., Peral, D., Porro, J. A., Díaz, M., de Lara, L. R., García-Beltrán, A., & Ocaña, J. L. (2015). Random-type scanning patterns in laser shock peening without absorbing coating in 2024-T351 Al alloy: a solution to reduce residual stress anisotropy. *Optics & Laser Technology*, *73*, 179-187.

[28] Guo, Y. B. (2011). Laser shock peening: modeling, simulations, and applications. In *Numerical Simulations-Applications, Examples and Theory*. InTech.

[29] Achintha, M., & Nowell, D. (2011). Eigenstrain modelling of residual stresses generated by laser shock peening. *Journal of Materials Processing Technology*, *211*(6), 1091-1101.

[30] Ivetic, G. (2011). Finite element analysis and comparison of laser shock peening and shot peening processes. *International Journal of Structural Integrity*, *2*(2), 135-144.

[31] Hu, Y., & Yao, Z. (2008). Numerical simulation and experimentation of overlapping laser shock processing with symmetry cell. *International Journal of Machine Tools and Manufacture*, *48*(2), 152-162.

[32] Abaqus, V. (2014). 6.14 Documentation. *Dassault Systemes Simulia Corporation*, *651*.

[33] Hu, Y., & Yao, Z. (2008). Overlapping rate effect on laser shock processing of 1045 steel by small spots with Nd: YAG pulsed laser. *Surface and Coatings Technology*, *202*(8), 1517-1525.

[34] Luo, K. Y., Liu, B., Wu, L. J., Yan, Z., & Lu, J. Z. (2016). Tensile properties, residual stress distribution and grain arrangement as a function of sheet thickness of Mg–Al–Mn alloy subjected to two-sided and simultaneous LSP impacts. *Applied Surface Science*, *369*, 366-376.

[35] Wu, B., Tao, S., & Lei, S. (2010). Numerical modeling of laser shock peening with femtosecond laser pulses and comparisons to experiments. *Applied Surface Science*, *256*(13), 4376-4382.

[36] Julan, E., Stolz, C., Taheri, S., Peyre, P., & Gilles, P. (2013). Simulation of laser peening for generation of a surface compressive stresses. In *21st Congress French Mechanics, Bordeaux, France, Aug* (pp. 26-30).

[37] Wu, X., Huang, C., Wang, X., & Song, H. (2011). A new effective method to estimate the effect of laser shock peening. *International Journal of Impact Engineering*, *38*(5), 322-329.

[38] Warren, A. W., Guo, Y. B., & Chen, S. C. (2008). Massive parallel laser shock peening: simulation, analysis, and validation. *International Journal of Fatigue*, *30*(1), 188-197.

[39] Achintha, M. N. D. S. K. W. P., Nowell, D., Shapiro, K., & Withers, P. J. (2013). Eigenstrain modelling of residual stress generated by arrays of laser shock peening shots and determination of the complete stress field using limited strain measurements. *Surface and Coatings Technology*, *216*, 68-77.

[40] Peyre, P., & Fabbro, R. (1995). Laser shock processing: a review of the physics and applications. *Optical and quantum electronics*, *27*(12), 1213-1229.

[41] Crudo, C. (2012). *Investigation on laser shock peening capability by FE simulation* (Doctoral dissertation).

[42] Peyre, P., Hfaiedh, N., Song, H., Ji, V., Vignal, V., Seiler, W., & Branly, S. (2011). Laser shock processing with two different laser sources on 2050-T8 aluminum alloy. *International Journal of Structural Integrity*, *2*(1), 87-100.

[43] https://www.lambdatechs.com/low-plasticity-burnishing-lpb/